478

FE-2029-4

FOSSIL ENERGY

GASIFICATION IN PULVERIZED COAL FLAMES

First Annual Progress Report, July 1975—June 1976

R. C. Lenzer
P. E. George
J. F. Thomas
N. M. Laurendeau

July 1976

Work Performed Under Contract E(49-18)-2029

Combustion Laboratory
Purdue University
Lafayette, Indiana

ENERGY RESEARCH AND DEVELOPMENT ADMINISTRATION

MASTER

DISTRIBUTION OF THIS DOCUMENT IS UNLIMITED

DISCLAIMER

This report was prepared as an account of work sponsored by an agency of the United States Government. Neither the United States Government nor any agency Thereof, nor any of their employees, makes any warranty, express or implied, or assumes any legal liability or responsibility for the accuracy, completeness, or usefulness of any information, apparatus, product, or process disclosed, or represents that its use would not infringe privately owned rights. Reference herein to any specific commercial product, process, or service by trade name, trademark, manufacturer, or otherwise does not necessarily constitute or imply its endorsement, recommendation, or favoring by the United States Government or any agency thereof. The views and opinions of authors expressed herein do not necessarily state or reflect those of the United States Government or any agency thereof.

DISCLAIMER

Portions of this document may be illegible in electronic image products. Images are produced from the best available original document.

NOTICE

This report was prepared as an account of work sponsored by the United States Government. Neither the United States nor the United States Energy Research and Development Administration, nor any of their employees, nor any of their contractors, subcontractors, or their employees, makes any warranty, express or implied, or assumes any legal liability or responsibility for the accuracy, completeness or usefulness of any information, apparatus, product or process disclosed, or represents that its use would not infringe privately owned rights.

This report has been reproduced directly from the best available copy.

Available from the National Technical Information Service, U. S. Department of Commerce, Springfield, Virginia 22161

Price: Paper Copy $6.75 (domestic)
$9.25 (foreign)
Microfiche $2.25 (domestic)
$3.75 (foreign)

Printed in the United States of America
USERDA Technical Information Center, Oak Ridge, Tennessee

FE-2029-4
Distribution Category UC-90c

GASIFICATION IN PULVERIZED COAL FLAMES

First Annual Progress Report
Energy Research and Development Administration
ERDA-FE-2029-4

R. C. Lenzer
P. E. George
J. F. Thomas
N. M. Laurendeau

950 0894

The Combustion Laboratory
School of Mechanical Engineering
Purdue University
West Lafayette, Indiana 47907
Report No. PURDU-CL-76-07

July 1976

NOTICE
This report was prepared as an account of work sponsored by the United States Government. Neither the United States nor the United States Energy Research and Development Administration, nor any of their employees, nor any of their contractors, subcontractors, or their employees, makes any warranty, express or implied, or assumes any legal liability or responsibility for the accuracy, completeness or usefulness of any information, apparatus, product or process disclosed, or represents that its use would not infringe privately owned rights.

MASTER
DISTRIBUTION OF THIS DOCUMENT IS UNLIMITED

THIS PAGE

WAS INTENTIONALLY

LEFT BLANK

ACKNOWLEDGEMENTS

The following Purdue undergraduate students have assisted in various phases of this investigation: James Varnau, David Waite, Scott Rodibaugh, Kris Dunn and Donald Moore. Special thanks go to Mr. Varnau for his work on the coal handling facility and to Mr. Waite for performing the equilibrium calculations. The exhaust hood for the coal handling facility was donated by Mr. James Rush of Rush Metal Products, Inc., Lafayette, Indiana. Prof. C. Ehresman aided us in obtaining electrical power and following various safety codes. Equipment acquisition was facilitated through the help of Mr. Frank Tymoski, Purdue Purchasing Department. The secretarial talents of Ms. Virginia Bass are especially appreciated.

We are grateful to the Energy Research and Development Administration for support of this investigation and to our contract monitor, Dr. Michael Biallas, for his patience and encouragement.

TABLE OF CONTENTS

	Page
LIST OF TABLES	vii
LIST OF FIGURES	viii
LIST OF SYMBOLS	ix
ABSTRACT	1
I. INTRODUCTION AND SUMMARY	2
A. Fundamental Concepts	2
B. Practical Gasification Processes	5
1. Counter-current Methods	6
2. Co-current Methods	9
C. Pulverized Coal Gasification: Criteria and Objectives	11
D. Pulverized Coal Gasifiers: Preliminary Discussion	13
1. The Confined Jet Gasifier	13
2. The Vortex Gasifier	16
E. Summary of Progress	19
II. GASIFICATION OF PULVERIZED COAL WITHIN SWIRLING FLOWS	20
A. General Concepts	20
B. Operating Variables	20
C. Gasification to a Middle BTU Gas	29
D. Gasification to a Low BTU Gas	30
E. Pressure Gasification	31
F. Slagging Operation	32
G. Conclusions and Correlations	33

Page

III. FLUID MECHANICS OF THE CONFINED SWIRLING JET GASIFIER: A PRELIMINARY STUDY 37

A. Fluid Mechanics 37
1. The Non-Swirling Jet 37
1.1 Free Jets 38
1.2 Confined Jets 40
2. Swirling Jets 42
2.1 General Aspects of Free Swirling Flows. 42
2.2 Development and Control of the Central Recirculation Zone. 46
2.3 Effect of Primary Jet 50
2.4 Rates of Spread/Entrainment and Effect of Confinement 50
3. Particle Behavior in Jets. 52

B. Heat Transfer. 54
1. Single Particle Heat Transfer. 54
2. Macroscopic Heat Transfer. 56
2.1 Radial Transfer 56
2.2 Longitudinal Transfer to Incoming Reactants . . 58
2.3 Transfer to the Reactor Walls 59

C. Design Considerations. 59
1. Swirl Generator. 59
2. Relation Between Chamber Diameter and Confinement. . 62

D. Summary. 63

IV. FLUID MECHANICS OF CYCLONE AND VORTEX FLOWS. 65

A. Flow Modeling. 65
1. Fundamental Concepts 65
2. Practical Vortex Reactors. 71

B. Flow Entry and Exit. 76

C. Geometric Chamber Parameters 77
1. Swirl Number, S. 77
2. Chamber Diameter, D. 80
3. Aspect Ratio, L/D. 81
4. Relative Throat Diameter, D_e/D. 81
5. Number of Tangential Nozzles, N 82
6. Relative Tangential Inlet Area, A_t/A_e. 82
7. Relative Wall Roughness, δ/D 82
8. Relative Tangential Nozzle Position, a/L 83
9. Tangential Nozzle Configuration, h/b 84

D. Combustion Effects in Cyclone Chambers 84

Page

E. Aerodynamic Resistance of a Cyclone Reaction Chamber 86
1. Resistance of the Air Distribution System 87
1.1 Secondary Air 87
1.2 Premixed Air and Fuel 88
2. Resistance of the Reaction Chamber 89

V. A PRELIMINARY REVIEW OF PULVERIZED COAL COMBUSTOR MODELS . . 92

A. Introduction 92

B. Mixing Theories 92
1. The Perfectly Stirred Reactor (PSR) 92
2. The Plug Flow Reactor (PFR) 93
3. Mechanistic Mixing Models 94

C. Kinetic Modeling of Pulverized Coal Combustion 96

D. Overall Models for Pulverized Coal Combustors 99

E. Equilibrium Gasification Model 100

F. Conclusions 112

VI. GASIFICATION FACILITY DESIGN 113

A. Test Cell 113
1. Flow System 113
2. Electrical System 129
2.1 The 240 VAC System 129
2.2 Safety Interlock and Control System 132

B. Coal Handling Facility 134

C. Cyclone Gasifier Design 137
1. Objectives 137
2. Reactor Sizing 137
3. Heat Transfer 139
4. The Reactor Assembly 141

D. Gas Sampling System 145
1. Mass Spectrometer 145
2. Calibration and Data Reduction 146
3. Sample Inlet System 146
4. Probes 148

VII. FUTURE EFFORTS 149

LIST OF REFERENCES 150

LIST OF TABLES

Table		Page
I	Products of Coal Gasification	3
II	Reactor Types for Coal Gasification	7
III	Power Gas Production via Two-Stage Coal Gasification Processes	7
IV	Single-Stage Coal Gasification Processes	8
V	Characteristics of Major Pulverized Coal Gasification Studies	21
VI	Definitions of Dependent Variables	24
VII	Typical Values for Independent Process Variables	25
VIII	Typical Values for Dependent Process Variables	26
IX	Make Gas Composition for Various Gasifiers	27
X	Pulverized Coal Gasification: Dependent Variable Behavior	28
XI	Typical Values of Geometric Chamber Parameters	78
XII	Mathmatical Models for Pulverized Coal Combustion	98
XIII	Assumed Dry Coal Analysis	101
XIV	Equilibrium Gasification Model: Input Conditions	101
XV	Equipment Status List	114
XVI	Mechanical, Electrical and Logic Symbols	126
XVII	Design Flow Rates for Test Cell	129
XVIII	Geometric Design Parameters for Cyclone Gasifier	139
XIX	Heat Loss Estimates for Cyclone Gasifier	142
XX	Temperature Estimates for Cyclone Gasifier Assembly	142

LIST OF FIGURES

Figure		Page
1	Concentric Jet Gasifier Schematic	14
2	Vortex Gasifier Schematic	17
3	Correlation Between Dependent and Independent Process Variables in Suspension Gasification	35
4	Regions of a Jet	39
5	General Impression of Streamlines in a Confined Jet	41
6	Diagram of PVC Geometry	44
7	General Impression of Streamlines in a Swirling Jet (S = 2.2)	47
8	General Impression of Streamlines in a Swirling Jet with Central Fuel Pipe (S = 1.57)	48
9	Comparison of Size and Shape of Reverse Flow Zones	49
10	Typical Flame Shapes	51
11	Swirl Generator	60
12	Correlation Between Swirl Coefficient σ and Swirl Block Position γ/γ_m	61
13	Generalized Cyclone Flow Chamber	66
14	Particle Movement in Rotary Flow	68
15	Cyclone Chamber Types	72
16	Aerodynamics of Cyclone Chamber: Type A	73
17	Aerodynamics of Cyclone Chamber: Type B	74
18	Velocity and Temperature Profiles in a Cyclone Chamber	79
19	Chamber Dimensions for Geometric Parameters	85
20	Dependence of Relative Drag of Cyclone Combustion Chambers (without air distribution losses) on D_e/D	91
21	Extended One-Dimensional Plug-Flow Model	95

Figure		Page
22	Equilibrium Predictions for Adiabatic Gasification at One Atmosphere	
	(a) H_2 and CO Concentrations	103
	(b) Gas Exit Temperature	104
23	Dependent Process Variables for Adiabatic Gasification at One Atmosphere	
	(a) Producer Gas Yield	105
	(b) Make Gas Heating Value	106
	(c) Cold Gas Efficiency	107
	(d) Hot Gas Efficiency	108
24a	Effect of Elevated Pressure on Adiabatic CH_4 Concentration	110
24b	Effect of Heat Loss on H_2 and CO Concentrations	111
25	Flow System Schematic	125
26	Test Cell Floor Plan	130
27	Three Phase Power Distribution System	131
28	Interlock Logic Diagram	133
29	Central Control Panel	135
30	Coal Handling Facility: Floor Plan	136
31	Coal Throughput Per Atmosphere Pressure for Various Size Reactors	138
32	Heat Release Rates for Various Size Reactors	140
33	Cyclone Reactor Assembly	143
34	Gas Sampling System Schematic	147

LIST OF SYMBOLS

A	particle surface area, cm^2
A_e	cross-sectional area of throat
A_t	total cross-sectional area of tangential inlets
a	distance from tangential nozzle to chamber endwall
B	particle burning rate, g/cm^2 sec
Bi	Biot number
b	width of tangential nozzle
C	point where entrainment stops
C_i	constants
c	constant
c_i	constants
D	diameter of chamber
D_e	throat diameter
d_p	particle diameter, cm
$\bar{d}_p$	characteristic particle diameter, cm
d_o	burner exit diameter
d'_o	equivalent burner exit diameter
$d_{primary}$	primary jet diameter
$d_{secondary}$	secondary (annular) jet diameter
E	activation energy, cal/mole
F	axial width of swirl generator flow channels
G_j	axial momentum flux of central jet

G_s	axial momentum flux of surrounding jet
G_x	flux of axial momentum
G_ϕ	flux of angular momentum
H_c	enthalpy of combustion for coal, BTU/lbm
H_p	enthalpy of combustion of products, BTU/lbm
ΔH_{pr}	difference in sensible enthalpy between products and reactants, BTU/lbm
H_2O/C	steam/coal ratio, lbm/lbm
h	height of tangential nozzle
I	beam intensity
I_o	initial beam intensity
K	acceleration coefficient
K_C	chemical reaction rate at the particle surface, g/cm^2 sec atm
K_D	oxygen diffusion rate to the particle surface, g/cm^2 sec atm
K_λ	absorption coefficient
k_D	oxygen diffusion coefficient, cm^2/sec
L	length of chamber
L_{div}	length of divergent quarl
ℓ	length
m	exponent
m_p	particle mass
$\dot{m}$	total mass flow
$\dot{m}_c$	coal throughput, lbm coal/hr ft^3
$\dot{m}_e$	entrained mass flow
$\dot{m}_j$	mass flow in central jet
$\dot{m}_o$	nozzle mass flow

$\dot{m}_r$	recirculated mass flow
$\dot{m}_s$	mass flow in surrounding jet
$\dot{m}_{primary}$	mass flow of primary jet
$\dot{m}_{secondary}$	mass flow of secondary jet
N	number of tangential inlets
Nu	Nusselt number
n	Rosin-Rammler distribution constant
OX/C	oxidizer/coal ratio, lbm/lbm
P	pre-exponential factor, g/cm^2 sec atm
P_x	point where jet strikes wall
PFR	plug flow reactor
PSR	perfectly stirred reactor
PVC	precessing vortex core
p	static pressure
P_{ox}	oxygen partial pressure, atm
Δp_a	pressure drop across air distribution system of cyclone, kgf/m^2
Δp_c	total pressure drop across cyclone, kgf/m^2
Δp_{cc}	pressure drop across cyclone chamber proper, kgf/m^2
Q	make gas heating value, BTU/SCF
q_{axial}	heat transfer rate in axial direction, BTU/hr
q_{radial}	heat transfer rate in radial direction, BTU/hr
q_{total}	total heat transfer rate, BTU/hr
R	radius of burner nozzle
R_c	radius of cyclone chamber
R_h	burner hub radius

R_u	universal gas constant atm cm^3/mole ^oK
Re	Reynolds number
Re_c	axial flow Reynolds number in vortex core
Re_{ex}	Reynolds number at exit cross-section of cyclone
Re_v	tangential flow Reynolds number
RR	weight percent of particle of diameter greater than d_p
RTD	residence time distribution
r	radial distance
r_i	radial distance in cyclone assembly
$r_{0.5}$	radius where velocity equals 1/2 of maximum velocity for that section
S	swirl number
$S_{isothermal}$	swirl number under isothermal conditions
T	temperature, ^oK
T_A	adiabatic flame temperature, ^oK
T_D	average cyclone exit design temperature
T_{in}	injection temperature of reactants, ^oK
T_{inlet}	temperature of entering flow
T_m	mean temperature in the particle boundary layer, ^oK
T_{outlet}	temperature of exiting flow
T_s	particle surface temperature, ^oK
T_{wall}	wall temperature, ^oF
Tr_i	radial temperatures in cyclone assembly, ^oF
Tx_i	axial temperatures in cyclone assembly, ^oF
t	time, sec
U	axial velocity
U_o	initial particle axial velocity

U_{out}	average axial velocity of reaction products at cyclone exit
V	reaction volume, m^3
$\dot{V}$	volume flowrate of reactants, m^3/sec
W	tangential velocity
W_{fuel}	velocity of tangentially injected fuel at the inlet cross-section, m/sec
W_{in}	velocity of tangential air at the inlet cross-section, m/sec
W_r	tangential velocity as a function of radius
x	axial distance from nozzle
x_o	axial distance to point theoretical entrainment begins
x_1	axial distance to point C
x_i	axial distance in cyclone assembly
Y_p	producer gas yield, SCF/lbm coal
z	number of movable or stationary blocks
α	mechanism factor
α_λ	monochromatic directional absorptivity
β	swirl block angle
Γ	dimensionless parameter relating to swirling jet confinement
γ	block position, degrees
γ_m	maximum block movement, degrees
Δ	particle range
δ	cyclone wall roughness
ζ	resistance coefficient
ζ_a	resistance coefficient of air distribution system
ζ_{ad}	resistance coefficient of air distribution system for dust-laden flow

ζ_c	overall resistance coefficient of cyclone
ζ_{cc}	resistance coefficient of cyclone chamber proper
η_c	percent coal (carbon) gasified
η_{cg}	cold gas efficiency
η_{hg}	hot gas efficiency
$\bar{\theta}$	Thring-Newby parameter
λ	wavelength
μ	dynamic viscosity
ρ	density
ρ_a	ambient density
ρ_{in}	density of air (or air-dust mixture) at the inlet cross-section, kg/m^3
ρ_{out}	density of cyclone reaction products at T_D, kg/m^3
ρ_o	nozzle exit density
σ	swirl coefficient
$\bar{\tau}$	mean residence time, sec^{-1}
τ_r	relaxation time
ϕ	velocity half-angle
ϕ_o	velocity half-angle with no swirl
$\psi(t)$	residence time distribution function, sec

ABSTRACT

This project concerns the production of power and synthesis gases from pulverized coal via suspension gasification. Swirling flow in both concentric jet and cyclone gasifiers will separate oxidation and reduction zones. Gasifier performance will be correlated with internally measured temperature and concentration profiles.

A literature review of vortex and cyclone reactors is complete. Preliminary reviews of confined jet reactors and pulverized coal reaction models have also been completed. A simple equilibrium model for power gas production is in agreement with literature correlations; cold gas efficiency is not a suitable performance parameter for combined cycle operation.

The coal handling facility, equipped with crusher, pulverizer and sieve shaker, is in working order. Test cell flow and electrical systems have been designed, and most of the equipment has been received. Construction of the cyclone gasifier has begun. A preliminary design for the gas sampling system, which will utilize a UTI Q-30C mass spectrometer, has been developed.

I. INTRODUCTION AND SUMMARY

The energy crisis demands greater use of our vast coal resources (Hottel and Howard, 1971). An environmentally acceptable method is coal gasification; in particular, gasification to synthesis and power gases (Squires, 1974; Osborn, 1974). Synthesis gas is a major feedstock for the production of methane, methanol, hydrogen, ammonia and liquid hydrocarbons. Clean power gas may be used as an industrial fuel, or more importantly, in combined cycles, boilers and MHD devices to generate electricity.

In general, coal consumption is hampered by four major problems: (1) mine safety, (2) transportation costs, (3) water requirements and (4) sulfur/nitrogen removal. Fortunately, the last three drawbacks can be largely eliminated by gasification-slurry pipeline systems (Laurendeau, 1975a). Conversion of coal to power gas will minimize SO_x and NO_x, since H_2S and NH_3 are favored under gasification conditions. Stack gas cleanup will remove the latter compounds; ammonia can be sold to the fertilizer industry.

A. Fundamental Concepts

This investigation is primarily concerned with the formation of a clean power or synthesis gas from coal. As indicated in Table I, synthesis gas is predominantly composed of carbon monoxide and hydrogen. Power gas is essentially a synthesis gas diluted with nitrogen. Its heating value is about one-half that of synthesis gas and one-sixth that of natural gas. Mixtures such as synthesis gas or power gas are sometimes called producer gas.

Producer gases are primarily generated by the endothermic steam-carbon reaction,

TABLE I

PRODUCTS OF COAL GASIFICATION

Product	Major Components	HHV(BTU/SCF)[a]
SNG	CH_4	900-1050
Synthesis gas	CO, H_2	250-400
Power gas	CO, H_2, N_2	100-250

[a]Higher heating value of the clean, dry product.

$$C(s) + H_2O\ (v) \rightarrow CO + H_2 \qquad \Delta H^o_{298} = 31.38 \text{ kcal/gmole},$$

which is favored at high temperatures ($T > 1200^oK$) and moderate pressures ($P < 20$ atm). Further gasification occurs via

$$C + CO_2 \rightarrow 2CO \qquad \Delta H^o_{298} = 41.21 \text{ kcal/gmole}.$$

Initial producer gas formation is, of course, a result of rapid coal pyrolysis. Final product composition is often determined by water-gas equilibrium:

$$CO + H_2O \rightleftarrows CO_2 + H_2 \qquad \Delta H^o_{298} = 9.83 \text{ kcal/gmole}.$$

As suggested by Table I, significant increases in heating value result if even small levels of methane are produced. Most CH_4 formation occurs via devolatilization; high pressure char hydrogasification ($C + 2H_2 \rightarrow CH_4$) can also contribute.

The necessary gasification temperatures are usually obtained by burning a portion of the coal with air or oxygen:

$$C + 1/2\ O_2 \rightarrow CO \qquad \Delta H^o_{298} = -26.42 \text{ kcal/gmole}$$

$$C + O_2 \rightarrow CO_2 \qquad \Delta H^o_{298} = -94.04 \text{ kcal/gmole}.$$

The use of oxygen results in synthesis gas; the use of air results in a low BTU power gas, due to the large quantity of nitrogen in the final mixture. In either case, maximization of the $CO/H_2/CH_4$ content and minimization of the CO_2/H_2O content of the product will clearly optimize its energy value (Laurendeau, 1975a). For power gases, high CO/H_2 ratios are favored since most combustion processes do not allow water condensation (Squires, 1974).

For chemical equilibrium at 1500°K, the gasification process may be represented by (Laurendeau, 1975a)

$$2C + H_2O + O_2 + 4N_2 \rightarrow 0.53\ CO_2 + 0.53\ H_2 + 1.47\ CO + 0.47\ H_2O + 4N_2.$$

Air and steam must be preheated to about 550°K to maintain adiabatic conditions. Note that water-gas equilibrium clearly predicts the impossibility of simultaneously reducing the H_2/CO ratio, CO_2 and H_2O. Thus, practical single stage processes should operate at residence times controlled by chemical kinetics and/or turbulent mixing.

Realistic two-phase gasification models, incorporating both fluid mechanics and chemical kinetics are not available (Laurendeau, 1975a). Knowledge of even homogeneous turbulent reactions is minimal; furthermore, simple overall rate data governing the reactions between pulverized char and O_2, H_2O, CO_2 or H_2 are not reliable (Mulcahy and Smith, 1969; von Fredersdorff and Elliott, 1963). Moreover, such data are only applicable over limited ranges of temperature, pressure, stoichiometry and coal type.

Coal generally reacts in two somewhat separable stages (Howard and Essenhigh, 1967). Initially, heat transfer to fresh coal particles causes pyrolysis and devolatilization; residual chars subsequently undergo heterogeneous combustion or gasification. Gasification is slow compared to combustion and pyrolysis; hence gasification kinetics will control residence time requirements.

The type and rate of volatile evolution depends mostly on local temperature history (Howard and Essenhigh, 1967). Pulverized coal combustion however depends on both particle size and temperature, since these parameters control the relative effects of mass diffusion and

chemical kinetics (Mulcahy and Smith, 1969). The slow gasification reactions are often controlled solely by chemical kinetics. In most cases, however, diffusive effects persist since most chars react both externally and internally, due to the existence of an extensive pore structure. Moreover, the pore structure itself changes dramatically during reaction (Walker et al., 1959).

Coal gasification favors formation of H_2S and NH_3, compared to SO_x and NO_x, due to the availability of molecular hydrogen. Commercial absorption methods remove both H_2S and NH_3 via liquid scrubbing near 400^oK. High temperature H_2S cleanup ($T > 1200^oK$) via in situ or exhaust scrubber systems will improve gasifier thermal efficiency, but leaves ammonia in the producer gas. Combustion will probably convert over half of the NH_3 to NO. As a result, NO_x emissions approach the 2 $lb/10^6$ BTU of coal level, an unacceptable value (Laurendeau, 1975a).

Of the three gasification products (Table I), power gas is the least expensive and makes the best use of our coal resources. Production of synthesis gas requires an oxygen separation plant, which represents a 40% increase in capital cost, plus a 10% increase in energy input (Farnsworth et al.,1973). Conversion of synthesis gas to SNG entails a 20% energy loss, plus expensive hardware (Squires, 1974). Moreover, for many purposes, we are really interested in the heating value per volume of product, not per volume of fuel. On this basis, power gas has a heating value only 15% less than that of natural gas (Squires, 1974).

Since synthesis gas is a chemical feedstock, maximization of $CO + H_2$ content, or chemical enthalpy, is important. However, low BTU fuels for combined cycles must be available at high temperatures (1300-1700^oK) and pressures (15-30 atm) to optimize overall thermal efficiency. Hence, for power gas, we must maximize chemical plus sensible enthalpy, yet minimize exhaust levels of ammonia and carbon.

B. Practical Gasification Processes

Three methods are available for the commercial production of a producer gas from coal: (1) stationary fuel beds, (2) fluidized beds, and (3) suspension beds. In general, fixed beds employ lump coal (1-10 cm),

fluidized beds crushed coal (10^{-2} - 1 cm) and suspension beds pulverized coal (10^{-4} - 10^{-2} cm). At present, the Lurgi process (a high pressure stationary bed technique) is the principle industrial method for the manufacture of producer gas, and the only method compatible with combined cycle operation. Fluidized bed and entrained flow processes are inherently superior, and are only now receiving warranted attention. The advantages and disadvantages of each method are listed in Table II (Laurendeau, 1975; Lenzer and Laurendeau, 1976).

The production of power or synthesis gas may be accomplished by either a two-stage (Table III) or single-stage (Table IV) process (Laurendeau, 1975a). Single-stage gasification processes are characterized by (1) simplicity of design, (2) high product temperature and (3) low methane content. Two-stage methods promote methane enrichment by separating gasification and pyrolysis steps. As a result, the final product possesses a higher chemical heating value, but its temperature is limited to 1000°K (Laurendeau, 1975a).

1. Counter-current Methods

Standard stationary and fluidized methods operate via an upward flow of air and steam through a coal bed. In both cases, the resulting gas composition is largely determined by the bed depth and the flow velocity. In a stationary bed, large coal chunks rest on a fixed or moving grate, while in a fluidized bed, small pieces of coal are held in turbulent suspension by the rapidly moving flow.

In a fixed bed gasifier, optimization of energy content is promoted by a natural separation of the oxidizing and reducing zones (Laurendeau, 1975a). The exothermic carbon-oxygen reaction dominates in the lower portion of the bed, thus supplying heat for the endothermic carbon-steam and carbon-carbon dioxide reactions in the upper portion. Pulverized coal gasifiers should make use of this principle, as gasification efficiency will increase substantially.

Renewed interest in fluidized bed methods has been spurred by recent increases in operational temperatures. Early processes were limited to temperatures (1200-1300°K) somewhat lower than the ash fusion

TABLE II

REACTOR TYPES FOR COAL GASIFICATION

Type	Advantages	Disadvantages
Fixed	Developed technology, countercurrent flow, high pressure operation	Non-uniform flow, clinker formation, temperature control, ash removal, tar formation, low capacity, coal fines unacceptable, high H_2O levels
Fluidized	Solids handling, uniform temperature, gas solid contact, countercurrent flow, *in situ* sulfur removal, high gasification rate	Pretreatment of caking coals, multistaged beds, carbon efficiency, ash disposal
Entrained	Highest volumetric reaction rate, slagging conditions, gas-solid contact, coal type irrelevant, high product temperature, compatible with coal slurries and froth flotation	Ash separation, temperature control, co-current flow, coal pulverization

TABLE III

POWER GAS PRODUCTION VIA TWO-STAGE COAL GASIFICATION PROCESSES

Process	Type	P(atm)	HHV(BTU/SCF)[a]
BI-GAS	entrained	70-100	175
SYNTHANE	fluidized	30-70	200
HYGAS	fluidized	70	235
Westinghouse	fluidized	10-20	140
BCR Multibed	fluidized	16	150

[a]Higher heating value of the raw gas on a dry basis

TABLE IV

SINGLE-STAGE COAL GASIFICATION PROCESSES

Process[a]	Type	Ash Removal	Product[b]	P(atm)	T(^{o}K)	HHV(BTU/SCF)[c]
Gas Producer (C)	fixed	agglomerates	PG,SG	1	∿1000	140-280
Stirred Producer	fixed	agglomerates	PG	7	∿900	150
Lurgi (C)	fixed	agglomerates	PG	2-30	850	165
			SG	2-40	900-1100	300
Winkler (C)	fluidized	powder	PG	1	1250	120
			SG	1	1100-1400	275
U-GAS	fluidized	agglomerates	PG	24	1300	150
Ignifluid (C)	fluidized	agglomerates	PG	1	1450-1550	140
Koppers-Totzek (C)	entrained	slag	SG	1	2200	300
Combustion Engineering	entrained	slag	PG,SG	1	1400-2000	125-285
Texaco Partial Oxidation	entrained	slag	PG	15	1500-1800	140

[a](C) denotes a commercial process

[b]PG - power gas; SG - synthesis gas

[c]Higher heating value of the raw gas on a dry basis

temperature ($\sim 1500^{o}K$) to avoid clinker formation. However, the development of Godel's ash-agglomerating fluidized bed (Ignifluid) allows temperatures of $1450-1550^{o}K$. Here, high fluidization velocities apparently limit clinker size; carbon losses are minimized by recycling coal fines (Squires, 1974). The ash-agglomerating fast-fluidized bed (Squires, 1974) suggests even higher fluidization velocities. The U-GAS and Westinghouse processes are being developed along these lines (Tables III-IV).

Both two-stage and single-stage counter-current methods have been reviewed by Laurendeau (1975a) and Bodle and Vyas (1973). Two-stage producers are usually overdesigned, since they were originally intended for SNG production. Exceptions are the Westinghouse and BCR methods (Table III). Single-stage methods, on the other hand, have been explicitly designed for manufacturing producer gas. Unfortunately, counter-current methods still suffer due to (1) low temperatures, (2) pretreatment/caking coal problems, (3) high H_2O and H_2/CO levels and (4) carbon efficiency problems.

2. Co-current Methods

Entrained flow methods appear to offer the most viable means of using U. S. bituminous coals (Table II). Experience with pulverized coal burners indicates that either caking or non-caking coals are acceptable. In addition, entrained techniques generate high temperatures, a condition required for optimization of thermal efficiency in combined cycles. High temperatures are, of course, a result of the large surface area, and hence high heat release rate per unit volume, generated by small particles, particularly at high pressures and large relative gas-particle velocities. High temperatures also suppress both clinker and tar formation, and allow ash removal under slagging (liquid) conditions (Hottel and Howard, 1971).

Compatibility with caking coals, combined cycles, and coal slurries are significant advantages; however, the entrained gasifier's lack of counter-current flow cannot be dismissed. Co-current flow reduces coal inventory; establishment of endothermic regions becomes

difficult, and thus product heating value decreases. Therefore, entrained gasifiers must generate artifical recirculation zones characterized by large residence times and reducing conditions; swirl or vortex designs are necessary.

The benefits of entrained flow have prompted the development of the so-called fast fluidized bed, a fluidized bed using pulverized coal, and hence strongly approaching co-current conditions. The ash-agglomerating fast fluidized bed combines ash agglomeration and fast fluidization, thus allowing reaction with both crushed and pulverized coal (Squires, 1974).

Hottel and Howard (1971) assert that the most desirable future gasifier will use direct gasification of pulverized raw coal with steam and air at elevated pressure under slagging conditions. In the present investigation, we are primarily concerned with this type of gasifier. Unfortunately, industrial entrained flow devices do not allow for efficient separation of oxidizing and reducing regions (as suggested by early gas producers). The significant advantages of pulverized coal systems must be realized; however, new gasifier designs are necessary, particularly for high pressure operation. At present, the Koppers-Totzek, Combustion Engineering, and Texaco Partial Oxidation processes represent single-stage methods (Table III); BI-GAS is the only two-stage method (Table IV). These processes have been reviewed by Laurendeau (1975a) and Bodle and Vyas (1973).

In the Koppers-Totzek system (Farnsworth et al., 1973) pulverized coal/oxygen/steam mixtures are delivered through water-cooled burners at high speeds to prevent flashback. Slag is collected in a water-quench tank at the bottom section of the gasifier. Synthesis gas leaves the upper portion at around 1450°K. Steam is generated along the reactor walls. In most cases, water must be sprayed into the gas to lower its temperature so that ash matter will not stick to downstream tubes. Less than 0.1% CH_4 and 20% CO_2 + H_2O are present in the final product (Bodle and Vyas, 1973). The excess temperatures created by this method suggest that oxygen might be replaced by air or an air/O_2 mixture, thus forming power gas. Apparently, this relatively simple procedure has never been attempted (Squires, 1974).

In the Combustion Engineering process (Patterson, 1976), the principles of Koppers-Totzek gasification have been used to produce power gas rather than synthesis gas. In this case, endothermic reactions are promoted by arranging burners into four vertical levels. Each level consists of eight individual tangentially-fired burners, spaced equally in a circular pattern. The two lower levels burn a coal/air mixture; the upper levels use coal/steam mixtures, thus producing a methane enriched power gas. (Note that the geometric configuration of this process separates the endothermic and exothermic zones).

The Texaco Partial Oxidation process (Hottel and Howard, 1971) is a linear flow (no swirl), atmospheric system. Fuel is fed into the gasifier via a coal-water slurry. On a weight basis, the H_2O/coal ratio is 0.75 and air/coal is 2.6. Most of the ash appears as slag. Ninty-five percent of the entering coal is gasified in about three seconds. Low BTU fuel is generated near 1500°K in water-gas equilibrium.

The BI-GAS system (Hottel and Howard, 1971) uses two stages to separate the exothermic and endothermic zones. Coal and steam are fed into the upper reactor by four nozzles; heat is supplied by the hot gases emanating from the lower reactor. Entrained char, separated from the raw gas in a cyclone, feeds the vortex flow of the gasification-combustion stage, which operates on air or air/oxygen mixtures.

C. Pulverized Coal Gasification: Criteria and Objectives

Based on the obvious advantages of pulverized coal operation (Table II), this investigation seeks to perfect entrained flow gasifiers using currently available pulverized coal burners, hence minimizing development time. We are concerned more with power gas than synthesis gas; hence air or air/oxygen mixtures will be used rather than pure oxygen. To optimize power gas production, the previous discussion suggests that we attempt to satisfy the following criteria:

(1) Slagging gasification via single stage vortex designs
(2) Compatibility with combined cycle operation, i.e., high pressures (1-20 atm) and temperatures (1400-1800°K)
(3) Separation of oxidation and reduction zones, thus

avoiding chemical equilibrium

(4) High carbon and thermal efficiency

(5) Short gasifier residence times

(6) Maximization of chemical plus sensible enthalpy

(7) Maximization of the $CO/H_2/CH_4$ content (minimize CO_2 and H_2O) and the CO/H_2 ratio

(8) Minimization of residual NH_3 and H_2S.

Two types of pulverized coal gasifiers will be considered: (1) the annular confined jet with secondary swirl and (2) the vortex tube with tangential entry. The first burner is characterized by a single axial injector of high primary velocity; secondary swirl is used to control mixing and residence times. The second burner is modeled after the cyclone combustor; long particle residence times and slagging operation should lead to high carbon efficiencies. In both cases, high temperatures generated in the combustion region will support the endothermic gasification reactions. Axially injected, preheated steam will be surrounded by swirling air, thus promoting efficient gasification. Pulverized coal is carried by primary steam in the confined jet system, and by primary air in the vortex gasifier.

Both model gasifiers will be sized to handle 5-40 lb/hr of Indiana/Illinois bituminous coal. Successful operation with bituminous coals usually indicates that lignites or subbituminous coals will work, since gasification efficiency increases as coal rank decreases (von Fredersdorff and Elliott, 1963). External heating will be used to compensate for the excessive heat losses characteristic of small scale reactors. System shakedown will proceed in the following order: (1) coal/air combustion at atmospheric conditions, (2) coal/air/oxygen/steam gasification at one atmosphere, and (3) coal/air/oxygen/steam gasification at higher pressures.

The physical and chemical mechanisms controlling gasification characteristics will be determined by measuring temperature and concentration (CO, H_2, H_2O, CO_2, CH_4, N_2) profiles (axial and radial) both within and downstream of the flame region. Pollutants (NO_x, NH_3, SO_x, H_2S) will also be considered, especially NH_3 and H_2S. System

optimization will be obtained by correlation of these measurements with fundamental burner parameters such as pressure, solid/gas feed rates, swirl intensity, inlet temperature, and burner configuration. Our main purpose is to determine the feasibility of using available pulverized coal burners to produce power or synthesis gas from coal. It this phase is successful, simple models governing entrained flow systems will be developed to further interpret the experimental data.

D. Pulverized Coal Gasifiers: Preliminary Discussion

1. The Confined Jet Gasifier

The concentric confined jet gasifier is patterned after the traditional pulverized coal burner (Fig. 1). Separation of oxidation and reduction zones is attained by using coal/steam mixtures in the primary flow and swirling air in the secondary flow. Fundamental experimental data applicable to confined and free jets have been obtained for cold flow (Beer and Chigier, 1972), homogeneous combustion (Beer and Chigier, 1972; Heap et al., 1973) and pulverized coal combustion (Beer and Chigier, 1969; Heap et al., 1973). These results allow preliminary design of our confined jet gasification system (Chapter III).

The combustion process in a pulverized coal burner is dominated by the highly turbulent flow field produced by secondary swirl. At high swirl intensities ($S > 0.6$), an adverse pressure gradient exists along the axis, and thus a torroidal vortex type of recirculation zone becomes stabilized in the flow, hence promoting air/coal entrainment and high carbon efficiency. (The dimensionless swirl number S, where $S = G_\phi/G_x R$, characterizes swirling flows. Here G_ϕ and G_x are the fluxes of angular and axial momentum, and R is the burner radius.) The size of the recirculation zone depends primarily on the swirl number and the shape of the divergent quarl at the burner exit. Increasing swirl generally lengthens the recirculation zone while divergence broadens the zone (Beer and Chigier, 1972).

Gasifier performance will depend quite strongly on the extent of turbulent mixing between the fuel rich recirculation zone and the outer air flow. Entrainment must be sufficient to promote combustion,

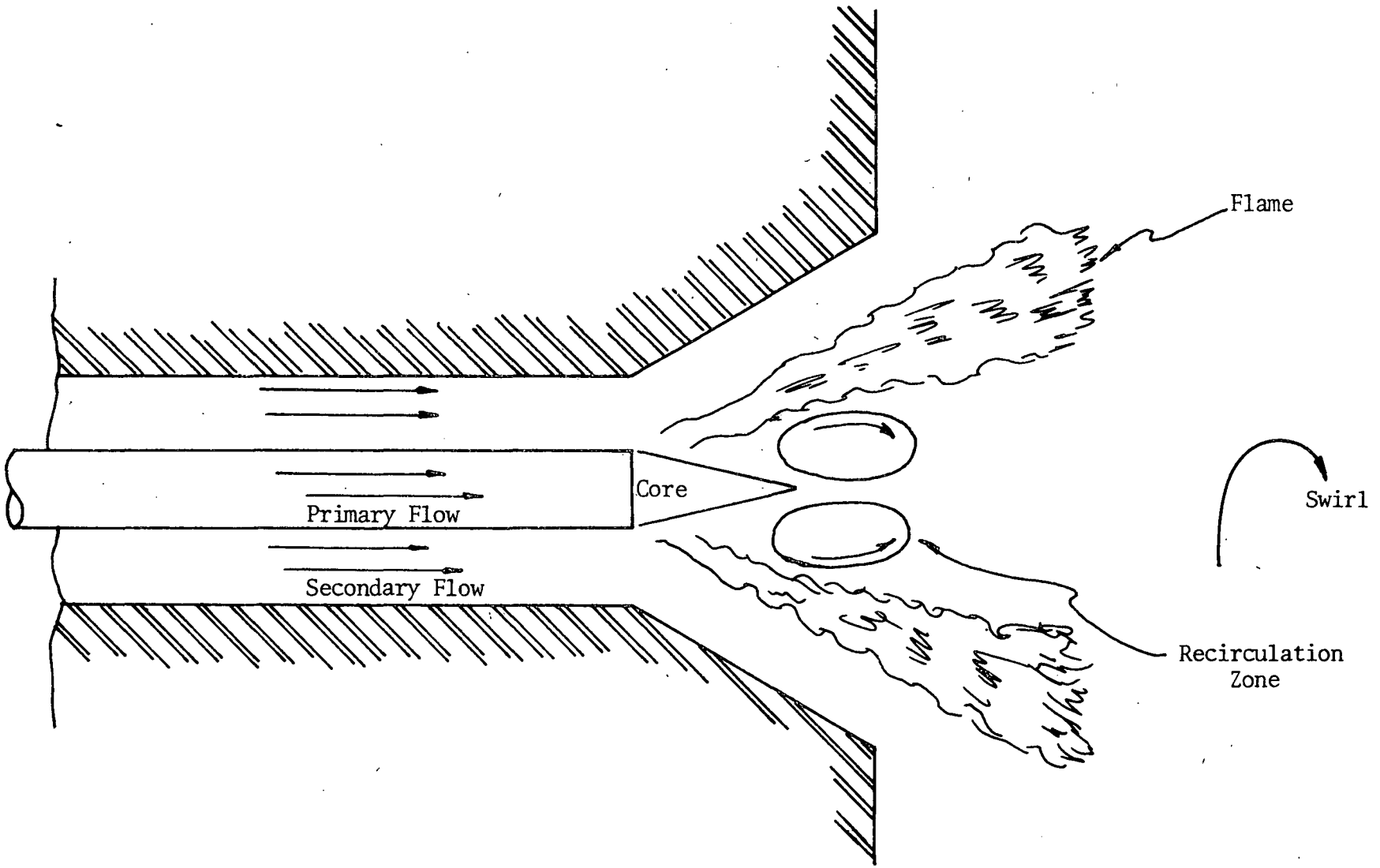

Figure 1. Concentric Jet Gasifier Schematic

but not enough to destroy the identity of the reduction zone. Previous work suggests that entrainment is largely controlled by the following burner parameters (Heap et al., 1973):

(1) secondary swirl
(2) primary/secondary composition ratios
(3) design and position of fuel injector
(4) primary velocity
(5) exit quarl divergence.

The first three parameters have the strongest effect, as they control flame shape during pulverized coal combustion. Our model concentric gasifier will be designed such that all parameters can be easily varied over reasonable ranges. To reduce entrainment and thus preserve the reduction zone, Heap et al. (1973) recommended a single hole, high velocity injector, with enough swirl to stabilize the reaction zone at the injector face. However, in view of carbon efficiency requirements, the appropriate choice of burner parameters is not at all obvious.

The half-angle of the water-cooled exit quarl will be initially designed for maximum performance ($\sim 35^{o}$), as suggested by Beer and Chigier (1972). Primary velocity and secondary swirl will be chosen to achieve both penetration (high primary velocity) and divergent (high swirl) flames. All fuel will be fed via the non-swirling primary jet. Secondary swirl will be controlled by a calibrated tangential entry or movable block swirl generator (Beer and Chigier, 1972).

If our confined turbulent flame is to model the free jet flame characteristic of large-scale industrial equipment, we must avoid excessive wall recirculation, caused by limitations in entrainment volume. (Wall recirculation may, however, be an alternative method of maintaining stability during gasification.) Confined jet analysis indicates that free jet conditions will be approached for Thring-Newby parameters $\theta < 0.1$, or $d_o/D < 0.05\text{-}0.10$, where d_o is the burner diameter and D the chamber diameter. Chamber length L should be somewhat greater than 3D, the distance required for flame-wall impingement (Beer and Chigier, 1972).

Although $\theta < 0.1$ allows free jet conditions, the entrained gas will probably be deficient in oxygen due to the presence of combustion products. Consequently, reaction length will increase compared to a

free turbulent system. However, our confined jet environment is not unrealistic, since multiple burner operation produces similar conditions.

For turbulent jets, comparison between model and prototype is aided by the unique profiles characteristic of all turbulent jets. More generally, however, partial modeling techniques have led to the development of rather simple similarity rules. If the following parameters are maintained equal in model and prototype, reliable extrapolation is assured (Beer and Chigier, 1972):

(1) stoichiometry and initial density
(2) residence time
(3) swirl number
(4) d_o/D and L/D
(5) $\dot{m}_{primary}/\dot{m}_{secondary}$
(6) $d_{primary}/d_{secondary}$.

2. The Vortex Gasifier

The tangential entry vortex tube gasifier is patterned after the cyclone burner (Fig. 2). Separation of oxidation and reduction zones is attained by tangential flow of coal/air mixtures coupled with axial steam injection. Fundamental experimental data for both homogeneous and heterogeneous (two-phase) cyclone chambers have been obtained for cold flow (Strickland, 1973), homogeneous combustion (Schmidt, 1970; Syred and Beer, 1974) and pulverized coal combustion (Syred and Beer, 1974). These results allow preliminary design of our vortex gasification system (Chapter IV).

The vortex gasifier possesses several advantages compared to the concentric jet system (Syred and Beer, 1974): (1) greater turbulent mixing levels, (2) ease of operation at high pressures and (3) larger particle residence times. These three factors promote high temperatures and slagging conditions, and hence good carbon and gasification efficiencies. There are disadvantages, however: (1) chamber wall temperatures are much higher, causing material and heat transfer problems; (2) slagging operation presents difficulties due to heat losses and residue disposal; (3) injection of coal/air vs coal/steam mixtures

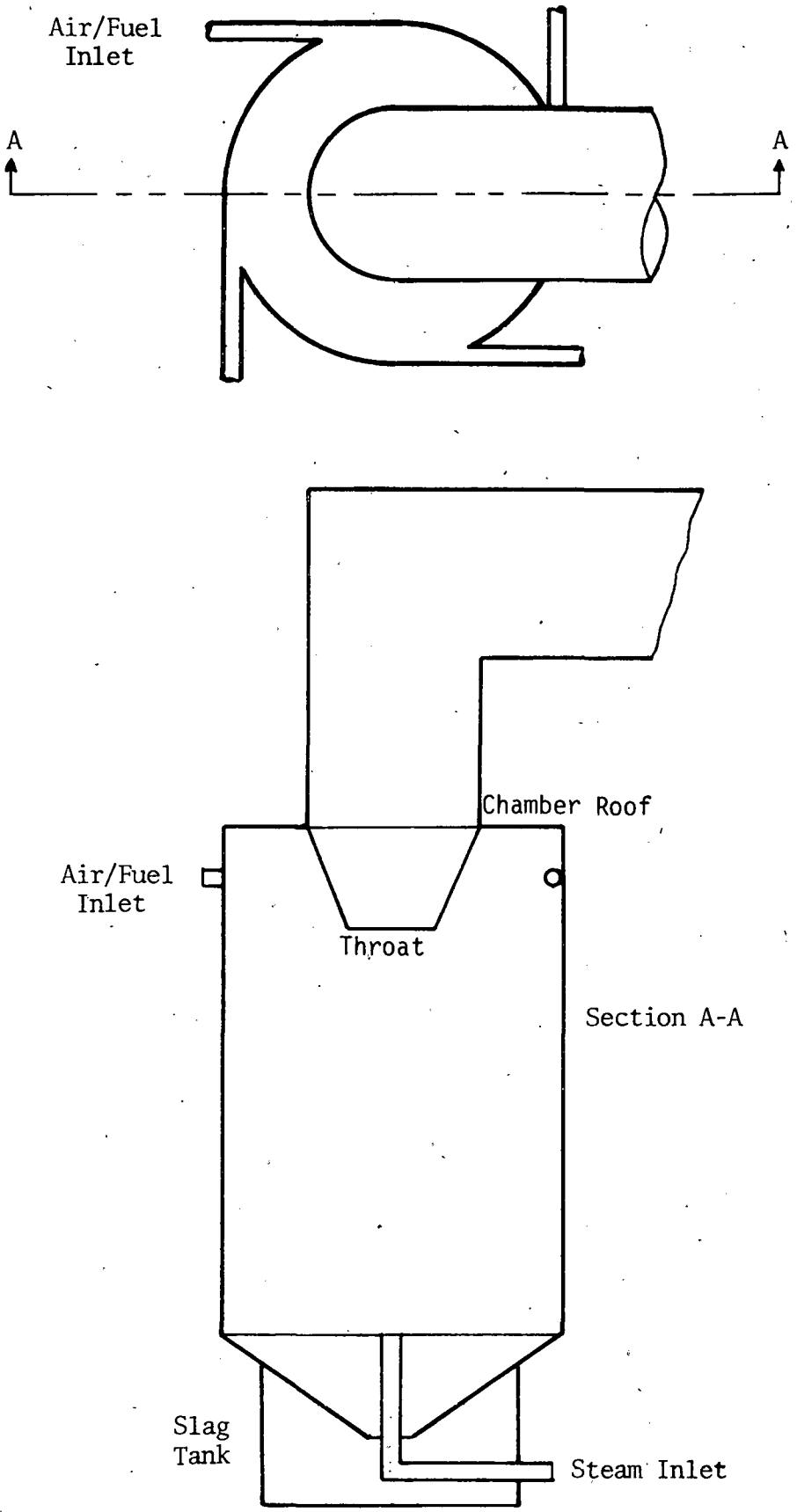

Figure 2. Vortex Gasifier Schematic

increases the opportunity for spontaneous combustion at high pressures.

Turbulent mixing and particle residence times in vortex tube systems are primarily determined by the tangential swirl velocity (Strickland, 1973). This dominant velocity profile is satisfactorily described by the Rankine model, i.e., potential or free vortex flow ($W_r \alpha r^{-1}$) near the wall, and rotational or forced vortex flow ($W_r \alpha r$) at the chamber core. In idealized rotary motion (Schmidt, 1970), the free vortex zone is characterized by downward axial flow, while the rotational zone is characterized by upward flow. Thus coal particles move downward via a helical path, followed by upward movement along a helical path of smaller radius. Lighter particles will of course undergo more rapid migration to the center of the chamber.

In Fig. 2, tangential air/coal injection occurs at the top of the cyclone to avoid slag buildup around the injection ports. If higher particle residence times are required, air/coal entry may be attempted at the bottom. In this case, two flow reversals occur; one at the throat annulus and another at the slag port (Schmidt, 1970). The half-angle of the throat quarl will probably determine much of the flow structure, regardless of bottom or top injection. Flow structure is also affected by the chamber endwall boundary layer (Schmidt, 1970); for example, average particle residence times are apparently increased by attaching rectangular fences radially to the closed endwall. Similarly, axial vs. radial steam injection will generate different mixing patterns, and hence affect gasification efficiency (axial injection promotes greater separation of oxidizing and reducing zones). At low steam velocities, mixing will be dominated by vortex entrainment in the core (Strickland, 1973).

Our proposed design is characterized by three important features: (1) entrained vortex flow, (2) coal/steam/air rather than coal/steam/oxygen and (3) separation of oxidation and reduction zones. The third characteristic has not been considered previously; the first two have received limited attention, most notably in the Ruhrgas process (von Fredersdorff and Elliott, 1963).

To our knowledge, the only extensive investigation of pulverized coal gasification in a <u>small-scale</u> cyclone system was conducted

by Yagi and Kunii (1957). Production of both power gas and synthesis gas was correlated with carbon efficiency, and hence reduction zone temperature (1300-1650°K). By externally heating the 20 cm diameter chamber, 70-80% of the ash appeared as slag. Their preliminary results are quite encouraging, thus providing impetus for our vortex gasifier design.

E. Summary of Progress

Much of the first contract year has been spent on an extensive review of the literature. Previous work on pulverized coal combustion and gasification is reviewed in Chapter II. The important independent and dependent variables are identified; a new method of interpreting their interrelationships is presented. Literature results suggest the importance of obtaining temperature and concentration profiles within the reactor.

The fluid mechanics of the confined jet and cyclone systems are reviewed in Chapters III and IV. The limited work on two-phase flows is also considered; design parameters are presented. Reactor models for gasification of pulverized coal are discussed in Chapter V. Turbulent, reacting, two-phase flow models are considered; a macroscopic model involving perfectly stirred and plug flow components is suggested for the present investigation. Results of an equilibrium model are presented.

Chapter VI details the experimental work accomplished thus far. The coal handling facility has been completed; design of the gasification system is essentially complete. Most components will be received by the end of the summer; construction work began in July, 1976. Initial shakedown runs are expected by October, 1976. The sampling system and cyclone gasifier will be built and tested in the next three months. Future efforts are outlined in Chapter VII.

II. GASIFICATION OF PULVERIZED COAL WITHIN SWIRLING FLOWS

A. General Concepts

Reviews of reactor types for coal gasification (von Fredersdorff and Elliott, 1963; Laurendeau, 1975a) indicate the attraction of entrainment systems (Table II). However, cocurrent flow inhibits interaction between coal inventory and fresh gasifying media. Furthermore, difficulty in establishing endothermic reaction zones results in decreased product heating value. Fortunately, these disadvantages can be circumvented by proper swirl design. Moreover, relative velocities may be induced between particles and gas thereby increasing the rate of boundary layer diffusion. Pore and boundary layer diffusion become the dominant rate controlling steps at high chamber temperatures (Elliott et al., 1952; Sebastian, 1952; Traenckner, 1953).

Heat required to support endothermic gasification reactions is provided by one (or more) of three methods: (1) by transfer through the chamber wall, (2) by generation within the process ($C + O_2 \rightarrow CO_2$), or (3) by introduction as sensible heat in the gasifying medium. Ordinarily, the gasifying medium consists of some combination of air, oxygen and steam. Oxygen is used to produce middle BTU synthesis gas; air, to produce low BTU power gas. Steam is the primary hydrogen source ($C + H_2O \rightarrow CO + H_2$). Table V summarizes the chamber flow type, method of heat supply and gasifying medium for the major pulverized coal gasification studies.

B. Operating Variables

Von Fredersdorff and Elliott (1963) have reviewed much of the previous work on fully-entrained suspension gasification. It is immediately apparent that many operating variables are involved. Most

TABLE V

CHARACTERISTICS OF MAJOR PULVERIZED COAL GASIFICATION STUDIES

Author(s)	Flow		Heat Supply			Gasifying Media					
	Plug	Swirling	External	Internal	Entering Reactants	Air	O_2	Air-O_2	Air-H_2O	O_2-H_2O	Air-O_2-H_2O
(1) von Fredersdorff (1949)		x		x	x			x			x
(2) Perry et al. (1950)		x		x	x					x	
(3) Elliott et al. (1952)		x		x	x					x	
(4) Sebastian (1952)	x			x	x		x			x	
(5) Traenckner (1953)		x		x	x	x					
(6) Nistler (1957)		x		x	x	x					
(7) Yagi and Kunii (1957)		x	x	x	x				x		x
(8) Holden et al. (1960)	x			x	x					x	
(9) Strimbeck et al. (1960)	x			x	x					x	x
(10) Coates et al. (1975)	x		x	x	x					x	x

authors classify these variables as either independent or dependent process variables.

Independent process variables are defined (Sebastian, 1952) as operating conditions independently chosen and varied at will, but maintained as constant as possible during a given run. Dependent process variables are defined as operating results obtained as functions of the chosen operating conditions. Variables related to gasifier design, fuel type, and method of reactant feed are considered independent, since they generally are held fixed. However, the case for most variables is not as clearly cut; in many instances it is purely a matter of choice.

The most common independent variables are related to reactant feed rate and temperature and to chamber temperature and pressure. More common dependent variables include some indication of process efficiency and relations determined from the make gas yield and composition. The following classification, revised from Sebastian (1952) and Coates (1975), is chosen from a practical operating standpoint:

I. Independent process variables
   1. Shape and dimensions of gasifier
   2. Method of feeding reactants
   3. Composition and physical properties of the coal
   4. Particle size
   5. Coal throughput ($\dot{m}_c$) or feed rate
   6. Injection temperature of the reactants (T_{in})
   7. Oxidizer/coal input ratio (OX/C)
   8. H_2O (steam)/coal input ratio (H_2O/C)
   9. Chamber pressure and temperature

II. Dependent process variables
   10. Percent coal (carbon) gasified (η_c)
   11. Make gas (total) as yield and producer gas yield (Y_p)
   12. Make gas composition and heating value (Q)
   13. Thermal efficiency and cold gas efficiency (η_{cg})
   14. Gas exit temperature
   15. Heat loss from gasifier
   16. Type, quantity, and size of residue.

Many frequently mentioned variables, which are not listed, can be defined in more fundamental terms. Gas residence time, for example, is related to gasifier design, coal throughput, O_2-air-H_2O/coal ratios, and chamber temperature and pressure. Similarly, the gas output rate (SCF/hr) can be found from the coal feed rate and make gas yield. Note that coal throughput (lbm/ft^{3}hr) is a more fundamental variable than coal feed rate (lbm/hr) since reactor volume is eliminated as a criterion in evaluating gasifier performance.

Definitions of the major dependent variables are listed in Table VI. The coal gasified, total yield, and make gas composition are probably the three most useful dependent variables. Make gas heating value and H_2/CO ratio can obviously be calculated from the composition. Producer gas yield and cold gas efficiency can be computed from composition and total yield. Knowledge of the gas exit temperature plus the independent variables are required to calculate the thermal efficiency, steam decomposition and heat loss. Typical values for both the independent and dependent process variables are given in Tables VII, VIII and IX.

The primary independent variables appear to be coal throughput, oxidizer/coal ratio, steam/coal ratio, reactant inlet temperature and chamber pressure. The dependent variables most indicative of gasifier performance are percent coal gasified, make gas heating value, producer gas yield, and cold gas efficiency. Table X depicts the qualitative behavior of these dependent variables as a function of primary independent variables for the major gasification studies listed in Table V. The effects of chamber pressure, omitted here, are discussed in a later section.

As expected, percent carbon gasified strongly increases with oxidizer/coal ratio (von Fredersdorff, 1949; Perry et al., 1950; Strimbeck et al., 1960). The dependence on coal throughput is not as clear: Perry reports no dependence but Sebastian (1952) reports increases at higher feed rates (due to lower heat loss). The effect of varying H_2O/coal ratio on carbon gasified seems to depend on the steam temperature; carbon efficiency increases with high temperature steam and decreases with lower temperature steam (Sebastian, 1952; Yagi and Kunii,

TABLE VI

DEFINITIONS OF DEPENDENT VARIABLES

Dependent Variable	Definition
coal (carbon) gasified (η_c)	percent of coal input converted in reactor
total yield	amount (SCF/lbm coal) of gas leaving reactor
producer gas yield (Y_p)	amount (SCF/lbm coal) of producer gas ($CO + H_2$) generated in reactor
make gas heating value (Q)	chemical heating value (BTU/SCF) of the gas produced
make gas composition	percent (by volume) of each gaseous species in reactor exhaust
H_2/CO ratio	volumetric ratio of H_2 to CO in exhaust gas
thermal efficiency	percent of total heat input (chemical and sensible) available in the raw make gas
cold gas efficiency (η_{cg})	percent of coal chemical heat input recoverable as make gas heating value
steam decomposition	percent of steam delivered to gasifier which reacts
gas exit temperature	temperature (^{o}K) of reaction products in exhaust stream
heat loss	percent of total heat in coal feed transferred through the reactor walls

TABLE VII

TYPICAL VALUES FOR INDEPENDENT PROCESS VARIABLES

	Coal Throughput ($lbm/hr\ ft^3$)	Air/Coal Ratio (lbm/lbm)	O_2/Coal Ratio (lbm/lbm)	OX/C Ratio (lbm/lbm)	H_2O/C Ratio (lbm/lbm)	Reactant Temperature (^oK)	Chamber Pressure (atm)
von Fredersdorff (1949)	20	.40	.75	.85	.5		1
Perry et al. (1950)		---	1.08	1.08	.79		1
Elliott et al. (1952)	10.6	---	.81	.81	.55	1010 (O_2,H_2O)	1
Sebastian (1952)	40.2	---	.75	.75	.15	600 (H_2O)	1
Traenckner (1953)	81.2	4.71	---	.99	---	950 (air)	1
Nistler (1957)					---	980 (air)	1
Yagi and Kunii (1957)	12.9 14.8	4.47 .90	--- 1.16	1.04 1.37	1.03 .60	430 (H_2O) 480 (H_2O)	1 1
Holden et al. (1960)	335 525		.80 .79	.80 .79	.30 .31		5 20
Strimbeck et al. (1960)	37.1 32.6	--- .68	.86 .64	.86 .80	.52 .32		1 1
Coates et al. (1975)	558	.23	.75	.80	.63	560 (O_2) 840 (H_2O)	6

TABLE VIII

TYPICAL VALUES FOR DEPENDENT PROCESS VARIABLES

	Carbon Gasified (%)	Total Yield (SCF/lbm)	Producer Gas Yield (SCF/lbm)	Make Gas Heating Value (BTU/SCF)	H_2/CO Ratio (SCF/SCF)	Cold Gas Efficiency (%)	Gas Exit Temperature (^{o}K)	Heat Loss (%)
von Fredersdorff (1949)	72			210		53		
Perry et al. (1950)	62				.78		1580	23.1
Elliott et al. (1952)	89		26.4				1510	
Sebastian (1952)	72		20.9		.68	59.1	1330	8.9
Traenckner (1953)		78.6		112	.57	63		22.5
Nistler (1957)		70.8		100	.35	61		
Yagi and Kunii (1957)	89.6 91.3		9.0 20.2		.69 .57			
Holden et al. (1960)	83.1 88.1		24.0 27.3				1900 1675	7.2 4.1
Strimbeck et al. (1960)	96.6 83.7		28.8 21.9					6.8 6.8
Coates et al. (1975)		31		260	.93	64		

TABLE IX

MAKE GAS COMPOSITION* FOR VARIOUS GASIFIERS

	CO (%)	H_2 (%)	CH_4 (%)	CO_2 (%)	N_2 (%)
Perry et al. (1950)	25	19.5		49.2	
Sebastian (1952)	48.5	33.2		13.9	
Traenckner (1953)	22.1	12.6		5.3	60.0
Nistler (1957)	22.8	8.0		5.1	64.1
Yagi and Kunii (1957)	6.5	4.5	.6	12.2	75.7
	33.0	18.8	.7	18.8	28.5
Coates et al. (1975)	41.0	38.2	.4	14.8	2.6
Koppers-Totzek (Tillman, 1976)	55.9	35.4		7.2	1.1
Lurgi (Tillman, 1976)	15	23	4	15	42
Wellman-Galusha (Tillman, 1976)	28.6	15	2.7	3.4	50.3

*Moisture-free basis

TABLE X

PULVERIZED COAL GASIFICATION:
DEPENDENT VARIABLE BEHAVIOR*

	$\dot{m}_c$ (lbm/ft^{3}hr)	OX/C Ratio (lbm/lbm)	H_2O/C Ratio (lbm/lbm)
η_c (%)	0 [2] + [4]	+ [1,2,9]	0 [7]
Q (BTU/SCF)		M [1]	-[1]
Y_p (SCF/lbm coal)	+ [2,4]	+ [3,9] M [8]	
η_{cg} (%)	+ [4]	M [1]	+ [1]

*Numbers in brackets indicate author(s) listed in Table V:

(-) dependent variable decreases with an increase in independent variable
(0) no dependence upon independent variable
(+) dependent variable increases with an increase in independent variable
(M) dependent variable reaches a maximum, then decreases with further increase in independent variable

1957; Strimbeck et al., 1960). Yagi and Kunii found that carbon efficiency increases with reduction zone temperature, which is consistent with improved performance found at higher oxidizer/coal ratios.

Von Fredersdorff (1949) reports that make gas heating value is maximized near 0.7 lbm O_2/lbm coal, but is lowered by high H_2O/coal ratios (1.0 to 1.5 lbm H_2O/lbm coal). Similarly, producer gas yield and cold gas efficiency are maximized at 0.9 lbm O_2/lbm coal (Holden, 1960; von Fredersdorff, 1949). Producer gas yield and cold gas efficiency are both improved by increasing coal throughput; cold gas efficiency also increases with the introduction of steam at low (< 0.5 lbm/lbm) steam/coal ratios when oxidizer/coal ratio is optimum (Perry et al., 1950; Sebastian, 1952; von Fredersdorff, 1949).

C. Gasification to a Middle BTU Gas

Perry et al. (1950) and Elliott et al. (1952) tested a 2 ft diameter chamber with tangential oxygen-steam entry and axial coal entry. Chamber lengths varied from 2 to 36 in. Excessive heat loss (Table VIII), favored at lower throughputs, resulted in a high CO_2 concentration in the product gas (Table IX). The low carbon efficiency (Table VIII) reported in Perry's work is due to the loss of coal fines from the reactor; improved feeding techniques resulted in the higher carbon efficiency reported by Elliott et al. These authors concluded that for a given set of feed conditions any means of increasing carbon conversion will improve gas quality. Furthermore, percent carbon gasified, producer gas quality and the throughput range are all strongly dependent on the uniformity and method of coal distribution.

Sebastian (1952) gasified coal in a 6 in diameter tube, 7 ft long, into which the reactants were axially introduced. Several runs were made using three different types of fuel: subbituminous coal, bituminous coal, and anthracite. As lower rank coals replaced higher rank coals, the quality of gas produced, the percentage of carbon gasified, and the cold gas efficiency all increased. Higher reactivity, resulting from higher oxygen and volatile matter content, partially accounts for the greater ease in gasifying lower rank coals. Gasification

of higher rank coals can be improved, however, by modifying chamber design to provide longer contact times and higher mass transfer rates. These results are consistent with those obtained by Strimbeck et al. (1960) in similar tests.

As expected, runs made with smaller particle-size consists (90.8% through 200 mesh) yielded better gasification results than did runs with larger particle-size consists (63.1% through 200 mesh). Improvement using the finer coal was attributed to faster reaction rates resulting from the increased surface area per unit weight of coal.

Elliott et al. (1952) and Sebastian (1952) find the H_2/CO ratio dependent on the O_2/coal and H_2O/coal ratios. The H_2/CO ratio decreases with an increase in O_2/coal ratio, but increases with an increase in H_2O/coal ratio. These opposing effects apparently operate via the rapidly established water-gas shift equilibrium,

$$CO + H_2O \rightleftarrows CO_2 + H_2 \ .$$

Strimbeck et al. (1960) and Coates et al. (1975) gasified coal using both oxygen-steam and air-oxygen mixtures. Gasifiers used by Strimbeck generally have been two stage reactors ranging in diameter from 27 to 36 in, the primary stage being approximately 30 in long. The reactor used by Coates also consists of two chambers: a 3-5/8 in diameter combustion chamber, and a 5-1/8 in diameter pyrolysis chamber. Coates' work must be developed further before reliable performance data can be obtained. However, Strimbeck, who has published results which are consistent with expected trends, reports that gas exit temperature increases with higher coal throughput (heat loss effect) and O_2/coal ratio, but shows no dependence on H_2O/coal ratio.

D. Gasification to a Low BTU Gas

Von Fredersdorff (1949) used both air-oxygen and air-oxygen-steam mixtures in a 22 in diameter chamber, 3 ft long. Flow entry and exit were both tangential. Several basic conclusions were drawn: (1) slagging operation can be applied successfully to suspension gasification at

atmospheric pressure; (2) low gas residence time is advantageous in increasing make gas calorific value; (3) tangential firing promotes removal of more than 50% of the ash in the form of slag; (4) a central combustion tube provides no thermal advantage. Steam addition lowered combustion zone temperatures by as much as 110°K. However, increasing steam inlet temperatures should improve gasifier performance.

Traenckner (1953) reports use of air and air-steam mixtures to gasify coal in the Ruhrgas pilot plant (chamber diameter - 32 in; length - 39 in). Similarly, Nistler (1957) reports operating results from the Ruhrgas commercial plant, which gasified 100 tons of coal per day in a 79 in diameter main reaction chamber. Performance data are presented in Tables VII, VIII and IX, but sufficient data to determine trends are not available.

Yagi and Kunii (1957) studied the effect of independent control variables upon carbon efficiency in a pulverized coal cyclone gasifier, 20 cm in diameter and 34 cm long. Three types of operations were conducted in the chamber: combustion in air, air-steam gasification, and air-oxygen-steam gasification. In general, carbon efficiency increased with an increase in reduction zone temperature (and thus percent ash remaining in the chamber), stayed nearly constant with an increase in H_2O/coal ratio, and decreased with an increase in the rate of gasification. However, Yagi and Kunii concluded that the essential factor affecting carbon efficiency is the mean temperature of the reduction zone.

Of the works reviewed, only Yagi and Kunii (1957) and Coates et al. (1975) employ external heaters. Certainly, performance data from other air gasification experiments indicate that satisfactory operating results can be obtained without external heating, but these have been only for larger diameter chambers.

E. Pressure Gasification

The gasification of coal to middle and low BTU gases at super-atmospheric pressure is attractive for three reasons: (1) coal throughputs are higher due to decreased reactant volume (Table VII); (2) synthesis processes requiring H_2 and CO at high pressure realize a reduction in

compression costs since only the oxidizer need be compressed; (3) percent heat loss under pressure operation is reduced (Table VIII). If throughput is increased under pressure operation, percent heat loss can decrease due to a greater volumetric heat release rate for a fixed reactor surface area. Likewise, if throughput is fixed, an increase in chamber pressure can reduce convective heat loss due to increased boundary layer thickness at the chamber wall.

Holden et al. (1960) axially injected pulverized coal, oxygen, and steam into a 5-20 atm pressure gasifier (diameter - 8 in; length - 4 ft). Significantly, the relative impacts of gas residence time and percent heat loss vary as chamber pressure increases. For example, carbon efficiency, primarily a function of oxidizer/coal ratio, decreases with an increase in coal throughput at 5 atm (even though heat loss decreases as throughput is increased), but increases with throughput at 20 atm. Thus, residence time dominates at lower pressure while percent heat loss, though relatively low, dominates at higher pressure. This behavior probably explains the lack of a distinct relation between percent carbon gasified and coal throughput in Table X. Like carbon efficiency, producer gas yield experiences a similar effect: producer gas yield decreases with increasing throughput at low pressure, but increases with throughput at higher pressure. Holden also found that gas exit temperature decreases with increasing pressure. This is consistent with the increased producer gas yield observed at higher pressure.

F. Slagging Operation

Hoy et al. (1958) have done an extensive study of coal combustion in a cyclone chamber. Their chief concern was the combustion efficiency and factors affecting it. Under optimum conditions, combustion efficiencies in excess of 98% were achieved. Although coal gasification was not an objective of this work, useful insight into successful slagging operation is provided. Slagging operation under gasification conditions has been achieved by von Fredersdorff (1949) and Yagi and Kunii (1957), though neither provides the detail offered by Hoy.

The temperature-viscosity behavior of the slag is characterized by the silica ratio of the ash. An increase in ash silica ratio or a decrease in chamber temperature increases slag viscosity, hence narrowing the operating range over which performance is satisfactory. Furthermore, the heat capacity of the slag leaving the chamber must be sufficient to compensate for any heat loss from the slag stream to the quenching chamber.

Hoy et al. (1958) maintained air/fuel ratios within 0.8 to 1.2 of stoichiometric. However, the optimum range was found to be from 1.05 to 1.10. For air rich mixtures, chamber temperature dropped too low to provide sufficient heat transfer to maintain the slag in a fluid state. This led to the accumulation of slag on the walls below the air inlets which, in time, reduced swirl velocity and combustion efficiency. For fuel rich mixtures, combustion efficiency was lowered by increased quantities of incompletely burned particles passing through the slag-tapping hole.

For coals with ash characteristics suitable for cyclone firing, combustion efficiency depended mainly on swirl velocity. At too low a swirl velocity, lack of recirculation caused combustion efficiency to drop due to unburned carbon being carried into the slag chamber. At too high a swirl velocity, combustion efficiency was reduced due to unburned carbon being carried from the chamber in the exhaust gases. Moreover, at excessively high velocities, slag droplets became entrained in the exhaust gases, which led to the obstruction of air inlets and gas outlet equipment.

G. Conclusions and Correlations

Oxidizer/coal ratio influences gasifier performance more than either coal throughput or steam/coal ratio since it markedly affects every major dependent variable (Table X). The data of Table VII indicate that oxidizer/coal ratios are consistently in the 0.5 - 1.4 lbm/lbm range. Similarly, steam/coal ratios are typically in the 0.3 - 1.0 lbm/lbm range. Ratios promoting optimum performance are always found within these ranges.

Steam inlet temperature and coal throughput vary widely among gasifiers (Table VII). Several authors acknowledge the benefits of increased steam inlet temperature; however, experimental data is scant. Variation in gasifier design probably accounts for variation in coal throughput at atmospheric pressure. Pressure gasification will allow significant increases in coal throughput.

The dependent variable behavior reported in Table X suggests the generalized correlation between dependent and independent process variables illustrated in Fig. 3 (Laurendeau, 1975b). Depending on operating conditions, gasification performance can increase, decrease, or peak with an increase in one of the independent process variables. For example, producer gas ($CO + H_2$) yield and cold gas efficiency are maximized at OX/C = 0.9, and make gas heating value is maximized near OX/C = 0.7 (von Fredersdorff, 1949; Holden et al., 1960). Clearly, experiments conducted at OX/C > 0.9 would only reveal a degradation of gasifier performance (von Fredersdorff, 1949; Holden et al., 1960). Studies indicating no dependence, e.g., the effect of coal throughput on carbon efficiency (Perry et al., 1950), may have occurred near the flat peak of the performance curve (Fig. 3).

The behavior depicted in Fig. 3 must, of course, be explained on physical grounds. Consider first the effect of coal throughput. At low coal throughputs, shorter residence times prevent CO and H_2 oxidation thus increasing performance; as throughput is increased, residence time becomes so short that entering reactants cool the gasifier faster than combustion reactions can supply heat. The resulting temperature drop causes a decrease in gasifier performance.

The effects of reactant inlet temperature and oxidizer/coal ratio are similar. Initially, higher temperatures improve performance. Eventually, producer gas oxidation and heat losses may dominate. For steam/coal ratio, initial increases are beneficial in forming producer gas. However, higher steam/coal ratios decrease gasifier temperature and performance.

Performance of any gasification system depends on the classical chemical kinetic parameters of stoichiometry, temperature and time.

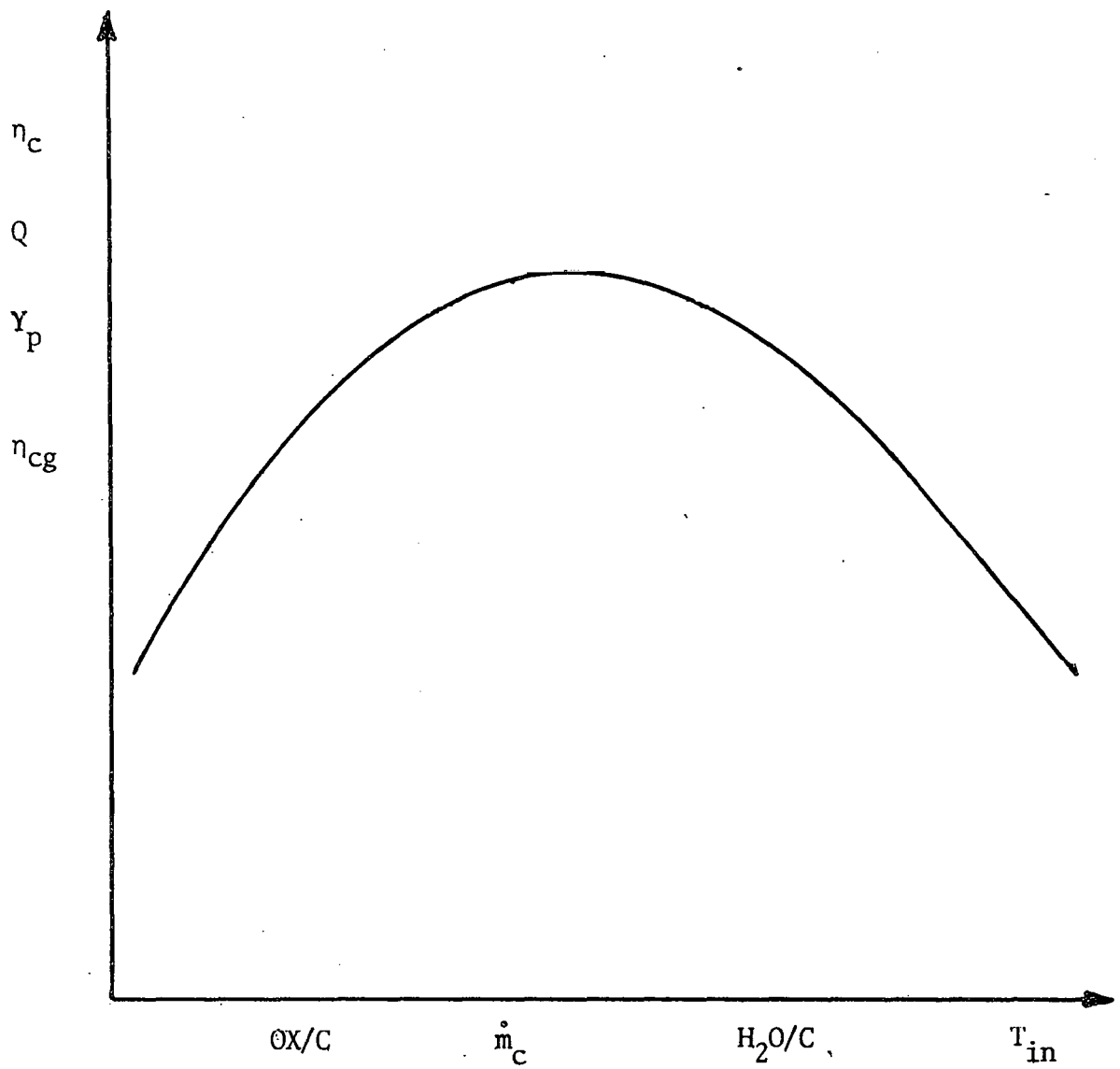

Figure 3. Correlation Between Dependent and Independent Process Variables in Suspension Gasification

Since local stoichiometry and temperature are controlled by turbulent mixing (and, ultimately, by chamber design), measurements of oxidizer/coal input ratio, steam/coal input ratio, coal throughput and reactant inlet temperature are necessary but insufficient for a thorough understanding of gasifier performance. Fundamental concepts can only be investigated by internal probing for both temperature and composition.

III. FLUID MECHANICS OF THE CONFINED SWIRLING JET GASIFIER: A PRELIMINARY STUDY

The jet gasifier we are proposing will be a jet of coal suspended in steam or air/steam mixture surrounded by a swirling jet of secondary air, as shown in Fig. 1. As noted in Chapter I, use of discrete reaction zones will improve gasification. Based on our review of literature concerning swirling jets, we find the fluid mechanics of such a jet favor the formation of discrete zones, and that by proper variation of swirl and burner configuration these zones may be shaped to promote optimum gasifier performance.

We have concentrated on three major areas in our literature search: (1) fluid mechanics, (2) heat transfer, (3) design parameters. In reviewing each of these areas, we are primarily concerned with effects which are important to gasification, although the literature reviewed concerned only cold flow or combustion systems.

A. Fluid Mechanics

The fluid mechanics of a turbulent highly swirling jet are so complex that effective mathematical analysis is nearly impossible (Beer and Chigier, 1972). Unswirled jets and jets with low swirl have, however, been analyzed successfully (Abromavich, 1963; Field et al., 1967; Beer and Chigier, 1972). An understanding of swirling jets must build on the basics derived from unswirled jets.

1. The Non-swirling Jet

Most mathematical jet analyses assume a one dimensional jet, either round or planer. Analyses have included free jets issuing into both stagnant and moving environments, and confined jets. The only jets we will consider are turbulent since laminar jets are of very limited applicability.

1.1 Free Jets. A free jet is not influenced by any surface effects other than those at the nozzle, i.e. it issues into an infinite atmosphere. Buoyant jets, jets issuing into cross and co-flowing streams and co-axial jets have been studied (Beer and Chigier, 1972), but only stagnant environments and co-axial jets are important to our present work.

As a turbulent jet issues into a stagnant environment a shear layer develops between the moving jet fluid and the still fluid of the surroundings. This shear layer, which develops much like a boundary layer at the entrance to a pipe, transfers momentum from the jet to the environment, causing fluid to be entrained and the jet width to grow. As this shear layer develops, it eventually absorbs the central jet. Figure 4 shows the regions of jet development. After the potential core (jet core with same properties as the nozzle) is absorbed, the jet goes through a mixing region. After the mixing region (approx. 10 diameters) the jet is fully developed and the velocity profiles (also, concentration and temperature profiles) are similar at each cross-section. Jet analyses rely on the similarity of these velocity profiles to simplify mathematical considerations (Field et al., 1967; Beer and Chigier, 1972).

Beyond the mixing and development regions, annular and co-axial jets behave like simple roundjets (Field et al., 1967). They can be described by the same mathematical formulas if the origin and diameter are correctly adjusted. The adjustment compensates for the various mixing and entrainment processes occurring before the jet is fully developed. The adjustment to the diameter d_o to give the equivalent diameter d_o' is based on defining a single round jet with equivalent velocity and momentum. For a co-axial jet system (Beer and Chigier, 1972),

$$d_o' = \frac{2\,(\dot{m}_j + \dot{m}_s)}{\pi\,\rho\,(G_j + G_s)^{0.5}}$$

where $\dot{m}$ is mass flow, G is axial momentum flux, subscript j refers to the central jet and subscript s refers to the annular or surrounding jet. Experimental correlations have also been reported for effective nozzle

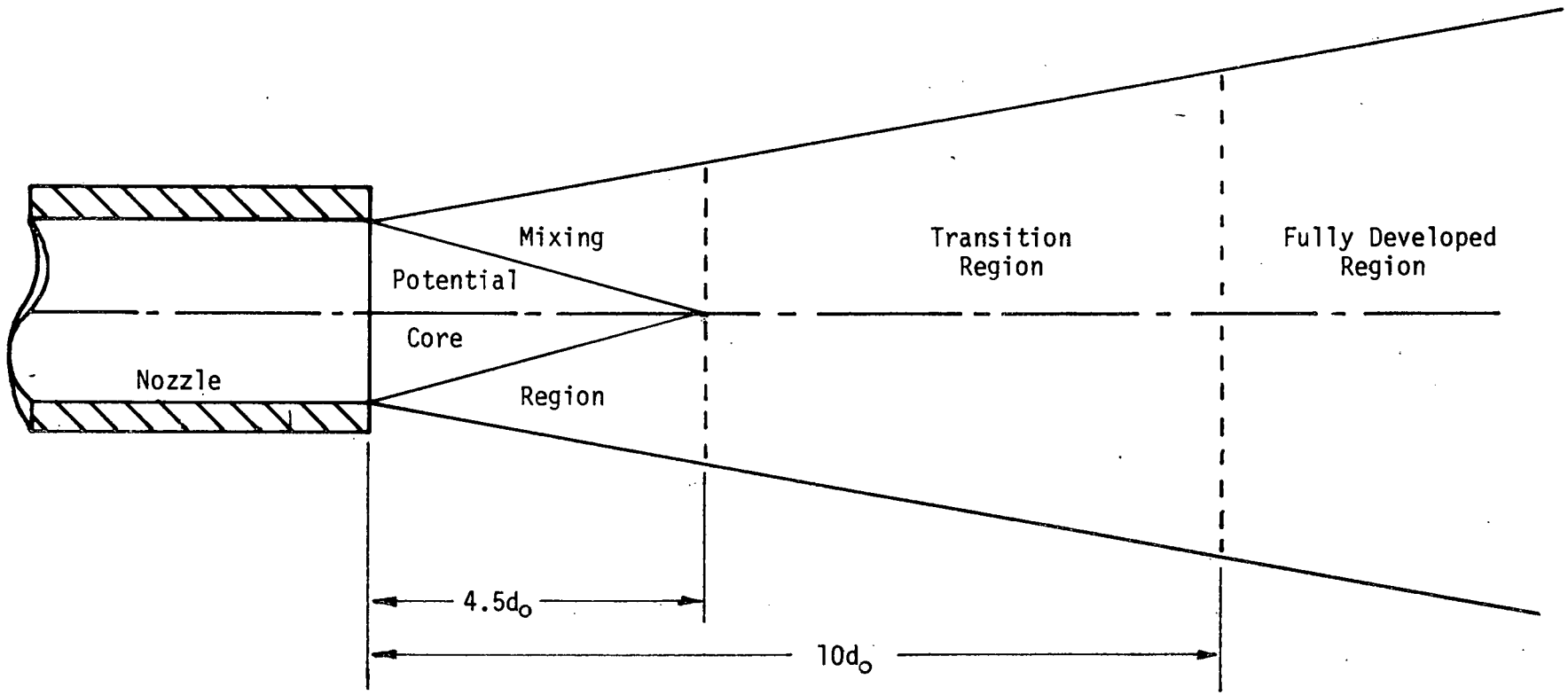

Figure 4. Regions of a Jet (from Beer and Chigier, 1972)

displacements (Chigier and Beer, 1964).

Combusting jets are approximated as low density jets issuing into a higher density environment. The non-dimensionalized velocity in a jet is found to be proportional to $(\rho_o/\rho_a)^{1/2}$, where ρ_o is the density at the jet exit and ρ_a the density of the surroundings (Field et al., 1967). This correlation will be used here although application to gasifying systems is questionable. In pulverized coal combustors the principle reaction ($C(s) + O_2 \rightarrow CO_2$) produces no additional volume, whereas the primary gasification reaction ($C(s) + H_2O \rightarrow H_2 + CO$) doubles the gas volume and will therefore distort the jet.

The mixing region of co-axial jets is characteristized by a recirculation zone at the boundary between the two jets near the nozzle. The size of the recirculation zone is a function of the cross-sectional area blocked by the wall of the central jet, with larger recirculation zones developing behind thicker pipes. The mixing of the primary jet fluid with the secondary jet increases as the ratio of secondary to primary velocity increases (Field et al., 1967).

1.2 Confined Jets. All jets of practical importance to gasification experience some degree of confinement, i.e., the supply of fluid for entrainment is limited. Figure 5 shows typical streamlines for a confined jet directed longitudinally in a duct. The jet entrains fluid and expands to contact the wall at point P_x. Since the jet fills the entire cross-section of the duct and thus prohibits backflow, the fluid for entrainment must come from the jet itself. This fluid is stripped off the jet beyond point C and recirculated for entrainment. Flow downstream of P_x where the jet fills the entire duct is typical of fully developed pipe flow.

The Thring-Newby parameter θ, defined by

$$\theta = \frac{d_o'}{D} \left(\frac{\rho_o}{\rho_a}\right)^{1/2}$$

where D is the chamber diameter, has been shown to effectively characterize confined jet flow (Field et al., 1967; Beer and Chigier, 1974). Thring and Newby assumed the jet would entrain as a free jet up to point C,

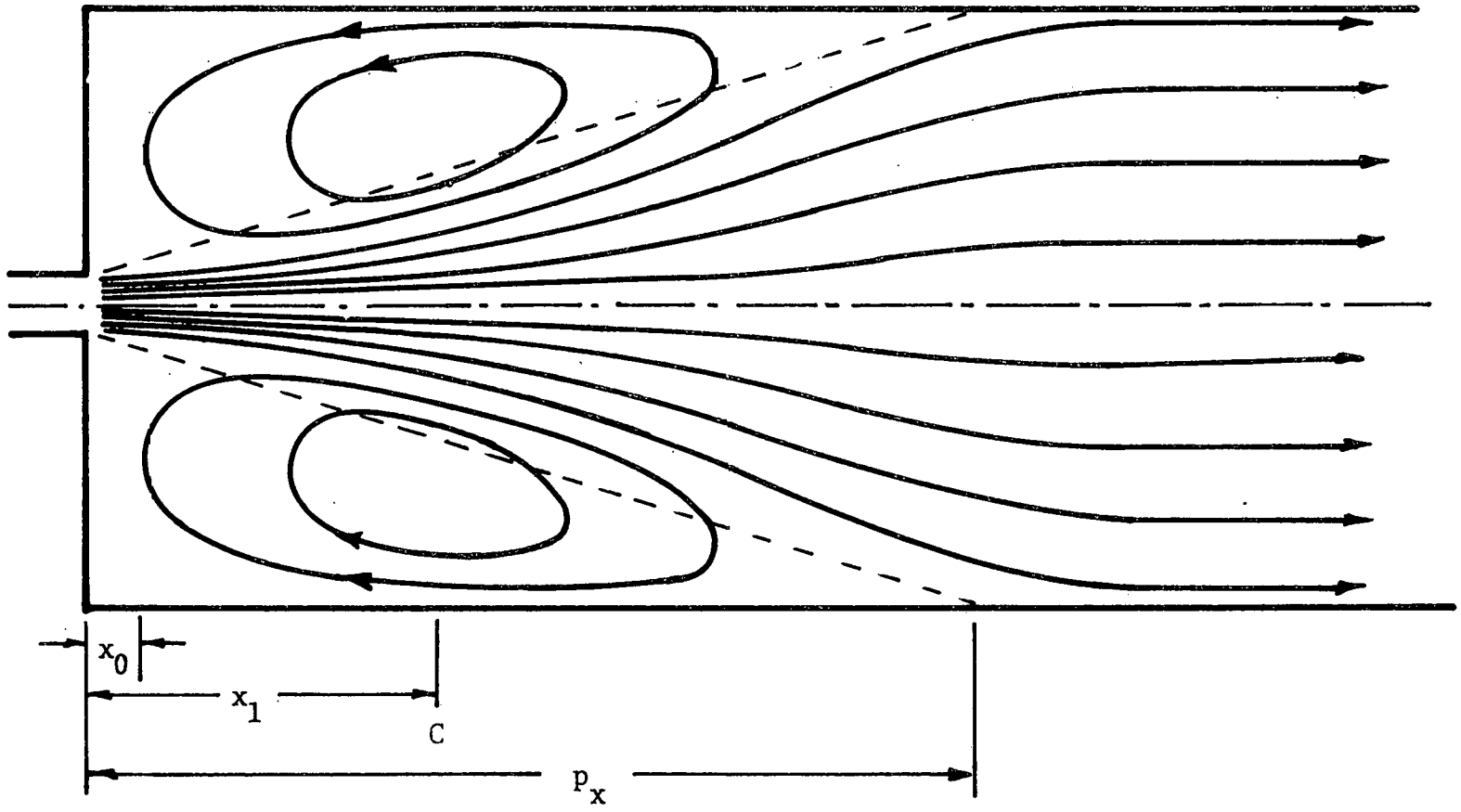

Figure 5. General Impression of Flowlines in a Confined Jet

half way between the position where theoretical entrainment begins and the point where the jet contacts the wall. On the basis of their analysis, they were able to predict the position of the recirculation zone and the quantity of recirculated fluid (Field et al., 1967; Beer and Chigier, 1972).

2. Swirling Jets

In both swirled and unswirled jets the axial and radial velocities decay in proportion to the inverse of axial distance (x^{-1}). For swirling jets the decay of tangential velocity is proportional to x^{-2}, so that the behavior of downstream portions of a swirling jet will be approximately the same as for a non-swirling jet (Field et al., 1967). The mixing and transition regions, the area of greatest importance to gasification, will be radically different.

2.1 General Aspects of Free Swirling Flows. In order to keep our discussion of general swirling flows as simple as possible, we will consider only flows created by tangential/axial entry generators. The discussion will be appropriate for a movable block generator as shown in Fig. 11 or a tangential entry type such as the one used by Syred and Beer (1974). The discussion is not applicable to flows created by vanes in the burner exit.

The swirl number S defined as

$$S = 2G_\phi/G_x d_o = G_\phi/G_x R$$

where G_ϕ is the axial flux of angular momentum, G_x the axial momentum flux and R the outer burner radius, has been shown to be an effective criterion for characterizing swirling flows (Field et al., 1967; Beer and Chigier, 1972; Kerr and Frasier, 1965). Swirl numbers of 0.6 to 2.5 are typical of industrial pulverized coal burners (Syred and Beer, 1974).

Most discussions of swirling jets are divided into two regions; $S < 0.6$ and $S > 0.6$. For $S < 0.6$, flows tend to be stable with very

little internal recirculation. At $S > 0.6$, the flow forms large recirculation zones. $S = 0.6$ is not a sharp division since swirling flows below this value are subject to instabilities and hysteresis effects (Syred and Beer, 1974). Only flows with $S > 0.6$ are relevant to our gasification work; such flows will be studied exclusively after a brief introduction to basic swirl concepts.

The structure of a swirling jet is a function of Reynolds number (Re) as well as swirl number. For low Reynolds numbers recirculation flows may not develop regardless of swirl number. Reynolds numbers greater than 18×10^3 should insure formation of recirculation zones (Syred and Beer, 1974); hence, further discussions only consider $Re > 18 \times 10^3$.

When swirl is imparted to a fluid flowing in a pipe, the fluid travels in a helical path. The tangential velocity profile will probably be of Rankine vortex form (Chapter IV) although we have only the data of Syred and Beer (1974) for high swirl numbers ($S = 2.2$) to support this claim. The relative portions of free and forced vortex will be related to the type of swirl generator and pipe length. The tangential velocity will die out rather rapidly due to viscous effects.

As the fluid leaves the pipe exit to form a jet, each fluid particle will tend to maintain its tangential and axial velocity. In addition the particle possesses radial momentum which is no longer counteracted by the radial pressure gradient. For low degrees of swirl ($S \leq 0.6$), the combined effect is an increased rate of spread of the jet, with associated increases in rate of entrainment and axial velocity decay. However, the axial velocity profiles retain their Gaussian shape; there is no internal recirculation (Beer and Chigier, 1972).

When $S > 0.6$ the adverse pressure gradient along the jet axis cannot be overcome by the kinetic energy of the fluid particles flowing in the axial direction; consequently, a recirculation zone develops on the jet axis (Beer and Chigier, 1972). In addition, the axis (or filament) of the central forced vortex core of the pipe flow becomes unstable. The forced vortex core filament, previously co-incident with the geometric axis, now begins to precess about the geometric axis like an unstable gyroscope (see Fig. 6). The frequency of this precession

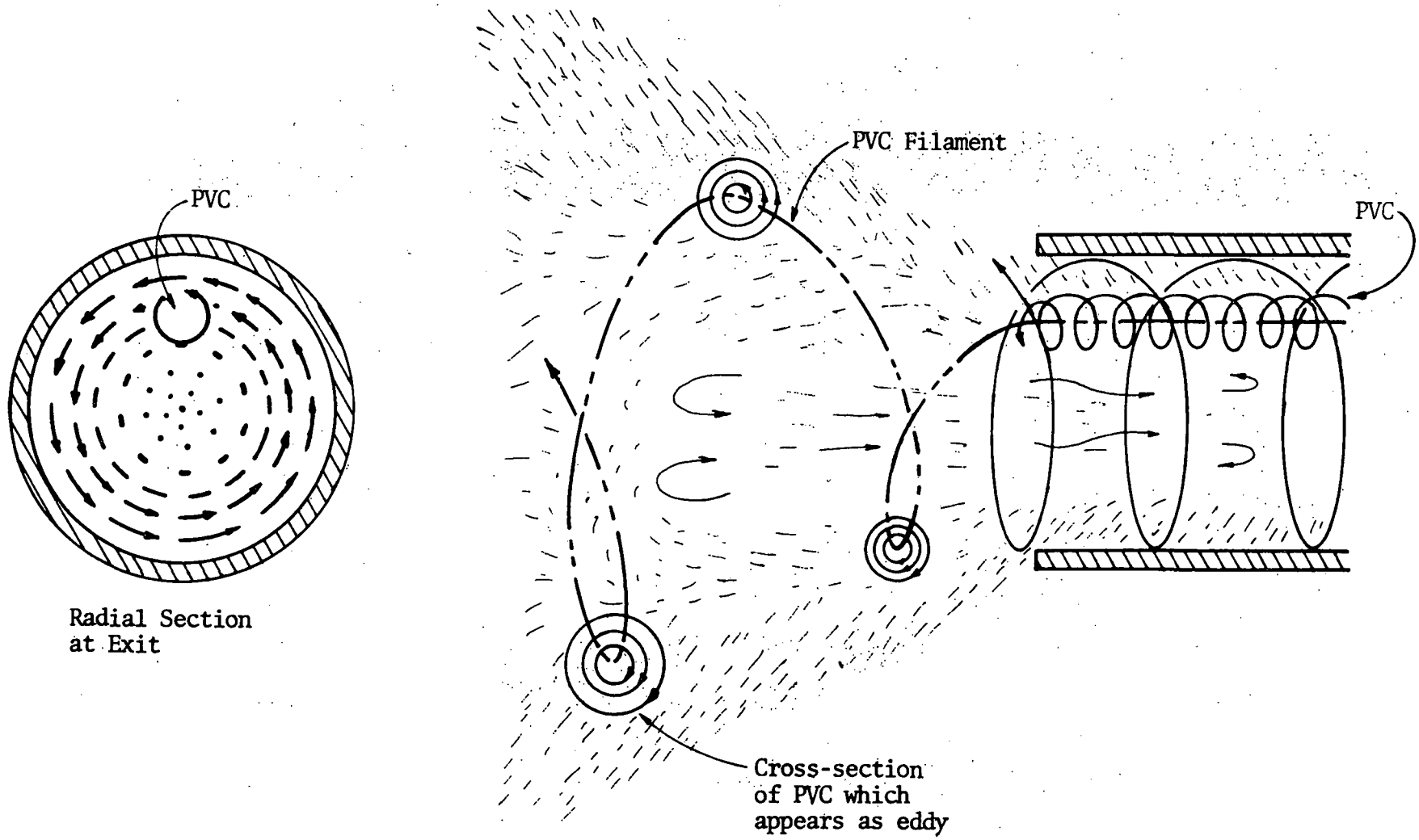

Figure 6. Diagram of PVC Geometry

may be 70 Hz or higher (Syred and Beer, 1974).

At swirl numbers just greater than 0.6, the deviation of the vortex filament from the geometric axis is slight; however, as the central recirculation zone grows radially and longitudinally, the filament is forced to precess in increasingly large circles. Figure 6 shows diagramatically the flow patterns at the exit of the swirl pipe. Note that the streamlines near the outer edge of the flow are still centered about the geometric axis. The central recirculation zone fills the center section. This section has little tangential velocity (Syred and Beer, 1974). The vortex filament and its associated vortex (generally referred to as the precessing vortex core or PVC) is located between the outer swirling and inner non-swirling zones and precesses about the geometric axis. This may be visualized as a fluid mechanical planetary gear system.

At the exit of the nozzle the PVC filament encounters a region of high turbulence and shear stress due to the restrictions imposed by the recirculation zone. Just downstream of this section, Syred and Beer (1974) noted the formation of radial-axial eddies which were shed at the same frequency as the vortex core precession. We suspect that when the PVC encounters the region of high turbulence at the nozzle exit, the filament is bent so that it crosses both the radial-tangential and radial-axial planes at an oblique angle. The filament then forms a conical helix which rotates about the geometric axis at the same frequency as the portion of the filament precessing within the swirl pipe (Fig. 6). Note that a longitudinal section through the swirling flow cuts the PVC filament so that an oblique cross-section is revealed. Hence, as the filament rotates, the investigator observes a shedding vortex.

Combustion conditions will damp the amplitude of the PVC, (Syred and Beer, 1974), as will the presence of a central fuel pipe. We believe that the damping of the large PVC will give rise to a series of smaller PVC's which again form conical helixes revolving about the geometric axis. A reduction in effective outlet area due to the enlargement of the central recirculation zone at high swirl numbers might also provide favorable conditions for the formation of more than

one PVC, although Syred and Beer report only one at S = 2.2.

The main importance of these PVC's lies in the intense mixing they promote between the outer section of the jet and the recirculation zone. It is important to have high levels of turbulence in the outer zone to promote the oxidation reactions, but the mixing promoted by the PVC's may make keeping segregated reaction zones difficult.

2.2 Development and Control of the Central Recirculation Zone. As noted above the central recirculation zone does not swirl, that is, it has no tangential velocity component. The lack of swirl in this region should result in large residence times, especially for long thin recirculation zones.

Figures 7 and 8 show conceptual streamline distributions for two different swirl conditions. In both cases the core of the recirculation zone forms near the swirl pipe outlet; the enlargement of the recirculation zones around the core restricts the flow from the pipe which causes high velocities and high turbulence intensities.

The size, shape, quantity of recirculation flow, and composition in the recirculation zone are all functions of swirl number, position and momentum of the primary jet, arrangement of the divergent nozzle, type of swirl generator, and to a lesser extent, degree of confinement (unless severly restricted). Figure 9a shows a comparison of recirculation zone sizes for various swirl numbers. Note that an exit vane swirl generator was used for this data. The recirculation zone increases in volume and length up to a swirl number of 2.0. At larger swirl numbers the volume and mass of recirculated flow increase, but the length is reduced. Figures 9b and 9c show the effect of different swirl generators and divergent nozzles respectively (Beer and Chigier, 1972).

The swirl generator we propose to use will be a combination of the two types shown in Fig. 9b (see Section C). It will have a central pipe, but swirl will be generated by radial/tangential fluid entry. We expect recirculation zones midway between the two types, depending on the effect of the primary jet (Section 2.3). Figures 9a and 9c indicate that recirculation zone size may be controlled by either swirl intensity or burner exit quarl geometry.

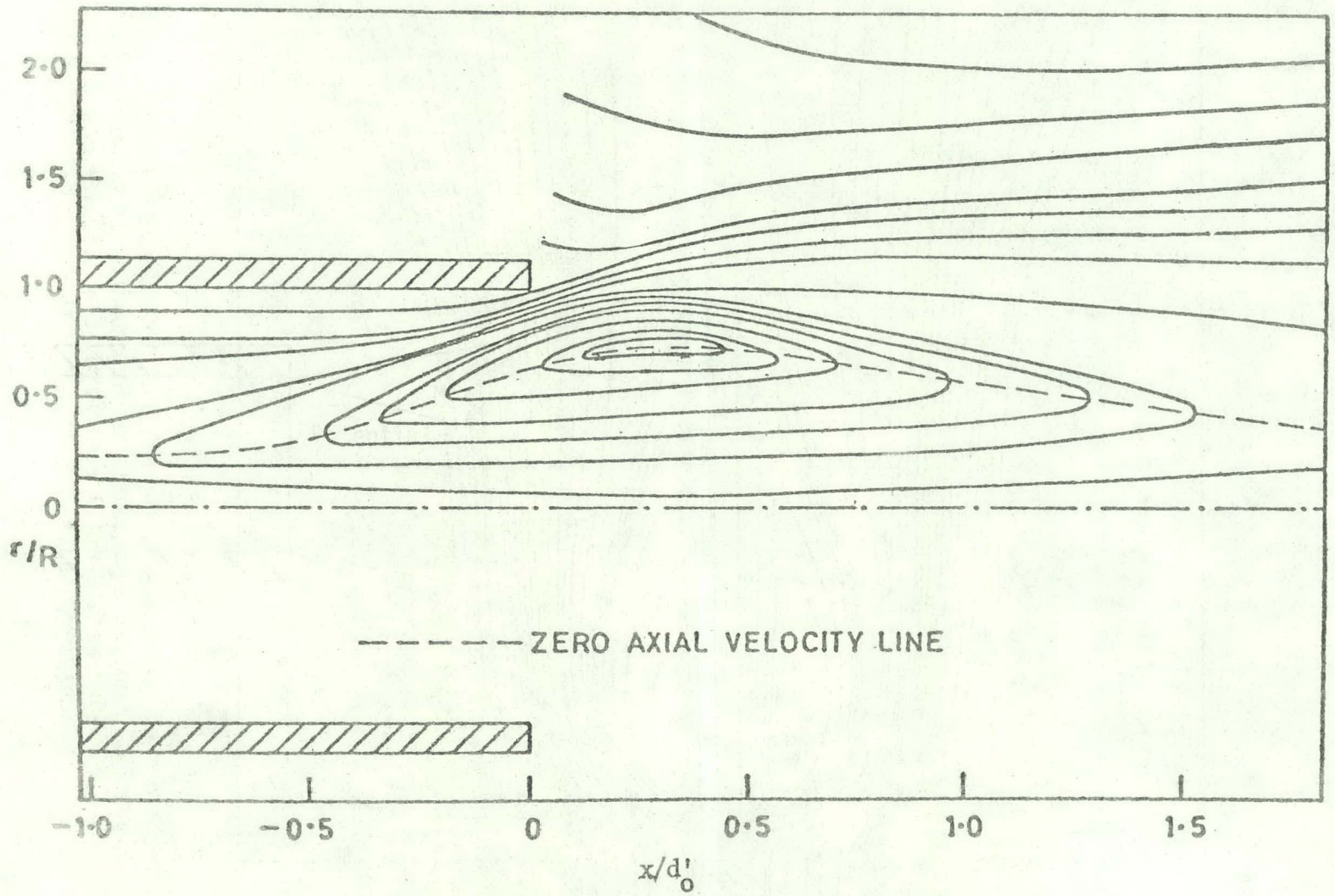

Figure 7. General Impression of Streamlines in a Swirling Jet, S = 2.2 (Syred et al., 1971)

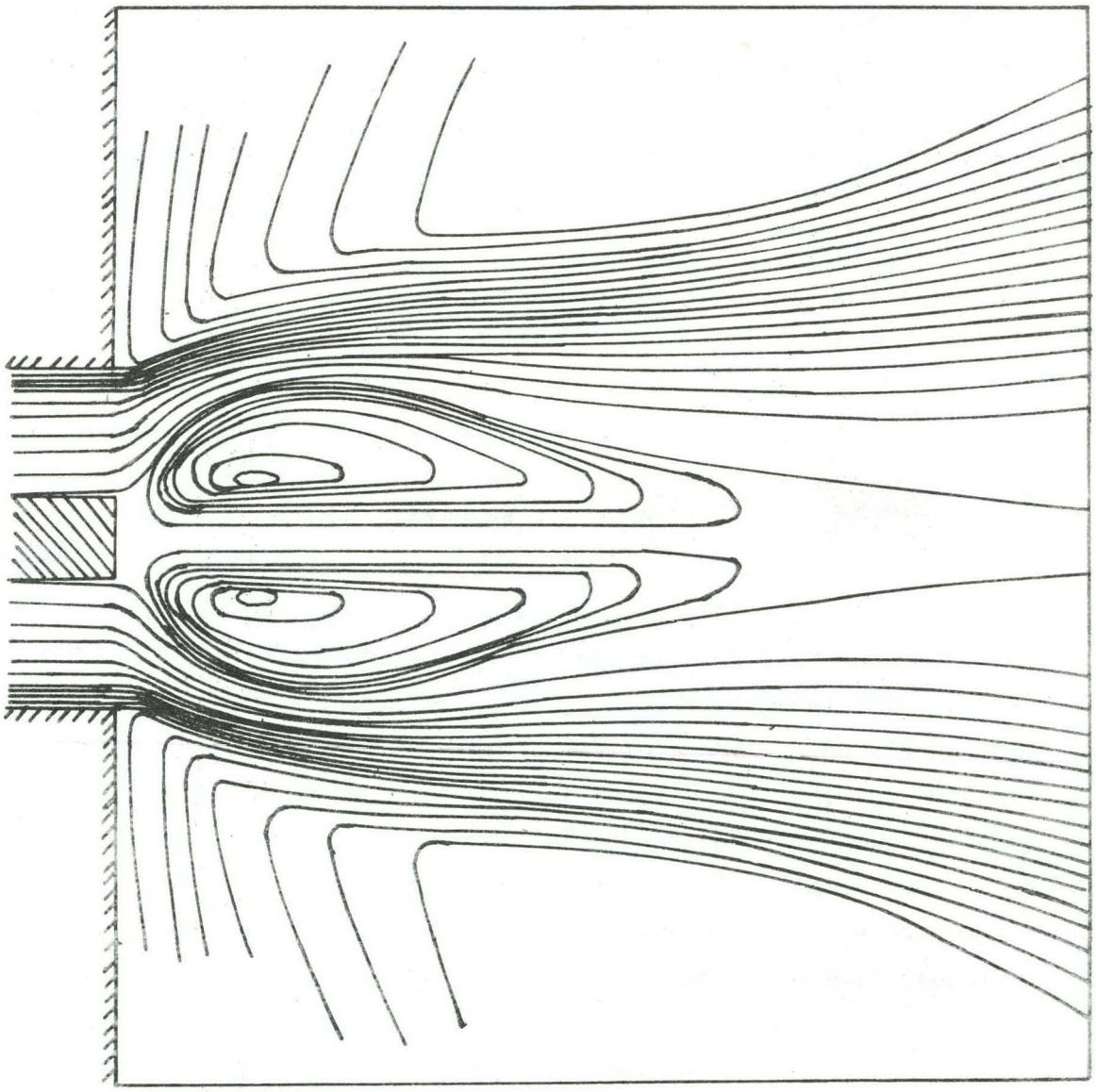

Figure 8. General Impression of Streamlines in a Swirling Jet with Central Fuel Pipe, S = 1.57 (Beer and Chigier, 1972)

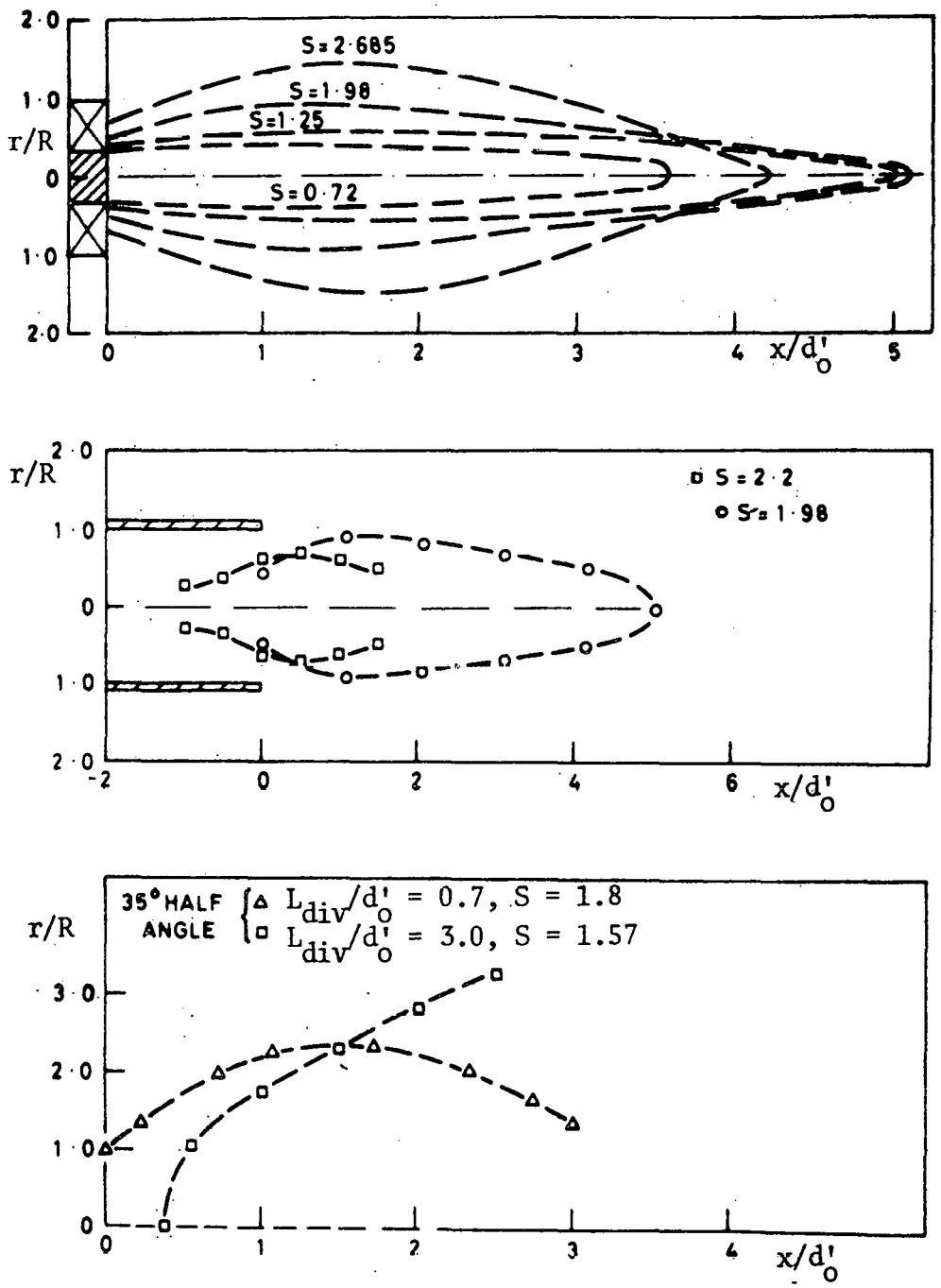

Figure 9. Comparison of the Size and Shape of Reverse Flow Zones. (a) After Vaned Swirlers. (b) Comparison of Vaned and Tangential Entry Swirlers. (c) Effect of Divergent Exit Nozzles (Syred and Beer, 1974)

2.3 Effect of Primary Jet. Very little work has been directed toward determining the effect of the central air/coal jet. The presence of a central fuel pipe will create a recirculation zone and affect PVC development. As the primary jet leaves the fuel pipe it encounters both the high turbulence levels of the nozzle exit and the reverse momentum of the recirculation zone. Depending on the pipe wall thickness, absorption by the secondary jet may begin immediately or be slightly delayed if a significant recirculation zone has developed in the wake of the pipe wall. In either case, entrainment at the primary-secondary interface will depend on the relative momentum and density of the jets.

In conventional swirling pulverized coal burners two types of flame are commonly encountered, divided and penetration (Heap et al., 1973c). In the divided flame (Fig. 10a), the entire primary jet is absorbed before the onset of recirculation. The primary and secondary jets behave like a single jet although the recirculation zone will be moved downstream from its no primary flow position. In the event that primary momentum is significantly greater than the reverse axial momentum of the recirculation zone, and entrainment in the secondary stream does not occur rapidly, a "penetration" flame will result. In this type of flame the primary jet entrains fluid from the secondary jet but retains its identity as it passes through the recirculation zone, causing a mushroom-shaped flame as noted in Fig. 10b. There will be an intermediate condition where the primary jet is not completely absorbed prior to the recirculation zone, but absorption is completed in the recirculation zone. This will charge the recirculation zone with fuel and steam rich gases in the gasification system, promoting separation of reaction zones. The optimum point for this partial penetration by the primary jet can only be determined by internal probing.

2.4 Rates of Spread/Entrainment and Effect of Confinement. Swirling jets entrain and expand much faster than non-swirling jets. As noted earlier, the parcels of fluid in a swirling jet have a radial momentum which forces them away from the jet axis. The relative velocity between the fluid particles and the stagnant atmosphere is greater due to the superimposed tangential component, so momentum

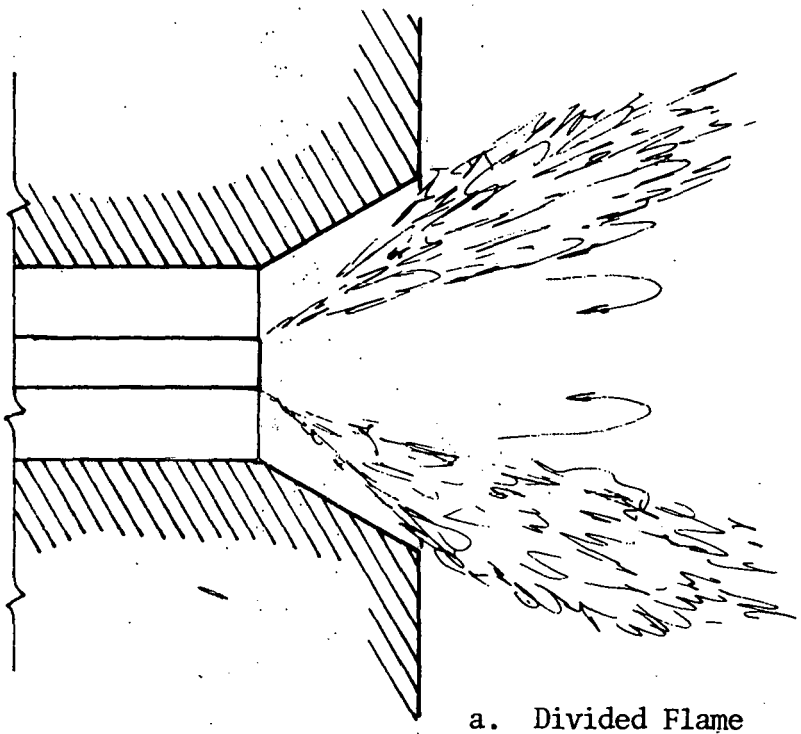

a. Divided Flame

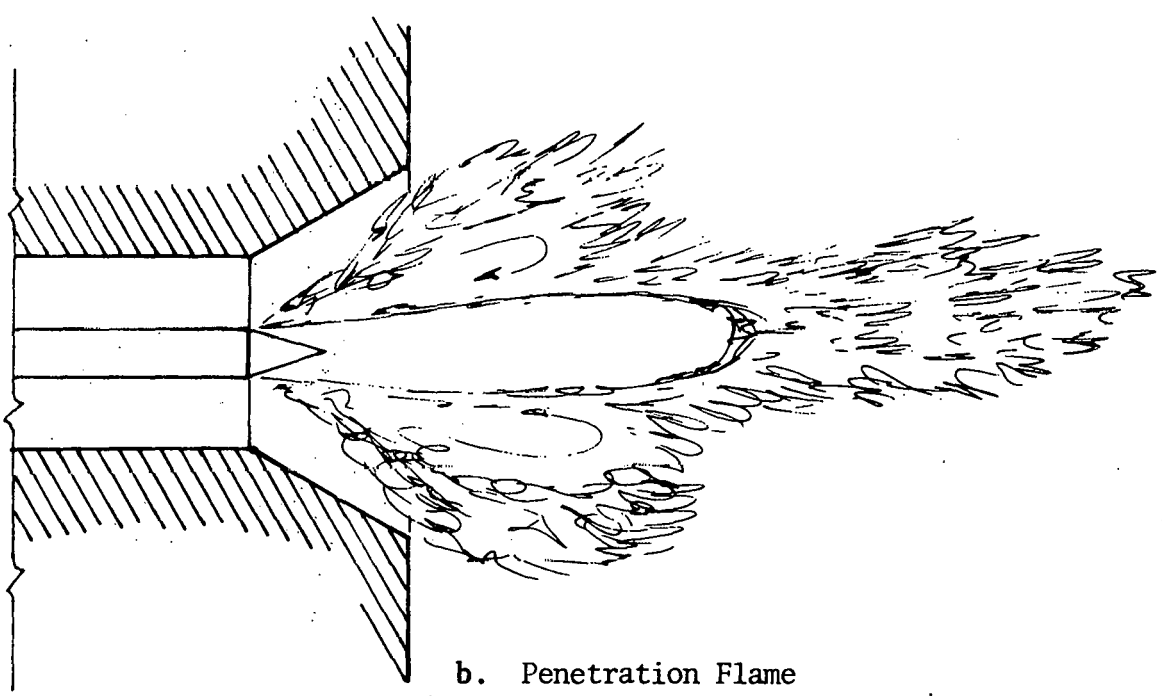

b. Penetration Flame

Figure 10. Typical Flame Shapes (Heap et al., 1973)

transfer is more rapid. Since jet expansion and entrainment is based on axial distance, and the fluid particles travel in a conical helix, the path length for a particle per unit axial length is greater for swirling jets. All these effects combine to determine swirling jet development.

Kerr and Frasier (1965) suggest the following correlations for jet spread and entrainment respectively ($S \leq 1.0$):

$$\tan \phi = (1 + C_1 S) \tan \phi_o$$

$$\dot{m}/\dot{m}_o = (x/d_o')(C_2 + C_3 S)$$

where ϕ is the velocity half angle (defined by $\tan \phi = r_{0.5}/x$, where $r_{0.5}$ is the radius at which the actual velocity equals one-half of the maximum value at the same cross-section), ϕ_o is the velocity half angle without swirl, $\dot{m}$ is the total mass flow ($\dot{m} = \dot{m}_o + \dot{m}_e$), $\dot{m}_o$ the mass flow at the nozzle, $\dot{m}_e$ is the entrained mass flow, d_o' the effective nozzle diameter and x the axial distance. C_1, C_2, and C_3 are constants for which Field et al. (1967) suggest the values: $C_1 = 2.85$, $C_2 = 0.35$, and $C_3 = 0.7$.

Although the behavior of confined swirling jets has not been effectively characterized, it is obvious that the effects of confinement will be more pronounced for swirling jets than for unswirled jets due to their higher rates of entrainment and spread. However, due to the rapid decay of tangential velocity, it appears that downstream entrainment and spread will be characteristic of unswirled jets. To gain some feeling for the effects of confinement, we have extended the Thring-Newby analysis to swirling jets, using the equations supplied by Kerr and Frasier. This analysis is presented in Section C.

3. Particle Behavior in Jets

The primary effect of a dispersion of particles in a gas jet is to increase the jet density and reduce the kinematic viscosity if the particles are small enough to allow the mixture to be considered homogeneous (Field et al., 1967). For a given primary jet velocity the momentum will increase with particle loading, and the effect on the

central recirculation zone will change as well. We expect that penetration flames will occur at lower primary to secondary air velocity ratios as particle loading is increased.

When the particles are not small enough to follow bulk fluid motion, then relative motion between fluid and particle will exist. The degree to which a particle will respond to changes in fluid velocity is directly related to the particle range in a stagnant fluid (Field et al., 1967). The range of a particle Δ is the distance it would travel in a stagnant environment before loosing 63% of its initial velocity. For a spherical particle

$$\Delta = U_o \tau_r$$

where U_o is the initial particle velocity and τ_r is the relaxation time (time required for $U = (1/e)U_o$). τ_r may be expressed as:

$$\tau_r = m_p/3\pi d_p \mu$$

where m_p is the particle mass, d_p the particle diameter, and μ the dynamic viscosity (Field et al., 1967).

For particles with ranges of 100 times the burner diameter or greater, the effect on or by the jet will be small since the particles will not respond to the level of turbulent and velocity fluctuations encountered (Field et al., 1967). The range of a 100 micron coal particle injected at 30 m/s into a 1800°K environment is 140 cm. For a 45 micron particle at the same speed the range is reduced to 30 cm. We suggest that one way to improve modeling of full scale equipment is to reduce particle size to maintain a constant particle range to burner diameter ratio.

For the jet gasifier, the preferred particle behavior would have the larger particles in the outer section with the faster oxidation reactions, and the smaller particles in the recirculation zone for the endothermic reactions. Recall that the turbulence levels in the recirculation zone are usually much lower than in the outer section.

Thus scrubbing of large particles to increase reaction rates will be promoted in the region which may be diffusion controlled. The ability of the swirling concentric jet arrangement to segregate particle sizes will depend largely on the mixing characteristics between the central and annular jets. The larger particles will advance further into the burner chamber before receiving significant tangential velocity (assuming the primary jet is not swirled), but once accelerated tangentially they will proceed across the stream much faster than the small particles, as evidenced by their longer range. This will throw the heavy particles to the outside while the smaller particles remain in the internal recirculation zone. Small particles are able to respond to small turbulent fluctuations, so they will experience better mixing in the recirculation zone than any remaining large particles.

B. Heat Transfer

Heat transfer in the swirling jet gasifier will have a significant effect on its performance. Heat transfer to incoming reactants, to the internal recirculation zone, and to the walls from the oxidation zone are the three dominant processes. Heat transfer will occur by convection and radiation on the macroscopic level, and by diffusion and radiation on the microscopic (single particle) level. We will first consider a single 60 micron particle suspended in a flowing air stream at 1800°K. Sixty microns was chosen as being representative of typical industrial pulverized coal. Although rigor requires a particle size distribution (Chapter V), a single size will serve to illustrate the basic principles. After the single particle is considered, we will discuss macroscopic heat transfer.

1. Single Particle Heat Transfer

A spherical coal particle is generally assumed for all calculations involving heat and mass transfer to pulverized coal (Field et al., 1967; Essenhigh and Csaba, 1963; Beer and Lee, 1965; Hottel and Sarofim, 1967). If we calculate the Reynolds (Re), Nusselt (Nu), and Biot (Bi) numbers based on a particle with a velocity of 90 m/sec

(three times expected inlet velocities), the viscosity of air at 1800°K (6.07×10^{-5} kg/m sec) and a thermal conductivity of coal of 2.5 W/m °K (Field et al., 1967) we find: a. Re = 17.5, b. Nu = 2.06, c. Bi = 0.09 (the Nu calculation is based on $Nu = 0.37\ (Re)^{0.6}$, $17 < Re < 18{,}000$ from Holman, 1963). For a particle in a stationary environment, the Nusselt Number is 2.00. Biot numbers less than 0.1 usually allow an isothermal assumption to be made for transient heat transfer. The particle can therefore be considered as stationary and isothermal for heat transfer calculations. A similar analysis will hold for species mass transfer to the particle, although chemical reactions will have to be considered.

The isothermal and stationary assumptions are not valid during the brief devolitilization period. When coal is devolitilized, the volatile matter is not simply generated at the surface of the coal particle, but due to the internal pore structure of coal it is driven off in small micro-jets. These jets disrupt the surrounding boundary layer and may increase heat and mass transfer from the particle. Fortunately this is an extremely rapid process which takes place near ignition, so the overall concept of a stationary particle is not disturbed.

Radiation heat transfer occurs between the particle and its surroundings. The effect of incident radiation on a small particle is not equivalent to interception by a large geometric body due to diffraction effects. For particles with diameters on the order of the wavelength of incident radiation, accurate treatment must be by the Mie equations (Hottel and Sarofim, 1967). Over 99% of the radiation from a black body at 1400°K will lie below 20 microns. Twenty five percent of the coal particles will lie below this value so there is an overlap. The bulk of the particles, however, will have a diameter (d_p) greater than $5\lambda/\pi$ which is the lower limit for geometric consideration suggested by Hottel and Sarofim (1967). For engineering approximations then, the coal particles will be considered geometric.

Even when a coal particle is considered as a black, spherical, geometric interceptor and radiator, radiation transfer is not straightforward. Radiation is exchanged with a volume emitting, frequency selective body (coal and ash suspensions in combustion gases) and with

a surface emitting and reflecting body beyond the gas and particle cloud (the chamber walls). Attempts to carry single particle considerations beyond a general description are not useful in an engineering sense because of the coupling of radiation effects to an ever changing environment.

2. Macroscopic Heat Transfer

It is not possible to provide a detailed analysis of heat transfer in a swirling jet without a fluid mechanical model. Convective transfer is obviously tightly bound to the fluid mechanics. Radiation transfer is more easily separated from flow conditions if regional boundaries can be defined, but it is dependent on particle and gas concentrations. Both the fluid mechanics and heat transfer are directly coupled to the rates of reaction due to variations in concentration, density, and temperature in the jet.

There are three primary heat transfer effects to be considered: (1) radial transfer from the oxidation zone to the central recirculating gasification zone; (b) longitudinal transfer from the oxidizing zone to the incoming reactants; (c) heat transfer from the jet to the chamber walls.

2.1 Radial Transfer. Convective heat transfer will be a result of the intense mixing caused by the downstream extension of the PVC's. The region between the outer zone and the inner recirculation zone is highly turbulent; however, we can say very little more about this as no studies of heat transfer in this region have been attempted.

Radiation will occur between the outer zone and the inner zone. The amount of radiation exchanged depends on the optical length of the gas region involved (Hottel and Sarofim, 1967). In order to pursue this, a brief review of radiation absorption by gases and particle clouds is in order.

A monochromatic beam of radiation passing through an absorbing, non-scattering medium will experience an exponential decay given by Beer's Law:

$$I = I_o e^{-\int_o^{\ell} K_\lambda dx} \quad \text{or } I = I_o e^{-K_\lambda \ell} \text{ if } K_\lambda \text{ is constant}$$

where K_λ is the monochromatic absorption coefficient, I the beam intensity, I_o the initial beam intensity and ℓ the depth of the medium. (A dispersion of scattering coal particles can be treated in the same way without undue loss of accuracy (Field et al., 1967).) The integral $\int_o^{\ell} K_\lambda dx$ can be considered an optical depth for the medium. A thin medium with a high absorption coefficient may absorb as much radiation as a thick medium with a low coefficient. An optically thick body will absorb most of the radiation which strikes its boundary. For a given gas thickness a monochromatic directional absorptivity can be defined so that the gas may be considered a surface with absorptivity α_λ such that:

$$\alpha_\lambda = 1 - e^{-\int_o^{\ell} K_\lambda dx}$$

As in solid body radiation, the monochromatic, directional emissivity is equal to the monochromatic, directional absorptivity. Methods for developing the absorption coefficient K_λ have been suggested by Field et al. (1967) and Hottel and Sarofim (1967) for dust clouds and gases of known composition.

It is generally preferable to do radiation exchange calculations on the basis of the grey body approximation. For gases with large optical depths in all wavelengths of importance this may be feasible, but for laboratory scale models the optical depth will probably be too short for grey body assumptions. A dispersion of particles in a transparent medium may behave well as a grey body, but in the presence of frequency selective gases, notably CO_2 and H_2O, the greyness is disturbed by bands of high monochromatic emissivity and absorptivity.

For radial radiative heat transfer the exchange will take place between two clouds of non-grey gases. The behavior of these clouds will depend on their depth in a given direction, and on the concentrations of absorbing gases and particles. Radiation will also occur indirectly via the chamber wall. The combustion zone will heat the wall which will

(1) reflect radiation into the central region and (2) emit radiation which passes through the recirculation zone.

2.2 Longitudinal Transfer to Incoming Reactants. Transfer of heat to the incoming reactants will be by: (1) convection of downstream hot gases to the jet entrance via the central recirculation zone; (2) convection of hot gases due to the external recirculation zone; (3) radiation from the oxidation zone; (4) indirect radiation from the oxidation zone via the furnace wall.

The central recirculation zone is given credit for effective heat transfer in combustion systems (Field et al., 1967; Beer and Chigier, 1969; Syred and Beer, 1974), but in gasification this will be the low temperature endothermic reaction zone; hence, effective upstream heat transfer may not occur. Convection exterior to the jet is a function of the degree of confinement, as noted in Section A. However, it is not clear that wall recirculation will transfer enough heat to the incoming reactants to stabilize the flame. Its behavior should be very similar to external recirculation zones in combustion systems, since it will interact most strongly with the external jet. Field et al. (1967) note that external recirculation zones are not as effective in reverse heat transfer as the central zone. The external recirculation region is also subject to cooling by the reactor walls.

Direct radiation between the oxidation zone and the incoming fuel will follow the basic laws suggested in Section 2.1. Radiation transfer to the unmixed secondary air jet will be minimal since it contains very few absorbing gases. Radiation transfer with subsequent mixing could play an important part in maintaining reactor stability.

Indirect radiation from the oxidation zone to the incoming gases via the chamber wall will be very important to our laboratory scale gasifier. The model gasifier will be plagued with very short optical depths and a high surface to volume ratio. We hope to use the chamber wall as a re-radiating surface to offset these effects. Dahmen and Syred (1975) found that radiation contributed significantly to stability in their cyclone combustor for low BTU gas. Since we have a coal particle suspension, we should realize even greater effects from wall radiation.

Basically the refractory wall will absorb radiation from the oxidizing zone. It will reflect a portion of the incident radiation and will also emit radiation based on its own temperature. In an industrial size gasifier, any radiation which left the jet would be lost to the cooled reactor walls.

2.3 Transfer to the Reactor Walls. As we mentioned in Section 2.2, the reaction zones will lose heat to the walls. This will be by radiant exchange from the combustion zone and convective exchange from the external recirculation zone. The amount of insulation and the thermal properties of the wall will determine the amount of heat lost from the reactor through the walls. The formation of slag on the walls will also affect the behavior of the reactor. In order to properly design a containment vessel, we will have to make estimates of the heat transferred through the walls. This will require some type of radiative transfer modeling under combustion conditions, but we have not yet formulated the model.

C. Design Considerations

Actual design of the gasifier has not begun. We have selected a swirl generator configuration and we are considering the type of analysis to be used for selecting a chamber diameter and length.

1. Swirl Generator

For our experimental gasifier we will use the movable block swirl generator of the type developed at IJmuiden. This swirl generator provides radial and tangential air inlets which can be varied to control swirl. Fig. 11 shows the generator used at IJumiden. We expect a similar design, although we will use a refractory quarl rather than the water cooled quarl shown. This type of swirl generator is easily changed from one swirl condition to the next, and the position of the swirl generator blocks is directly related to swirl number.

Figure 12 shows the correlation between swirl block opening and swirl coefficient σ. Swirl number is related to swirl coefficient by:

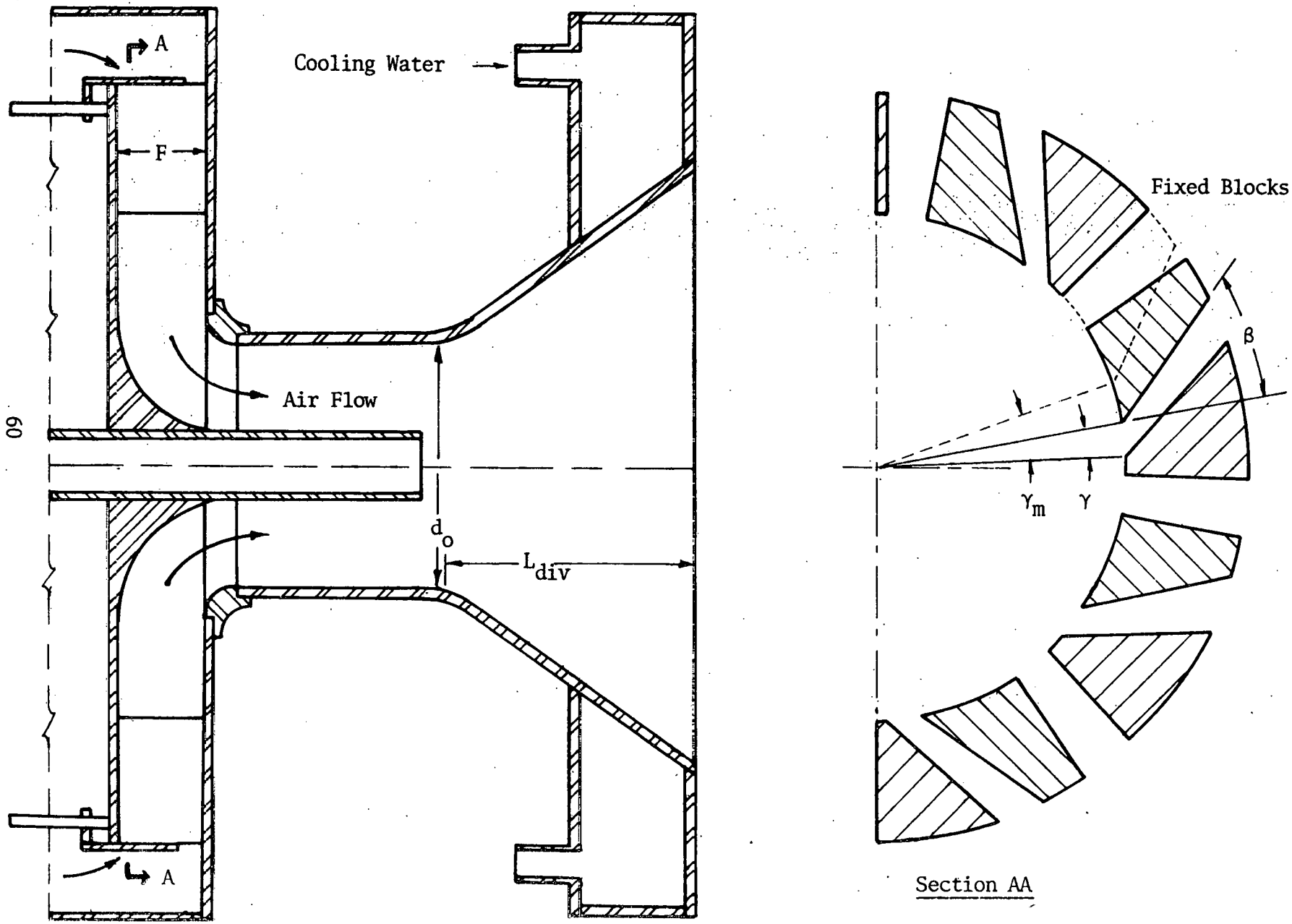

Figure 11. Swirl Generator (Beer and Chigier, 1972)

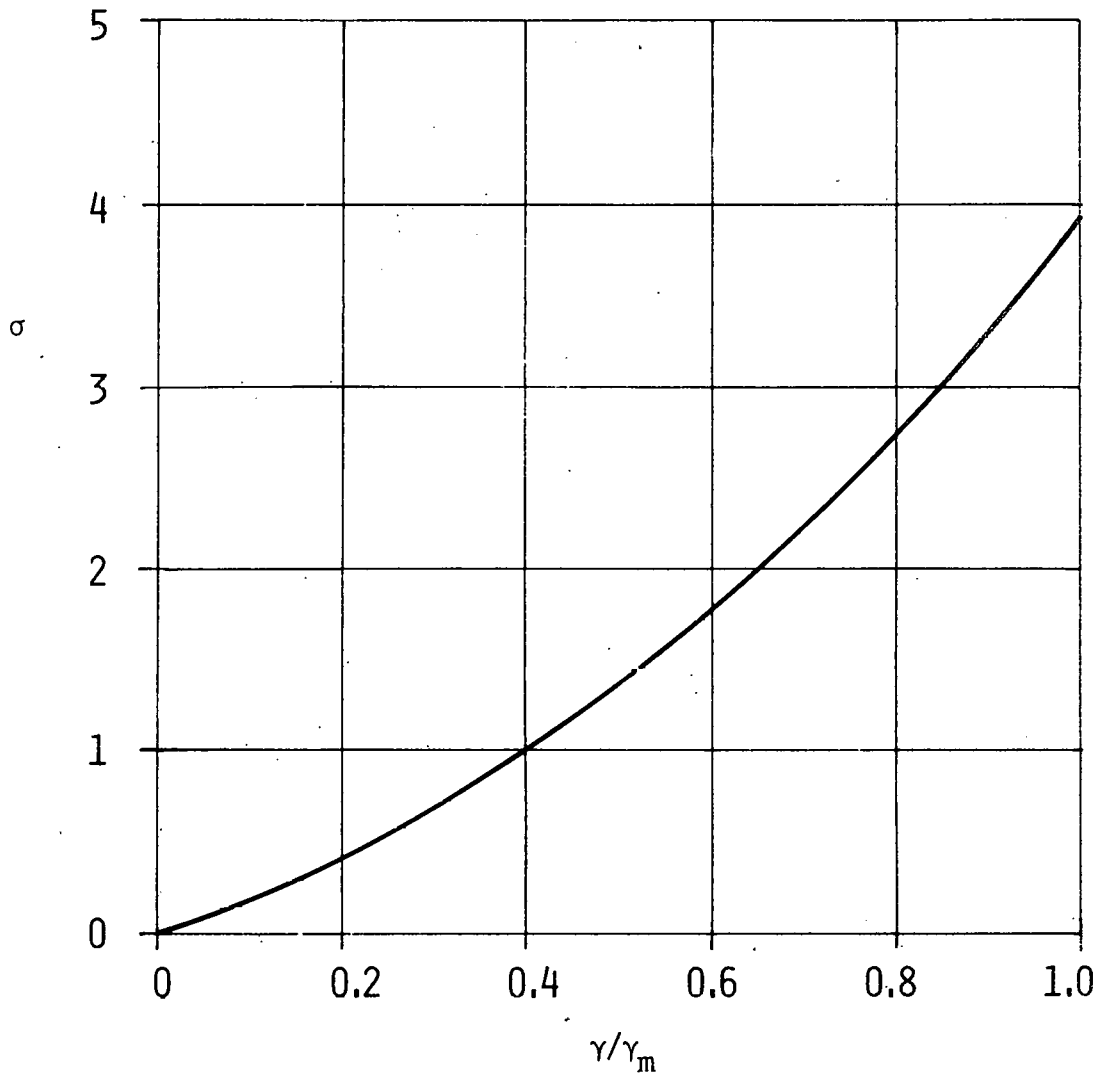

Figure 12. Correlation Between Swirl Coefficient γ and Swirl Block Position γ/γ_m (Beer and Chigier, 1972)

$$S = \sigma \frac{R}{F} (1-(\frac{r_h}{R})^2)$$

where r_h is the hub (fuel pipe) radius F the axial block width. This simple relation along with the theoretical curve for σ shown in Fig. 12 will allow quick determination of the swirl number from a position indicator or a micrometer screw adjustment.

2. Relation Between Chamber Diameter and Confinement

In order to provide some qualitative understanding of the effects of confinement, we have extended the modified Thring-Newby analysis as presented in Field et al. (1967) to swirling jets. To perform this analysis, we have extrapolated the equations of Kerr and Frasier (Section A-2.4) for rate of entrainment and spread to higher swirl numbers.

We first assume that the jet angle is equal to twice the velocity half angle (Field et al., 1967). This allows calculation of the point where the jet contacts the wall (P_x) by (Fig. 5):

$$P_x = (D/2) \tan 2\phi.$$

Field et al. show that the unswirled jet velocity half angle is 4.85^o. This value is used in the Kerr and Frasier equation for the rate of spread to give:

$$P = (D/2) \tan (2 \arctan (0.0849 + 0.241 S)).$$

Theoretical entrainment begins at a point x_o ($\dot{m}/\dot{m}_o = 1$) given by

$$x_o = d_o'/(0.35 + 0.7 S);$$

we then assume the jet entrains as a free jet up to a distance x_1 half way between x_o and P. After point "C" as shown on Fig. 5, disentrainment and recirculation begin. The axial distance to "C" (x_1) is given by:

$$x_1 = 1/2\ [(d_o'/(0.35 + 0.7\ S)) + ((D/2)\ \tan\ (2\ \arctan\ (0.849 + 0.241S)))].$$

The total fluid entrained, and hence the fluid recirculated is given by;

$$\dot{m}_r = \dot{m}_o\ [\ (x_1/d_o')(0.35 + 0.7\ S) - 1]$$

which is again based on the entrainment equation of Kerr and Frasier.

By defining a dimensionless parameter Γ:

$$\Gamma = (d_o'/D)\ \tan\ (\arctan\ (0.849 + 0.241\ S)$$

the recirculated flow can be expressed as:

$$\dot{m}_r = \dot{m}_o\ (\frac{0.0875 + 0.175\ S}{\Gamma} - 0.5).$$

For a non-swirling isothermal jet this reduces to:

$$\dot{m}_r = \dot{m}_o\ (\frac{0.51}{\theta} - 0.5)$$

which compares favorably with the non-swirling relation given by Field et al. (1967). (Note the Thring-Newby parameter θ.)

This analysis does not account for the central recirculation zone. Beer and Chigier (1972) found that highly swirling jets could be made to attach to the front chamber wall. The analysis cannot predict this. It does provide a "first cut" analysis for the recirculation flow in the absence of any other technique.

At present we belive that, with proper confinement, sufficient recirculation can be maintained ($2 < \dot{m}_r/\dot{m}_o < 4$) to (1) stabilize reactions via convective heat transfer and (2) recycle CO_2 to the endothermic reaction zone for reduction to CO ($C(s) + CO_2 \rightarrow 2CO$).

D. Summary

At this time, we have developed sufficient qualitative understanding of the proposed confined jet gasification system to feel that

the characteristics of the system will allow improvement over conventional entrained flow systems. In addition we are now able to begin design considerations. The jet gasifier will be designed to allow shaping the recirculation zone by regulating swirl number and changing burner quarl geometry. Reduced particle size and refractory walls will be used to offset problems caused by the smaller jet size. Reaction stability may be an important limiting factor.

IV. FLUID MECHANICS OF CYCLONE AND VORTEX FLOWS

Nearly all aspects of cyclone chamber aerodynamics (and hence design) can be classified under one of the following headings: (1) method of flow entry and exit, (2) chamber geometric parameters, and (3) combustion effects. Major topics considered under these headings include mixing, dimensionless geometric parameters, and the similarity of hot and cold flow.

These sections are preceded by a review of cyclone and vortex flow models, both theoretical and empirical. The chapter ends with a discussion of the aerodynamic drag in a cyclone.

A. Flow Modeling

1. Fundamental Concepts

Cyclone and vortex flow modeling discussions may be conveniently separated into two parts: (1) flow in the radial plane, in which tangential and radial velocities are considered, and (2) flow in the longitudinal plane, in which axial velocities and flow reversals are considered. A vortex may be described as a fluid motion in which the streamlines are concentric circles (Daily and Harleman, 1966). As will be seen, cyclone flow is more accurately characterized by streamlines which spiral radially inward.

For discussion purposes, a generalized cyclone flow chamber is illustrated in Fig. 13. Tangential flow entry has been divided into primary and secondary zones: entry is primary tangential at the closed end, and secondary tangential at the throat; combined primary and secondary entry describes chambers having axially distributed tangential entry. Axial flow entry has also been divided into primary and secondary zones: primary axial entry is central axial injection at the closed end; secondary axial entry is entry through the annular zone at the throat.

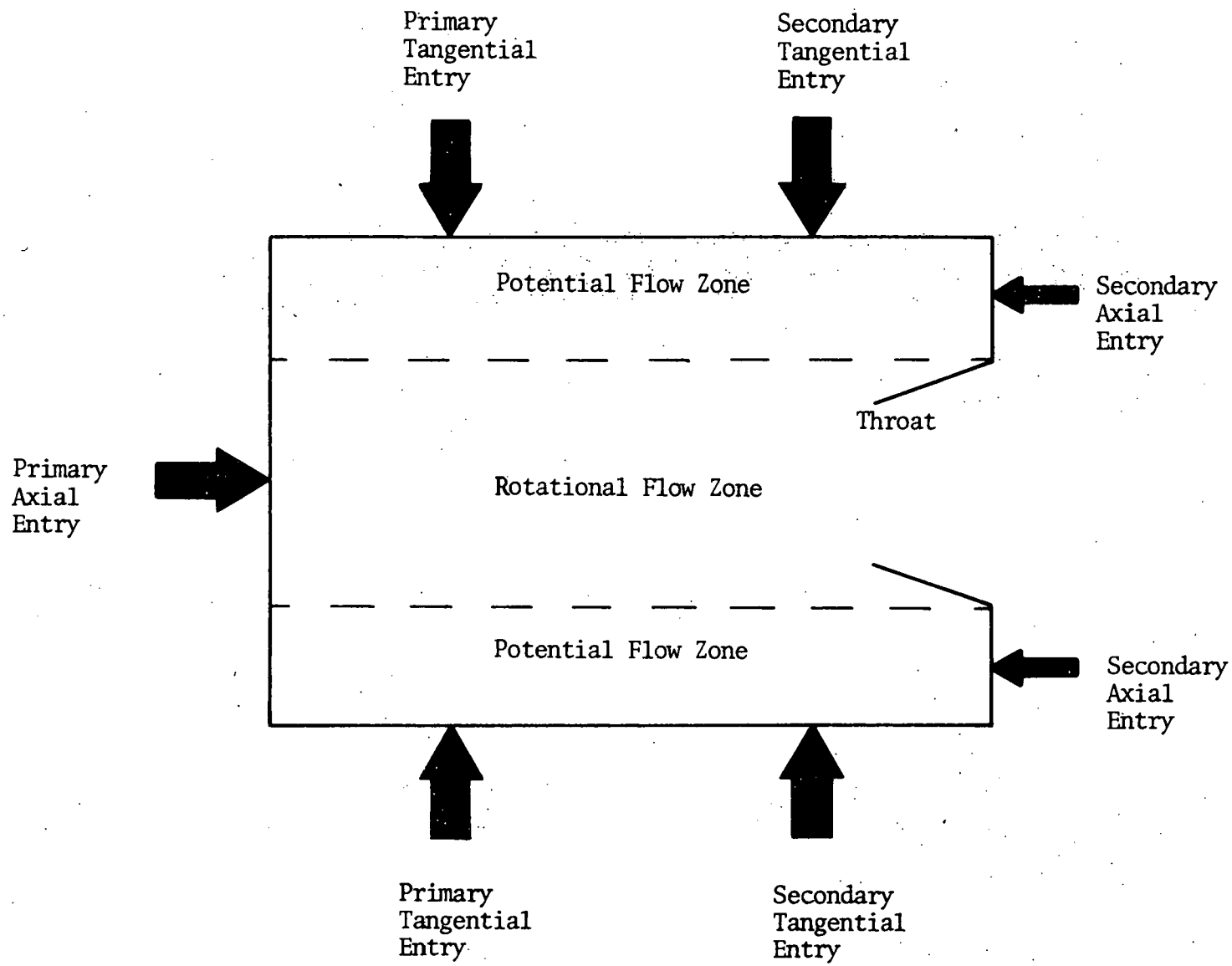

Figure 13. Generalized Cyclone Flow Chamber

It is extremely important to distinguish primary and secondary air from primary and secondary entries: primary air is air whose main function is to entrain fuel, while secondary air is the air required for combustion. On the other hand, primary and secondary entries designate location, not type of reactant.

The most prevalent flow model assumes a tangential velocity profile of Rankine form. In this model, the flow near the wall of the chamber is assumed to be a potential or free vortex flow in which angular momentum is always conserved. The tangential velocity is given by

$$W_r = c_1 \times r^{-1} \quad .$$

In the core of the chamber the flow is a rotational or forced vortex flow which follows the relation

$$W_r = c_2 \times r \quad .$$

Perry et al. (1950), Agrest (1965), Roschke (1966b), Ustimenko and Bukhman (1968), Schmidt (1970), and Dahmen and Syred (1975) have all cited part or all of this model. In addition, most of these investigations have indicated the existence of reverse flow regions; that is, the existence of regions within the chamber where the axial velocity changes sign.

In idealized rotary flow (Schmidt, 1970), i.e., flow with only primary and secondary tangential entry (Fig. 13), the potential flow zone has a downward axial flow (Fig. 14). At the chamber floor, flow passes through a free vortex sink to a forced vortex source and thus to the rotational flow zone, which has an upward axial flow. However, transitions from potential to rotational flow occur not only at the chamber bottom, but throughout the entire flow volume.

Agrest (1965) states that the rotational field at the axis is induced by the frictionless potential field in the annular region. In

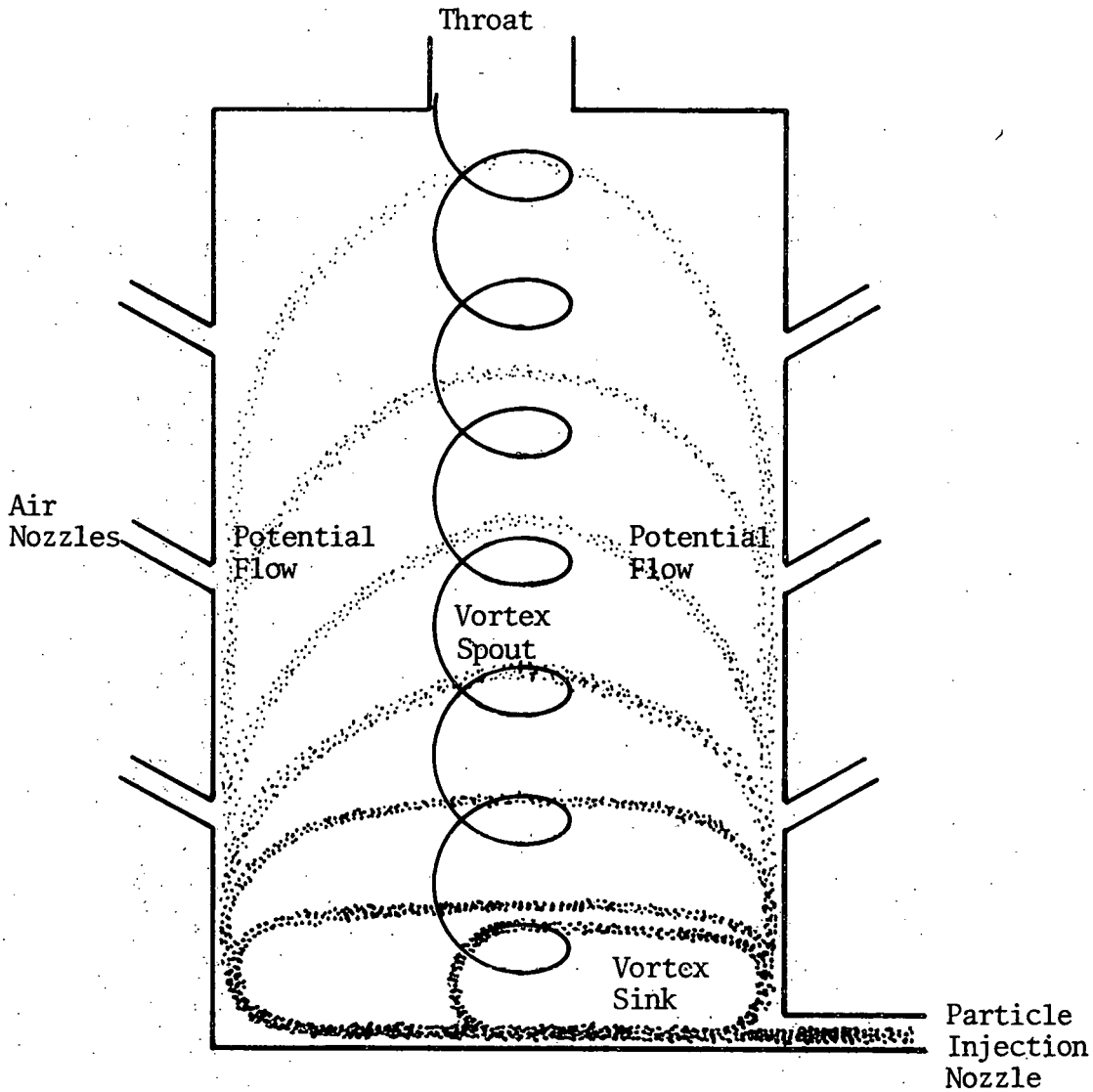

Figure 14. Particle Movement in Rotary Flow (Schmidt, 1970)

the boundary zone between the rotational and potential fields, a very turbulent boundary layer is formed. This turbulence is very favorable in promoting reaction. Similarly, Ustimenko and Bukhman (1968) acknowledge the existence of "quasipotential" and "quasisolid" flow regions. The turbulence intensity is approximately constant in the quasipotential flow region and increases in the quasisolid flow region.

Roschke (1966b), in investigation of confined, jet-driven water vortices with primary and secondary tangential entry (Fig. 13), presents a modified version of the free vortex region. This modification assumes that

$$W_r \propto 1/r^m \; ; \; m \leq 1 \quad .$$

Decreasing values of m indicate greater degrees of departure from a potential vortex. However, Roschke found agreement between model and experiment poor; moreover, agreement became worse as the aspect ratio (L/D) increased.

Roschke also points out that few closed-form solutions for static pressure distributions in vortex flows have been developed due to difficulties involved in integrating the radial momentum equation. He suggests that the Rankine combined vortex model may be more convenient. Static pressure distributions can, of course, be determined from any tangential velocity profile (Beer and Chigier, 1972).

Perry et al. (1950) have discussed particle entrainment in vortex flow. They cite three forces which act on an individual particle: (1) centrifugal force due to the particle's circular path, (2) the viscous drag of the gas stream, and (3) gravity. If the centrifugal and viscous forces balance for a non-reacting particle at some radius within the vortex, then the particle will move downward in a helical path. However, a particle undergoing gasification will react; the subsequent size reduction will promote movement toward the center of the chamber.

Agrest (1965) describes particle motion in a cyclone chamber with two flow reversals. Air entry is tangential through both primary and secondary zones (Fig. 13), while fuel entry is tangential through the primary zone only. A fuel particle entering here follows a helical

path in the potential flow zone to the annulus of the throat where the first flow reversal takes place. The particle returns to the closed end (floor) in a smaller diameter helix in the rotational flow zone. The turbulent boundary layer separates these two helical paths. Finally, upon reaching the floor, the second flow reversal takes place. The particle, still in the rotational flow zone, follows an even smaller diameter helical path to exit at the throat.

Schmidt (1970) refers to Agrest's chamber as a "rotary flow furnace." However, his description of particle motion differs from Agrest's. According to Schmidt (Fig. 14), particles introduced tangentially at the free vortex sink of the flow move first to the center of the forced vortex, and from there upward along the vortex axis (spout). Centrifugal force moves particles outward from the spout to the potential flow, which runs toward the chamber floor where the cycle starts anew. Heavier particles, which have a greater centrifugal force applied to them, are moved back to the potential flow sooner than finer particles. Consequently, finer particles move further or "higher" along the vortex spout.

Schmidt also reports the results of a cold flow vortex tube investigation. Of particular interest are the axial flows present in the chamber. In one test, secondary tangential air flowed directly to the exit, while primary tangential air flowed to the chamber floor, reversed axial direction and then exited. However, rectangular fences (6 mm high and 1 mm wide) attached radially to the chamber floor induced nearly all the entering air to the floor before a flow reversal carried it to the exit. Furthermore, the tangential velocity profiles were no longer of Rankine form. Thus, axial flow reversals may be strongly affected by the chamber endwall boundary layer.

Other authors have investigated the parameters affecting flow reversal. Roschke (1966a), for example, found axial flow structure strongly controlled by the aspect ratio (L/D); for $L/D < 4$, the number of axial flow reversals tended to decrease as aspect ratio increased.

2. Practical Vortex Reactors

Syred and Beer (1974) identify two main types of industrial cyclones. These are shown in Fig. 15. Type A is commonly used for fuels having high calorific value where slag, ash generation, and ash removal are not much of a problem. Type B is used for high ash content fuels, the combustion of which often results in slag formation.

Baluev and Troyankin (1967a) have thoroughly studied the gas flow pattern in the first type of cyclone. Five distinct annular flow zones were found. These are shown in Fig. 16. Two main downward flows, wall flow 1 and axial flow 3, rotate coaxially. In these two flows the tangential and axial velocities are both at relative maxima. Peripheral intermediate zone 2 is a reverse stream consisting of rising turbulent vortices branching from flows 1 and 3. Radial velocities pass through zero in zone 2, flow being toward the axis at shorter radii and toward the wall at larger radii. In zone 5, direct flow from the top and reverse flow in the exit move against each other. Turbulent mass transfer predominates in zone 4; consequently, the central flows in zone 5 are twisted by zone 3. Axial velocities in zone 4 decrease in the forward direction or even reverse, while the tangential velocities in both zones 4 and 5 increase from the axis toward the periphery. The peripheral recirculation zone present at the bottom of the chamber near the exit is particularly well-developed in chambers with aspect ratios (L/D) in the range 2.4 to 4.0 and with relative exit diameters (D_e/D) in the range 0.3 to 0.4.

The second type of cyclone chamber (B) is often used with only one air/fuel inlet. Velocity profiles, recirculation zones, and pressure distributions within the cyclone thus tend to be uneven and non-symmetrical. A diagram of the flow pattern is given in Fig. 17. Two main areas of reverse flow are distinguishable. One is near the top of the cyclone, inside the annulus formed by the conical outlet; the other is within the main body of the cyclone, at a radius slightly greater than that of the throat.

As shall be seen later, Baluev and Troyankin have studied the effects of variations in geometry on the first type of cyclone.

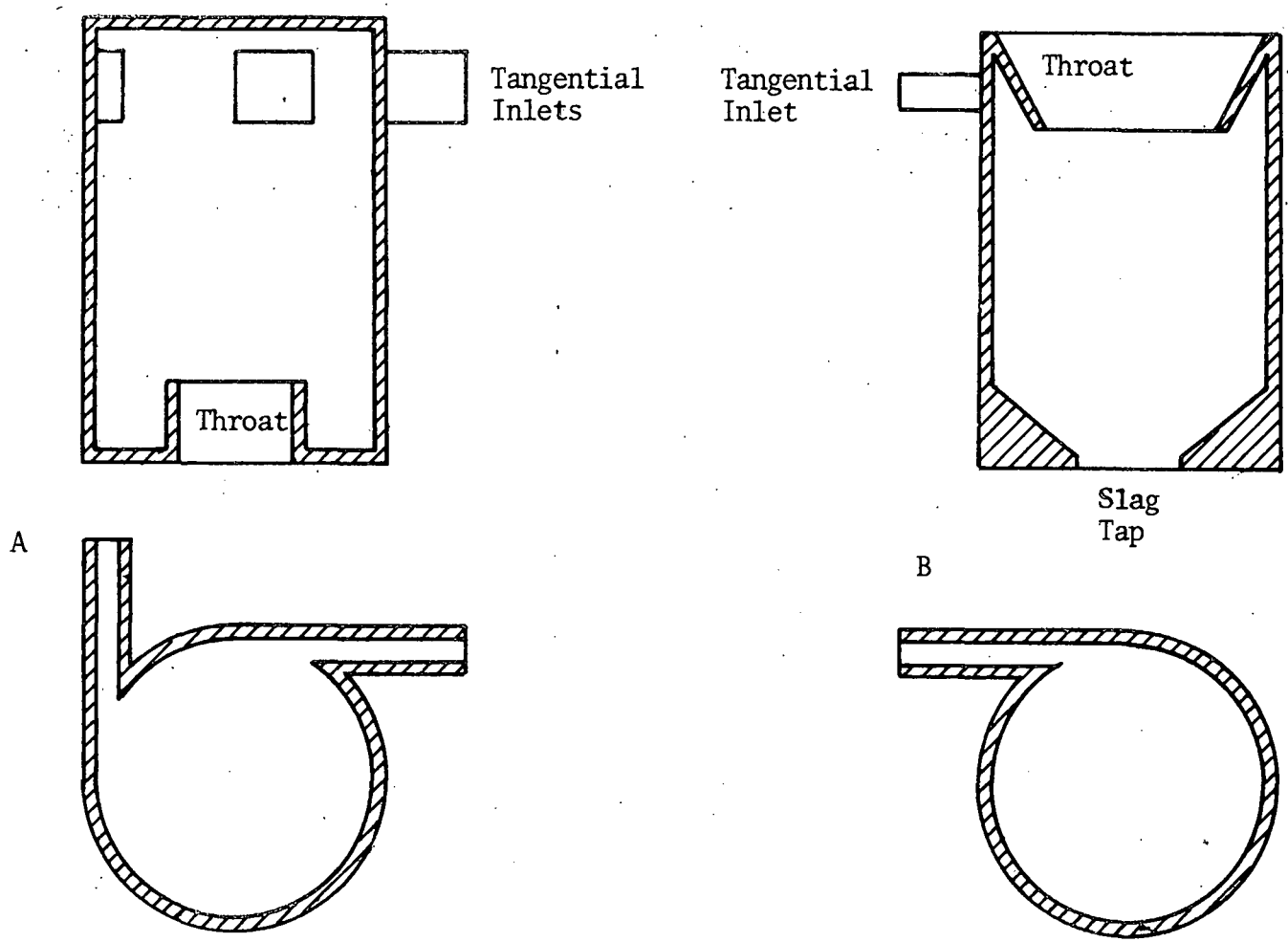

Figure 15. Cyclone Chamber Types (Syred and Beer, 1974)

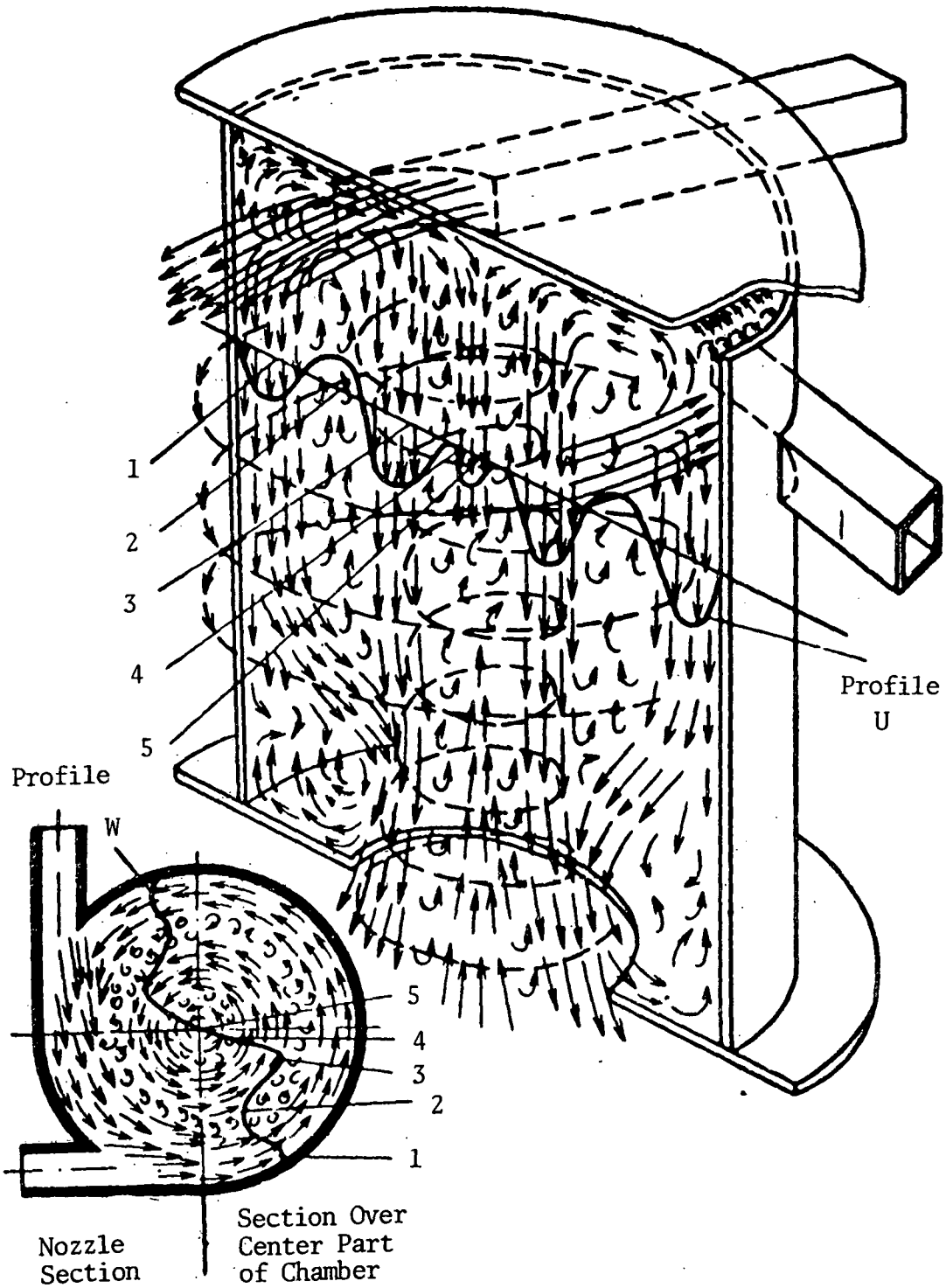

Figure 16. Aerodynamics of Cyclone Chamber: Type A
(Baluev and Troyankin, 1967a)

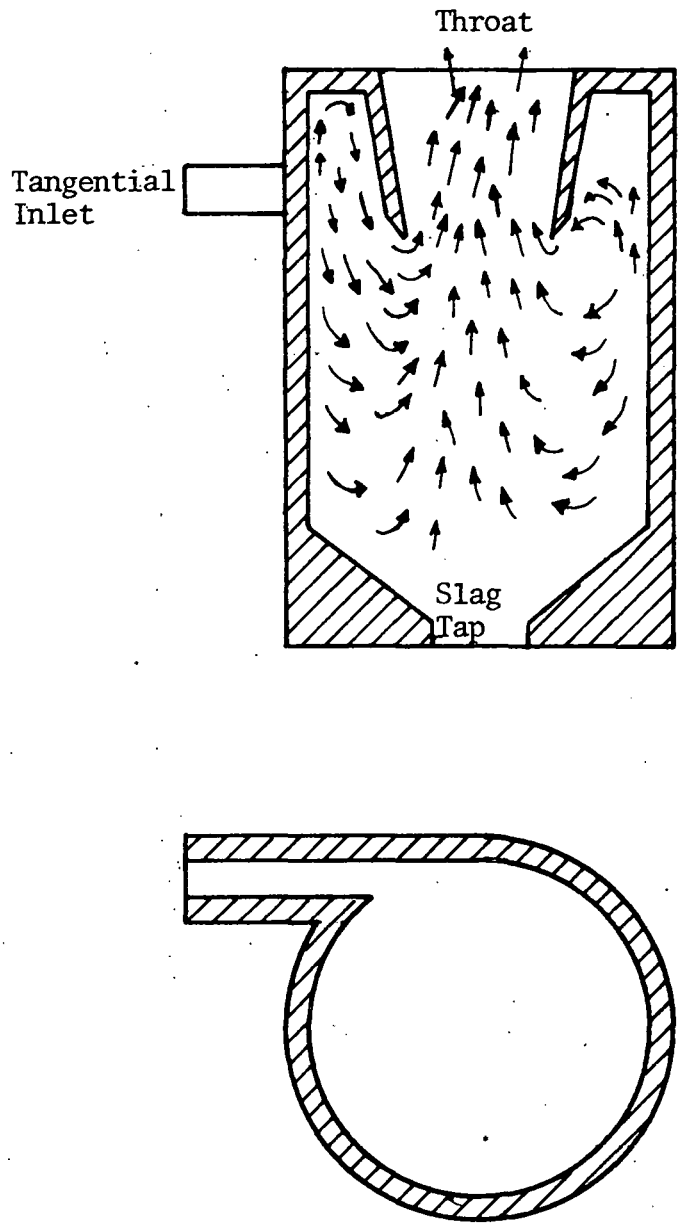

Figure 17. Aerodynamics of Cyclone Chamber: Type B
(Kalishevskii and Ganchev, 1966)

Unfortunately, little information of this sort is available for the second type. However, studies by Dahmen and Syred (1975), Hoy et al. (1958), and von Fredersdorff (1949) provide further insight into cyclones fired with pulverized fuel.

Dahmen and Syred (1975) have designed an experimental cyclone combustor for carbon black waste gas based on the solid-fueled devices described by Agrest (1965) and Schmidt (1970). As in most gaseous vortex systems, tangential entry is evenly distributed along the chamber length. Tangential velocity distributions (isothermal) are similar over the chamber length and follow a Rankine type profile (Fig. 18). The only reverse axial flow zone occurs at the chamber wall and extends over about 70% of the cyclone length. No central reverse flow zone was detected; however, flame observations and static pressure measurements indicate a toroidal recirculation zone at the throat.

Hoy et al. (1958) have investigated the combustion of crushed coal in a small cyclone combustor. Primary air and coal enter through secondary tangential nozzles (Fig. 13). Secondary air enters axially through a secondary annular swirl vane assembly (Fig. 13). Combustion products leave through a centrally located throat in the chamber roof. This configuration is a variation of type B in Fig. 15. No detailed flow information is provided. However, tangential velocity data indicate that swirl weakens as flow approaches the chamber floor.

The continuous gasification of powdered coal suspensions in a vortex chamber has been investigated by von Fredersdorff (1949). Two chamber arrangements were tested. The first consisted of two concentric cylinders. The coal suspension was introduced tangentially at the top of the inner cylinder and followed a tight helical path to the bottom of the inner cylinder where the flow was discharged to the outer cylinder. Auxiliary oxygen, air, and/or steam were introduced tangentially at the bottom of the outer cylinder; the combined flow then followed an upward helical path, exiting tangentially at the top of the annular region. In the second arrangement, the inner cylinder was eliminated. The coal suspension was introduced tangentially at the bottom of the chamber. Flow followed an upward helical path to exit tangentially at

the top. Auxiliary steam could be added at the top of the chamber if needed. In this arrangement, no zones of reverse flow were present.

B. Flow Entry and Exit

Methods of reactant entry and product exit influence the type and location of reaction and the residence time of the reactants. In autothermic gasification processes, for example, exothermic combustion reactions are required to supply the heat for the endothermic gasification reactions. The combustion reactions will generally occur in the oxygen-rich zones, while the gasification reactions occur in the oxygen-depleted zones. Consequently, it is important that oxygen be supplied only to those areas of the chamber intended for combustion, and that the chamber exit be accessible to the gasified products. Obviously, sufficient residence time must be provided for these reactions to take place.

It is important to distinguish particulate residence time from gas residence time. Gas residence time is determined primarily by reactor volume and volumetric flow rate. Particulate residence time can be significantly longer due to particle recirculation (Schmidt, 1970). Agrest (1965) reported particulate residence times 12 to 15 times longer than gas residence times in a non-slagging operation. Semenov and Semenenko (1969) describe how, in a slagging reactor, a coal particle will continually interact with the molten wall layer until it burns to such a size that it is carried away by gas flow.

Particulate residence time and reactant location can obviously be controlled by appropriate chamber injection methods, since these control mixing history. The two primary methods employ axial or tangential injection. Using a CO_2 tracer gas, Schmidt (1970) found that the central axial introduction of gaseous fuel was far from ideal and gave poor mixing of fuel and air. Tangential introduction of fuel yielded much better results. The number and size of tangential nozzles can also affect the flow field, since nozzle velocities will vary (Schmidt, 1970).

Strickland (1973) tested a vortex chamber having either axial coflow or counterflow. Axial flow entry is through the primary

zone (Fig. 13); tangential flow is primary in the coflow case, secondary in the counterflow case. Flow exits the chamber both axially and tangentially. Strickland found that the coflow configuration resulted in a more stable flow pattern than did the counterflow arrangement. In both cases, however, highest mass retentions (the percentage of the entering axial mass flow retained in the exiting axial mass flow) were possible when the inlet axial flow Reynolds number (Re_c) was low compared to the inlet tangential flow Reynolds number (Re_v). Under these conditions the dominant mode of mixing is vortex entrainment in the core. On the other hand, at lower Re_v core flooding of the vortex region occurs.

In most cyclones, however, entry is purely tangential; occasionally, tangential nozzles are canted a few degrees to provide a slight axial velocity component. Central axial exits predominate; an exception is the top tangential exit used by von Fredersdorff (1949).

C. Geometric Chamber Parameters

Table XI presents typical values of the important geometric chamber parameters for a variety of cyclone chambers. Various chamber dimensions are illustrated in Fig. 19. The effects of each geometric parameter on chamber design are considered in the following subsections.

1. Swirl Number, S

Tangential flows in free jets or flames are commonly characterized by a non-dimensional parameter known as the swirl number. Syred and Beer (1974) define the swirl number as the ratio of the axial flux of angular momentum to the axial flux of linear momentum divided by a characteristic length, the exit radius of the burner nozzle. In equation form

$$S = G_\phi/(G_x R)$$

where

$$G_\phi = \int_0^R U(\rho W r)2\pi r dr = c_3,$$

TABLE XI

TYPICAL VALUES OF GEOMETRIC CHAMBER PARAMETERS

Authors	S	L/D	D_e/D	N	A_t/A_e	δ/D	a/L	h/b
Elliott et al. (1952)		0.1-1.5		8				5.3
Baluev and Troyankin (1967b)		1.0-4.0	0.3-1.0	1-4	0.045-0.394	0-0.011	0.07-0.45	0.3-3.3
Syred and Beer (1974)	2-20	1.0-3.0	0.4-0.7	1-4				
Dahmen and Syred (1975)		2.6	0.4-0.5	16	0.261-0.464			

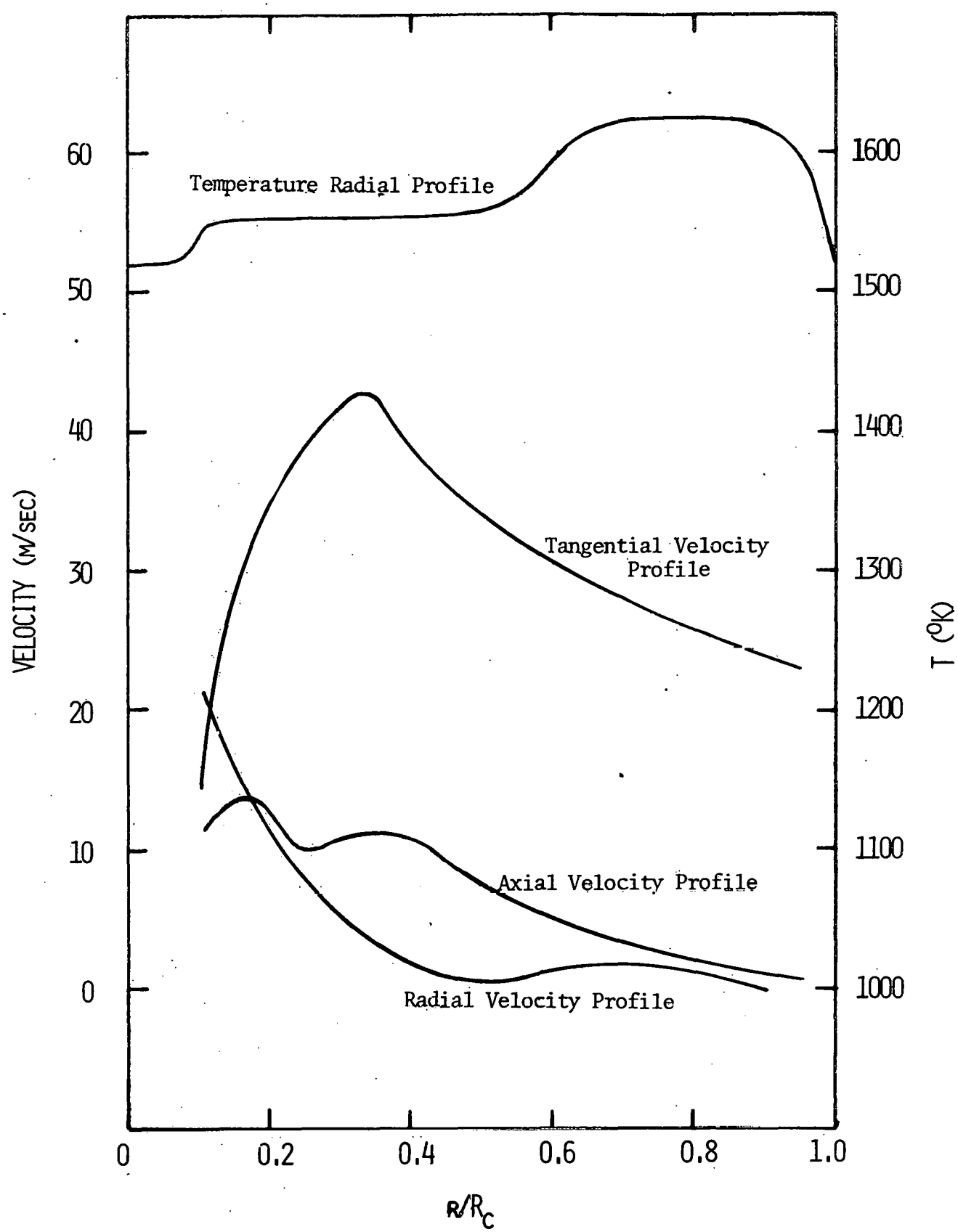

Figure 18. Velocity and Temperature Profiles in a Cyclone Chamber (Dahmen and Syred, 1975)

$$G_x = \int_0^R U(\rho U)2\pi r dr + \int_0^R p \cdot 2\pi r dr = c_4 .$$

Syred and Beer point out that the swirl number has not been used to characterize cyclones, but suggest that this may be done and that a means for comparing cyclones to swirl burners may be provided in the process. Thus, when a uniform exit axial velocity profile is assumed (Syred and Beer, 1974), $S = (\pi D_e D)/(4 A_t)$. This swirl number applies only to isothermal flows. Typical values of S vary from 2 to 20, depending on the cyclone type.

Under combustion conditions, flows generally are not isothermal. Inlet angular momentum stays approximately constant, but, due to the accelerating effects of combustion, the axial momentum of the fluid stream leaving the cyclone chamber is increased. Consequently, the swirl number is lower under combustion conditions than it is under isothermal conditions. As a suitable relation between the two swirl numbers, Syred and Beer offer the following:

$$S = S_{isothermal} \times T_{inlet}/T_{outlet} .$$

For some cyclones, combustion can reduce the swirl number by as much as 80%.

2. Chamber Diameter, D

The chamber diameter, by itself, is of significance only in a limited sense. Cyclones used in industrial applications generally have large heat release rates; hence, heat loss to the chamber walls represents only a small fraction of the total heat available. However, as chamber size is reduced to laboratory scale, the fractional heat loss becomes increasingly greater due to an increase in the surface to volume ratio. Consequently, in small chambers such as the 20 cm diameter chamber employed by Yagi and Kunii (1957), external heating of chamber walls becomes mandatory.

3. Aspect Ratio, L/D

Baluev and Troyankin (1967b) have done an extensive study of the effects of aspect ratio on the aerodynamics of type A cyclone chambers (Fig. 15). As L/D increases, tangential velocities diminish throughout the chamber volume. Also, flow 1 is intensified compared to flow 3 (Fig. 16). For $L/D \geq 2.5$, flow reversals in zones 4 and 5 disappear; one central descending flow predominates.

The relationship between the split (ascending and descending) flows of zone 1 also changes with increasing aspect ratio. At $L/D = 4.0$ and $D_e/D = 0.5$, the descending flow contains a substantially greater percentage of gas than the rising flow and the maximum tangential velocity in zone 1 is greater than in zone 3; at $L/D = 1.5$ and $D_e/D = 0.5$, these values are similar.

Baluev and Troyankin also found that increasing the aspect ratio varied the influence of other design parameters. The effect of throat diameter diminishes with increase in aspect ratio, as does the effect of the number of nozzles.

Roschke (1966a) found the aspect ratio ($0 < L/D \leq 12$) to have a strong influence on water flow in his confined, jet-driven vortex tube, especially for $0 < L/D < 4$. At these lower values, flow was dominated by endwall boundary layers and their interaction with the primary vortex flow. In general, as L/D increased, the diameter of the vortex core decreased. Axial flow patterns were not notably affected by changes in mass flow rate at low L/D values, but significant effects were sometimes observed at larger aspect ratios. Turbulence appeared to increase with aspect ratio; however, no turbulence was evident in the core region.

Baluev and Troyankin (1967b) recommend $1.5 \leq L/D \leq 1.8$; gas residence times are adequate and operation satisfactory.

4. Relative Throat Diameter, D_e/D

According to Baluev and Troyankin (1967b), the relative throat diameter appreciably affects (1) the mass ratio of gas in the rising and descending branches of the tangential streams and (2) the decay of

the tangential inlet velocity (Fig. 16). In a throatless chamber ($D_e/D = 1$), rising flow is almost non-existent. Flow 3 is much weaker than flow 1, and, consequently, only one clearly pronounced tangential velocity maximum, situated on the periphery, is present. At $D_e/D = 0.5$, percentages of gas in the rising and descending flows are nearly equal. As D_e/D continues to decrease, flow 3 becomes stronger at the expense of flow 1, and eventually one powerful central descending flow develops in zones 4 and 5 with reverse streams and dips disappearing.

Recommended values of D_e/D are 0.4 to 0.7. This range evidently combines sufficient mixing with reasonable drag losses.

5. Number of Tangential Nozzles, N

Ustimenko and Bukhman (1968), Baluev and Troyankin (1967b), and Syred and Beer (1974) all recommend the use of two or more nozzles to achieve greater symmetry. Baluev and Troyankin found that when a single nozzle is used, the axis of the main flow 3 does not coincide with the chamber axis. The distribution of axial velocities is less symmetrical and more irregular than that of tangential velocities. This non-symmetry of the aerodynamics with one tangential nozzle is particularly characteristic of chambers with $L/D \geq 1.5$ and $D_e/D \geq 0.5$. An increase in N is especially advisable for long chambers.

6. Relative Tangential Inlet Area, A_t/A_e

The A_t/A_e ratio noticeably affects the tangential and axial velocity profiles within the chamber. As this ratio increases, the saddle-like velocity profiles smooth out due to a decrease in axial and tangential velocities in zone 1 (Fig. 16). Flow reversals in zones 4 and 5 are replaced by a strong central descending flow. Typically, the A_t/A_e ratio falls within the range 0.04-0.4.

7. Relative Wall Roughness, δ/D

Baluev and Troyankin (1967b) report that the extent of roughness formed by ash fusion appears to range from $\delta/D = 0.005$ to $\delta/D = 0.011$,

depending on the cyclone diameter and the fuel characteristics. Increases in δ/D tend to decrease and tangential velocity maxima (zones 1 and 3), as well as the axial flow in zone 3. The zone 3 flows are the most strongly affected. Since flow 3 moves above the nozzles and under the roof, the roughness of these surfaces strongly determines the chamber aerodynamics as a whole.

Although Hoy et al. (1958) do not concern themselves with wall roughness, they do mention a different dimensionless parameter which is related to frictional drag. They cite the ratio of the internal surface area of the cyclone to the area of the air inlets. As this ratio decreases, the effectiveness of inlet velocity in producing swirl should increase. Measurements taken during operation with two swirl vane assemblies of different port area lend credibility to this conclusion.

While wall roughness is generally considered undesirable, Dahmen and Syred (1975) found that it actually improved their operation. Surface roughness resulted in increased stability limits for flames formed with weak waste gas. Smoother temperature profiles were obtained over most of the cyclone length during operation with rougher walls due to the increased radiative heat exchange brought about by increased surface area. Thus reactor performance can be enhanced by appropriate selection of surface material.

8. Relative Tangential Nozzle Position, a/L

The position of the tangential nozzles relative to the chamber roof, a/L (Fig. 19), governs the mass ratio of rising to descending flow and, therefore, the relationship between the magnitudes of the main flows 1 and 3 in the Baluev and Troyankin model (Fig. 16).

Varying nozzle position most strongly affects axial velocity distributions. With the nozzles very near the roof (a/L = 0.067), zone 1 axial flow is at its strongest, while zone 3 is at its weakest. As a/L is increased to 0.45, axial velocities decrease in zone 1 and increase in zone 3. Reverse flow 2 disappears. Tangential velocities throughout the chamber are relatively high at a/L = 0.06-0.1. However, as a/L approaches 0.5, tangential velocity maxima increase over most of the chamber.

The experimental data show that the nozzles should be positioned in the range $0.08 \leq a/L \leq 0.15$. Apparently, this range balances axial flows 1 and 3, while maintaining reverse flow 2 and strong tangential velocities. However, Baluev and Troyankin suggest that the type of fuel to be used, the method of fuel supply, and special features of the plant process be taken into account when selecting the nozzle position.

9. Tangential Nozzle Configuration, h/b

Baluev and Troyankin have concluded that the configuration of rectangular tangential nozzles does not exert a decisive effect on the aerodynamics of a cyclone chamber. Again, however, they suggest considering the class of fuel to be used and the nature of the plant process when selecting the nozzle configuration.

D. Combustion Effects in Cyclone Chambers

Syred and Beer (1974) present a fairly complete compilation of what is known about combustion effects in cyclone chambers. They point out, however, that there is far less information in this regard on cyclones than on swirl burners because the combustion of solid fuels, for which the cyclone has almost always been used, is not conducive to facility in measurement.

Flow patterns produced under burning conditions are usually similar to those in the isothermal state. Schmidt (1970), for example, comments on flame patterns for a vortex tube burning methane and propane. For cold flow studies, propane was replaced with carbon dioxide, whose concentration is more easily measured and whose molecular weight matches that of propane. Concentration profiles of carbon dioxide compared favorably with the flame patterns.

In a similar vein, Dahmen and Syred (1975) found that temperature measurements under combustion conditions substantiated velocity profiles obtained under isothermal conditions. Figure 18 illustrates typical velocity and temperature profiles found in the chamber. The velocity profiles indicate the presence of a reverse flow/recirculation

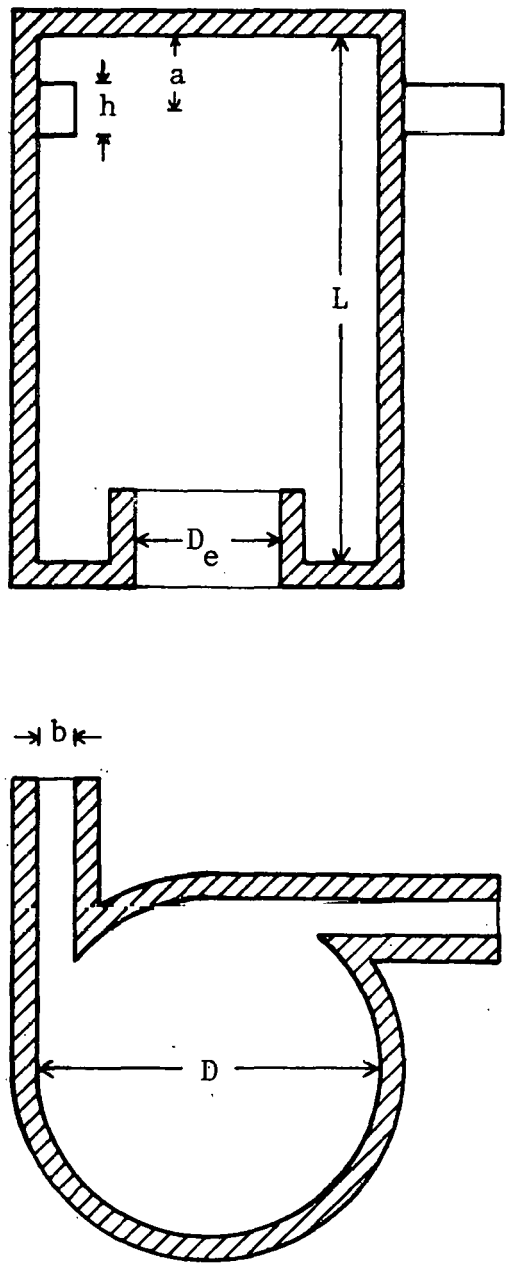

Figure 19. Chamber Dimensions for Geometric Parameters

zone close to the wall, where temperature is the highest. This combustion-promoting mixing zone (in addition to radiative heating from the chamber wall) apparently accounts for the higher temperature.

Syred and Beer believe that with due caution isothermal results can often be extrapolated to burning conditions. The combustion process seems to occupy most of the cyclone chamber volume; hence, strong radial density and pressure gradients, responsible for differences between isothermal and combustive states in many swirl burners, do not exist. However, we should note that combustion conditions tend to lower the swirl number.

An indirect effect of combustion on cyclone flow occurs under slagging conditions. The ash in solid fuels, especially coal, becomes molten at high temperatures ($T > 1600\ ^{o}K$). Coal particles interact with the resultant slag film formed on the cyclone walls, thus enhancing particulate residence time and carbon conversion. Although cleaner operation results due to reduced fly ash, chamber design possibilities are limited to prevent clogging and to permit slag removal.

E. Aerodynamic Resistance of a Cyclone Reaction Chamber

Tager (1971) has presented a method for calculating the aerodynamic drag of a cyclone. His analysis originates with the equation

$$\Delta p_c = \zeta_c \, (W_{in}^{2} \rho_{in})/2,$$

where Δp_c is equal to the pressure differential between the secondary air plenum and the chamber exhaust. This relation, obtained by analogy from the Bernoulli equation, does not allow the contributions to drag by different elements of the cyclone to be taken into account on an individual basis. Consequently, Tager splits the total drag into two terms:

$$\Delta p_c = \Delta p_a + \Delta p_{cc}$$

where Δp_a equals the pressure differential between the secondary air plenum and the cyclone chamber, and Δp_{cc} equals the pressure differential

between the cyclone chamber and the chamber exhaust. Essentially, Δp_a is the drag of the air distribution system and Δp_{cc} is the drag of the combustion chamber proper.

The energy lost due to the pressure drop across the air distribution system is a measure of the swirl imparted to the flow. On the other hand, the pressure drop across the chamber itself is due to vortex formation, wall friction losses, particle transportation, and exit losses at the throat. Of these latter losses, the pressure loss at the throat predominates.

The temperature and volume of combustion products at the exit of the cyclone are dependent on loading, type of fuel, completeness of combustion, heat losses, air temperature, and excess air. The velocity of products at the cyclone exit also depends on the ratio of throat diameter to cyclone diameter, D_e/D. Consequently, it can be seen that the aerodynamic drag of the cyclone is related both to combustion conditions and structural characteristics.

Cold model resistance data cannot be blindly transferred to an operating furnace since flow pattern and swirl may not be identical under the two conditions. Swirl number, for example, can change significantly. Tager recommends determining values of the resistance coefficient ζ under combustion conditions. However, this step is only necessary for the cyclone chamber, since the air distribution system operates at nearly isothermal conditions. Separate expressions for the resistances of the air distribution system and the reaction chamber will now be considered.

1. Resistance of the Air Distribution System

1.1 Secondary Air. The general form of the aerodynamic drag of the air distribution system is given by

$$\Delta p_a = \zeta_a \, (W_{in}{}^2 \rho_{in})/2$$

where ζ_a is the resistance coefficient of the air distribution system, W_{in} is the velocity of the tangential air in the exit cross-section of

the air inlets, and ρ_{in} is the density of the air (or air-dust mixture for premixed fuel) in the same cross-section. The W_{in} term is easily calculated from knowledge of inlet pressure and temperature, A_t and the tangential air flow rate at standard conditions.

The resistance coefficient is usually determined by running cold air through either a model of the air distribution system or the full scale cold furnace. Reynolds numbers obtained for this arrangement are normally between 5×10^4 and 1.2×10^5. This corresponds to the similarity region and determines the validity of transferring the found values of ζ_a to the full scale arrangement. Typically, ζ_a = 1.1-1.8 for vane swirlers and ζ_a = 1.3-2.0 for tangential injectors.

1.2 Premixed Air and Fuel. When premixing of pulverized fuel is taken into account, determination of the resistance coefficient becomes more complex. Naturally, one would assume that the aerodynamic resistance of the air distribution system would increase due to consumption of flow energy by particle acceleration and transportation.

As the absolute dimensions of the gasifier increase, particles have a greater distance over which they can be accelerated, and, consequently, more closely approach the flow velocity. This leads to greater energy consumption and, therefore, greater resistance. Tager recommends that resistance coefficients be calculated specially for each case.

For the special case where it can be assumed that the fuel particles are fully accelerated to the air flow velocity (i.e., fully entrained), a standard procedure for calculating air distribution coefficients has been adopted. An empirical expression for the resistance coefficient is given by

$$\zeta_{ad} = \zeta_a (1 + \kappa) + 2\kappa$$

where ζ_{ad} is the resistance coefficient of the air distribution system in operation with dust-laden air. The κ term is the mass concentration of dust, which is calculated by dividing the mass flow rate of fuel by

the mass flow rate of the air. The pressure drop across the air distribution system is then calculated by substituting the value of ζ_{ad} into the relation given above for the aerodynamic drag of the air distribution system.

An acceleration coefficient K, defined as the ratio of kinetic energy of the pulverized fuel at its actual velocity to its theoretical kinetic energy at the air flow velocity, can now be introduced to allow for the general case of only partial acceleration of the particles. This ratio reduces to

$$K = (W_{fuel}/W_{in})^2$$

The final expression for the air/fuel distribution resistance coefficient is now given by

$$\zeta_{ad} = \zeta_a \ (1 + K\kappa) + 2K\kappa$$

This value can now be used to calculate the pressure drop across the distribution chamber.

2. Resistance of the Reaction Chamber

The resistance expression for the cyclone chamber proper remains to be investigated. It is given by

$$\Delta p_{cc} = \zeta_{cc} \ (U_{out}{}^2 \rho_{out})/2$$

where ζ_{cc} is the resistance coefficient of the combustion chamber, U_{out} is the average axial velocity of reaction products at the exit cross-section, and ρ_{out} is the density of the reaction products at the average exit design temperature T_D. The U_{out} term is calculated from the fuel mass flow rate, A_e, and the gas volume per unit mass of fuel at standard conditions. The quantity T_D is calculated from a heat balance equation with allowance for such parameters as the amount of fuel burned, the amount of air blown in, the completeness of reaction, heat transfer,

and the dissociation of carbon dioxide and water at high temperatures. Experimental data indicate that ζ_{cc} is a function of exit Reynolds number: ζ_{cc} gradually decreases with increasing Reynolds number ($Re_{ex} > 5 \times 10^4$), approaching a constant value at $Re_{ex} > 10^5$ (Tager, 1971).

It was implied earlier that the dimensionless parameter D_e/D is related to the drag of the cyclone chamber. Furthermore, depending on use, relative diameters of exit ports may vary from one cyclone to another. Consequently, it has been found convenient to relate a relative drag term for the reaction chamber to the relative diameter of its exit port.

The relative drag term, $\Delta p_{cc}/(\Delta p_{cc})_{.45}$, is defined as the ratio of the actual drag of the chamber at the actual D_e/D value to the drag of the same chamber with $D_e/D = 0.45$. In Fig. 20, data from both vertical (either top or bottom gas exits) and horizontal chambers are plotted and found to share a common dependence, thus lending support to Tager's claim that exit losses predominate in the cyclone chamber. A suitable curve fit for the data has been found. It is given by

$$\Delta p_{cc}/(\Delta p_{cc})_{.45} = 0.9/(D_e/D) - 1$$

where D_e/D ranges in value from 0.3 to 0.7. Thus:

$$\Delta p_{cc} = [\zeta_{cc}(U_{out}{}^2\rho_{out})/2]_{.45}\,[0.9/(D_e/D) - 1] \quad .$$

Typically, $\zeta_{cc} \simeq 1.5\text{-}4.0$, depending on the type of exit port. For a simple vortex chamber, $\zeta_{cc} \simeq 2.0$; for cyclone type B, $\zeta_{cc} \simeq 4.0$.

Syred and Beer (1974) question the validity of Tager's approach; however, they indicate that this method accurately predicts the pressure drop in the Agrest combustor, as well as other cyclone chambers. Typical values of Δp_c (Hoy et al., 1958) range from 400 to 760 kgf/m^2 (16 to 30 inches of water).

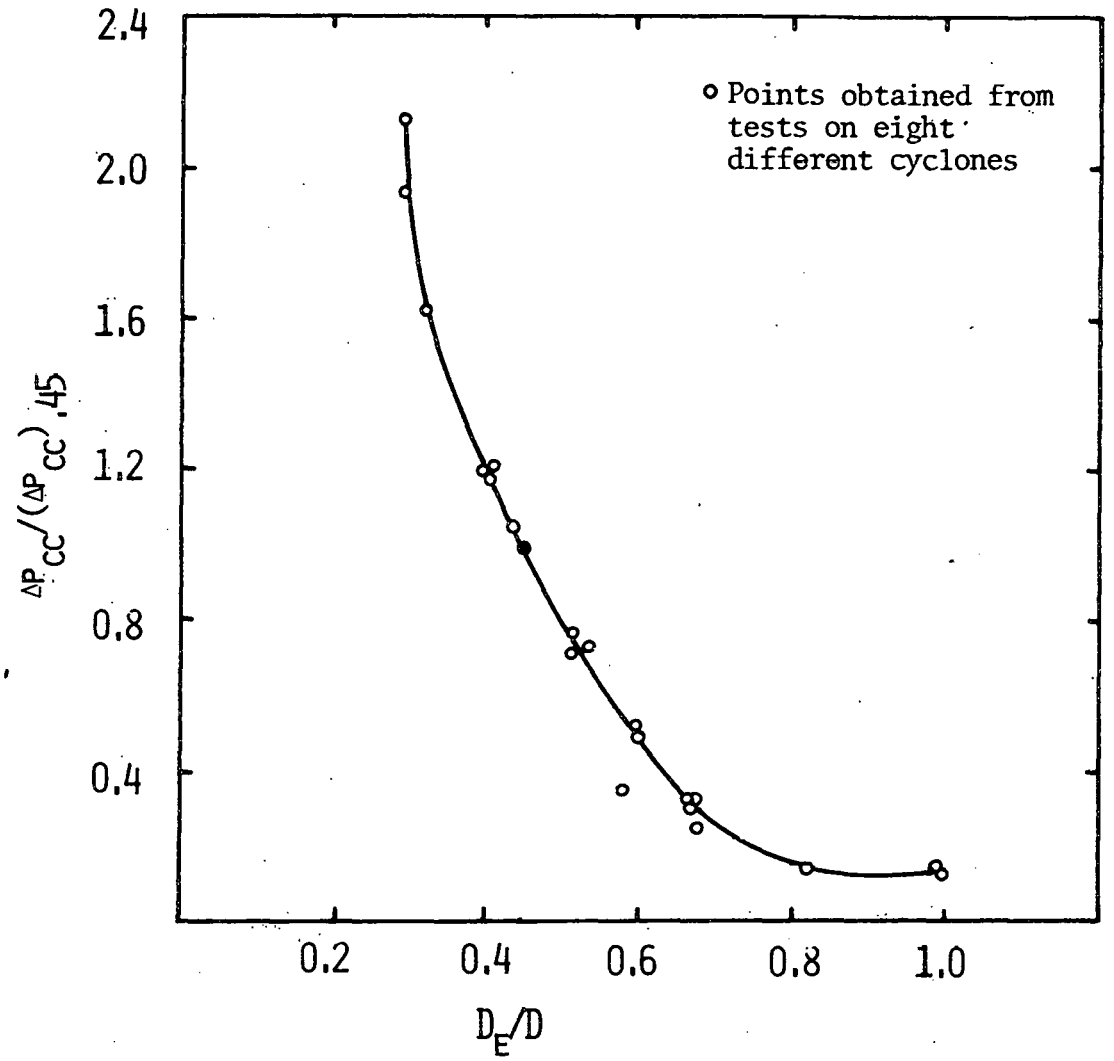

Figure 20. Dependence or Relative Drag of Cyclone Combustion Chambers (without air distribution losses) on D_e/D (Tager, 1971)

V. A PRELIMINARY REVIEW OF PULVERIZED COAL COMBUSTOR MODELS

A. Introduction

A preliminary review of pulverized coal combustor models was made to investigate modeling possibilities for coal gasification in entrained flows, particularly the cyclone chamber. The eventual goal is to formulate a simple model which will at least reveal gasification trends. Results of an equilibrium coal gasification model based on the NASA SP-273 computer program (Gordon and McBride, 1971) have been included and compared with the coal gasification literature.

A pulverized coal combustor model generally requires three types of information: the flow pattern and mixing, the heat transfer (internal and external), and the reaction rates which include devolatilization, gaseous combustion and surface burning. Because of the complexity of these phenomena, many simplifying assumptions must be chosen to formulate a theoretical model.

B. Mixing Theories

Mixing theories can be divided into two basic categories, the population balance theories and the mechanistic theories (Pratt, 1974). Population balance theories are concerned with residence time distributions (RTDs) and include such simple models as the perfectly stirred reactor and the plug flow reactor. Mechanistic theories are concerned with modeling turbulent flow phenomena, starting from the governing differential equations.

1. The Perfectly Stirred Reactor (PSR)

In perfectly stirred reactor theory, the incoming reactant streams enter a reaction volume in which mixing occurs at an infinite

rate. All properties in the reaction volume are uniform and are identical to those of the exit stream. The PSR is therefore known as a zero order model as there is no variation of properties with position within the reaction volume.

Two types of mixing, known as micromixing and macromixing, have been defined for PSR modeling use. In the micromixing case, complete mixing occurs on the molecular level, such that molecular homogeneity is present throughout the reaction volume. The macromixing case assumes that the reactants form relatively small pockets or fluid particles, which are evenly dispersed throughout the reactor volume. The molecules of a given fluid pocket are assumed to be completely mixed within that pocket, but they do not come into contact with molecules of other pockets. In an actual reactor, mixing occurs as some type of compromise between micromixing and macromixing.

The PSR model is applicable whenever the reactants are dispersed throughout the reaction volume in a time much less than the mean residence time $\bar{\tau}$. The residence time distribution $\psi(t)$ is useful for calculation purposes and is of the form

$$\psi(t) = \bar{\tau}^{-1} \exp(-t / \bar{\tau})$$

where

$$\bar{\tau} = V/\dot{V}$$

and V is the reaction volume and $\dot{V}$ is the volume flowrate of reactants. This RTD can represent either the individual molecules for the micromixed case or the fluid particles for the macromixed case.

Although no internal heat transfer is considered in the PSR model, external heat transfer can be included. Previous models, however, have only accounted for radiation transfer to the reactor walls (Table XII).

2. The Plug Flow Reactor (PFR)

Plug flow reactor theory assumes complete mixing in the radial direction with no mixing in the axial direction (direction of flow).

Any cross section normal to the flow is homogeneous and has uniform velocity; therefore, all fluid particles leaving the reactor have identical histories and residence times. Because these assumptions are unrealistic for combustor modeling, some modifications are usually included in PFR models.

PFR modifications are often made to include backmixing and heat transfer effects. Figure 21 illustrates the types of modifications that are included in PFR models while keeping the model one dimensional. Heat transfer for the PFR model is often simplified by using an isothermal or internally adiabatic assumption. The isothermal model assumes an average temperature throughout the chamber, while the internally adiabatic model assumes there is no heat transfer between fluid slices in the axial direction. External heat transfer can be included regardless of the internal heat transfer assumptions.

Backmixing is modeled by breaking the reaction volume into radial sections of uniform composition and temperature. Recirculated products and/or secondary air of known properties are then brought into each section. Iterative methods for calculating temperature and composition can be used until steady state conditions are achieved (Field et al., 1967).

3. Mechanistic Mixing Models

Mechanistic theories attempt to model turbulent phenomena directly rather than assume some type of mixing. The classical approach to this problem begins with the governing differential equations of mass, momentum, energy, and chemical species, along with the appropriate boundary conditions and simplifying assumptions. The resulting Navier Stokes equations can be solved by finite difference techniques.

The turbulent phenomena can either be modeled directly by choosing a computational mesh much smaller than the turbulent length scale, or indirectly by choosing a computational mesh larger than the length scale. Some work has been done using the direct technique without chemical reaction (Lumley et al., 1973; Harlow et al., 1971). Inclusion of chemical reaction is well beyond present numerical techniques

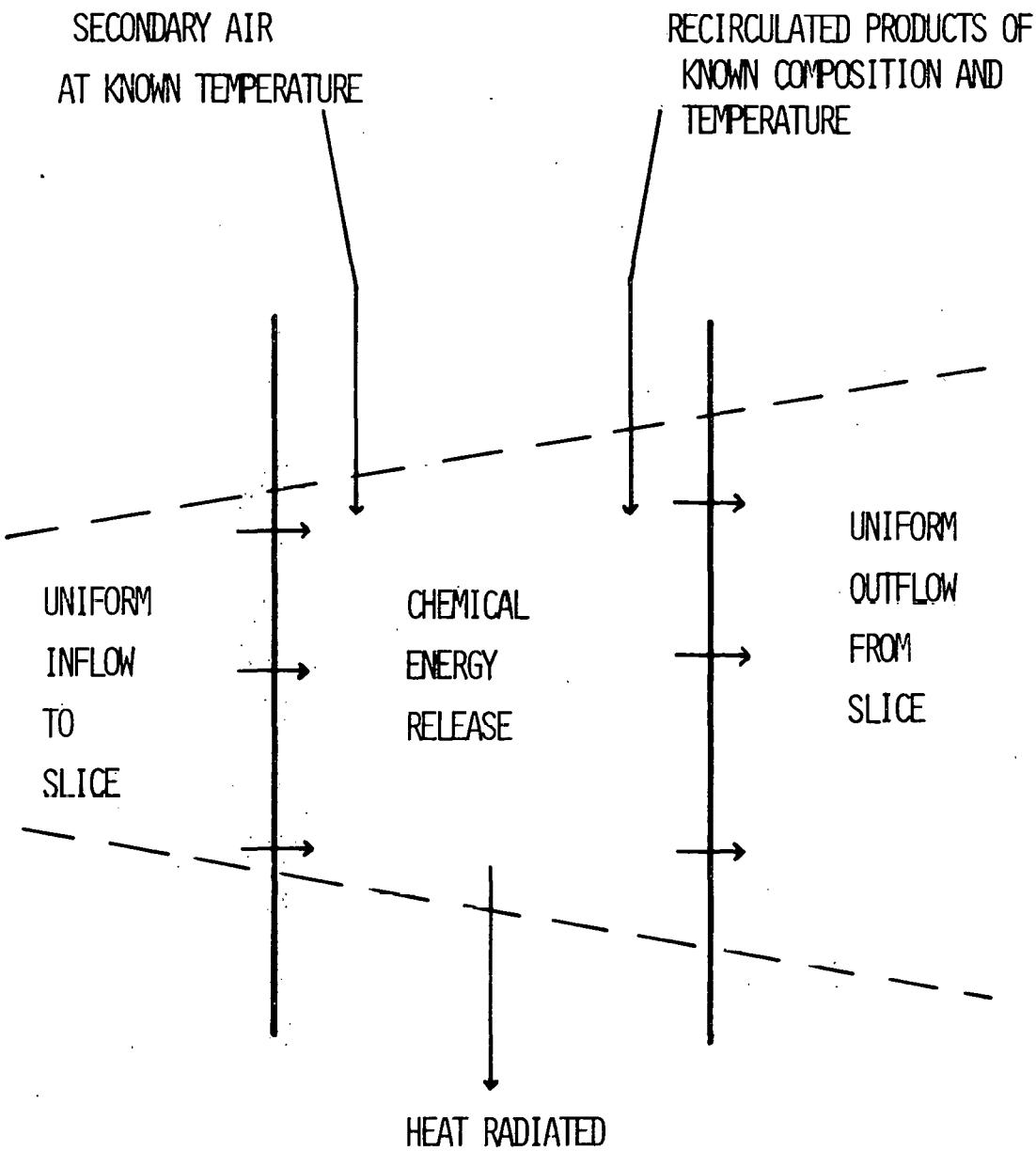

Figure 21. Extended One-dimensional Plug Flow Model (Field et al., 1967)

for direct (small mesh) turbulence modeling and therefore the indirect method is the serious candidate for future modeling use (Pratt, 1974).

The procedure in using the indirect, large mesh approach starts with the conservation equations in terms of time-steady and fluctuating components (Beer and Chigier, 1972). The resulting equations are known as the Reynolds equations, and the new terms which appear, that are not present in the laminar equations, are known as the Reynolds stresses. Solution procedures depend on how the Reynolds stresses are modeled and discussions of these methods are given by Mellor and Herring (1973) and Launder and Spalding (1972).

Regardless of the solution procedure, mechanistic models are weak in dealing with combustion chemistry and are unable to deal with the coupled effects of species concentration and temperature fluctuation (Pratt, 1974). Such a model applied to a pulverized coal combustor would have the added difficulties of modeling two phase flow, which involves solving conservation equations for both the gas and particles along with the coupling equations between phases (Crowe and Pratt, 1972).

C. Kinetic Modeling of Pulverized Coal Combustion

Many attempts have been made to model the kinetics of pulverized coal combustion. Only those which pertain to combustor modeling are considered here. In all models of Table XII, the burning rate of the volatiles was assumed infinite and thus only char combustion was considered. This approximation is reasonable as combustion of the volatiles takes only milliseconds, once they are mixed with air (Field et al., 1967).

Several different methods have been used to model char combustion. Theoretical char burning models usually assume combustion to be diffusion controlled, chemically controlled or both. This can be expressed by the equation

$$B = p_{ox}/(1/K_D + 1/K_C)$$

where B is the burning rate, p_{ox} is the oxygen partial pressure, K_D is the rate of oxygen diffusion to the particle surface, and K_C is the

chemical reaction rate at the surface (Beer, 1972). Field et al. (1967) suggest expressions for both K_D and K_C. From correlation of experimental data the expression

$$K_C = P \exp(-E/R_u T_s)$$

was developed, where P is a pre-exponential factor, E the activation energy, R_u the universal gas constant, and T_s the particle surface temperature. A theoretical expression for K_D is developed by Field et al. (1967) for a spherical carbon particle surrounded by a relatively thick stagnant gas layer through which oxygen diffuses. Assuming a mean temperature T_m in the stagnant layer, we have

$$K_D = 24\ \alpha\ k_D/d_p\ R_u\ T_m$$

where α is a mechanism factor ($\alpha = 1$ when CO_2 is the primary product and $\alpha = 2$ when CO is the primary product), k_D is the oxygen diffusion coefficient, and d_p is the particle diameter.

All models of Table XII use theoretical kinetics which consider both the oxygen diffusion rate and the chemical reaction rate, with the exception of the Beer and Lee (1965) model, which uses an empirical expression. Beer and Lee (1965) formulated an expression from data obtained via anthracite dust cloud experiments in a plug flow furnace. An equation for the burning rate of the form

$$B = c\ A\ p_{ox}\ T^{-1/2} \exp(E/R_u T)$$

was developed where c is an experimental constant and A the particle surface area. Such empirical models are usually easy to employ into overall combustor models, but they often fit only a narrow range of conditions (Field et al., 1967; Beer and Lee, 1965). Most dust cloud experiments have been done for anthracite and semi-anthracite, but little has been done for the more highly reactive lower rank coals.

TABLE XII

MATHEMATICAL MODELS FOR PULVERIZED COAL COMBUSTION
(Field et al., 1967)

Flow Type	Reference	Coal Size Distribution	Reaction Rate Dependency	Internal Heat Transfer	External Heat Transfer
Plug flow with controlled mixing	Vulis (1961)	Not specified	Diffusion or chemical control (fuel-rich case only)	Crude allowance for radiation back from flame, otherwise adiabatic	None
	Hedley and Jackson (1968)	Monosize	Semi-empirical power function of temperature oxygen concentration and particle size	Adiabatic	None
	Horn, Csaba and Street (1966)	Rosin-Rammler	Combined diffusion and chemical control	Adiabatic	Radiation to walls
	Field and Gill (1967)	Any size distribution	Combined diffusion and chemical control	Adiabatic or isothermal	Radiation to walls; calculated from solid-particle concentration with allowance for gas radiation
Stirred tank followed by plug flow	Beer and Lee (1965)	Monosize	Semi-empirical (exponential form)	Isothermal PSR section and adiabatic PFR section	None

D. Overall Models for Pulverized Coal Combustors

A summary of pulverized coal combustor models is given in Table XII. These models have been developed for a variety of uses. For example, Hedley and Jackson (1966) wanted to find the effects of recirculation of combustion products on the burnout rate, and Horn et al. (1966) wanted a model to predict concentration and temperature measurements along the axis of a pulverized coal combustion chamber (Field et al., 1967). All models except that of Beer and Lee (1965) are plug flow models modified to include recirculation.

The model by Beer and Lee (1965) is unique in that it is a combination PSR-PFR model for a pulverized coal furnace. Efficiency calculations based on the model were in agreement with experimental data obtained from a pulverized coal furnace. From their study it was concluded that combustor efficiency is maximized by the proper combination of a PSR (micromixed) followed by a PFR. Other models using PSR-PFR combinations have been developed, but not for pulverized coal combustion (Mcllor, 1972).

Interesting variations have been used in treating portions of the combustor models. Horn et al. (1966) accounted for the temperature difference between the particles and gas. An energy balance at the particle surface was used to calculate the surface equilibrium temperature. Volatile evolution was also accounted for, by simply assuming that volatiles were released when the particles reached 670°K. Although these two effects were modeled crudely, they are completely ignored in other models (Field et al., 1967).

Several different methods have been used to model heat transfer. Field and Gill (1967) used an isothermal plug flow model and calculated the equilibrium temperature using a simple energy balance. Usually, external heat transfer through the walls is compared to internal heat generation in an iterative procedure. The standard procedure for the adiabatic plug flow models is to perform a heat balance on a small radial "slice" of the reactor. A differential equation is derived from the heat balance for variation of temperature along the chamber, which is then solved simultaneously with a suitable equation for variation

of composition. Vulis (1961) used an adiabatic PFR model which included an approximation for radiation back from the flame, but the validity of the radiation model has been questioned (Field et al., 1967).

Often it is necessary to approximate the pulverized coal particle size distribution when modeling combustion, as burning rates are a function of particle size. It is commonly assumed that the particles are either monosize or follow a Rosin-Rammler distribution. Field et al. (1967) has shown that the monosize distribution can lead to considerable error, in contrast to the Rosin-Rammler distribution which can be quite realistic. The Rosin-Rammler distribution is described by the function

$$RR = 100 \exp (d_p / \bar{d}_p)^n$$

where d_p is the particle diameter, RR the weight percent of coal which is of a size greater than d_p, and $\bar{d}_p$ and n are adjustable constants (Rosin and Rammler, 1933). A standard Rosin-Rammler distribution for theoretical use was suggested by Field et al. (1967), with values of $\bar{d}_p$ = 53 microns and n = 1.2. These values approximate a pulverized coal sample 80% of which will pass through a 75 micron (200 mesh) sieve.

Mechanistic models for pulverized coal combustion have yet to be developed, although work is continuing in this area. A turbulent two-phase flow model has been developed by Pratt (1974), and an extension of this model to include pulverized coal combustion will be attempted by Pratt and Smoot (Pratt, 1976).

E. Equilibrium Gasification Model

As a first approximation, we have used the NASA SP-273 computer program (Gordon and McBride, 1971) to construct a simple equilibrium model for gasification of coal to a low BTU power gas. Equilibrium concentrations were calculated for the gasification of an Indiana Bituminous coal with steam and air. The coal analysis is indicated in Table XIII; input conditions are listed in Table XIV.

The input enthalpies reflect both the chemical and sensible enthalpy for the given input temperatures. The input enthalpy for the

TABLE XIII

ASSUMED DRY COAL ANALYSIS

Proximate:		Ultimate:	
Volatile matter	41.4%	Carbon	72.3%
Fixed carbon	48.2%	Hydrogen	4.8%
Ash	10.4%	Oxygen	8.3%
		Nitrogen	1.4%
Caloric Value:	12960 BTU/lb	Sulfur	2.8%
		Ash	10.4%

TABLE XIV

EQUILIBRIUM GASIFICATION MODEL: INPUT CONDITIONS

Reactants	Molecular Form	Input Enthalpy (cal/mole)	Input Temp (^{o}K)
Coal	$C_{6.718} H_{5.315} O_{.579} N_{.112} S_{.098}$ + SiO_2 (Ash)	-36100	298
Air	$N_{1.562} O_{.420} Ar_{.0093} C_{.0003}$	2950	700
Steam	H_2O	-53394	810

coal was calculated via its stoichiometric combustion reaction and the given heating value (Coates et al., 1975). The air to coal ratios (OX/C) were set equal to 2, 3 and 4 lbm air/lbm coal, while steam to coal ratios (H_2O/C) were set at .25, .50, .75 and 1.0 lbm H_2O/lbm coal.

These independent process variables were varied at a constant pressure of 1 atm under adiabatic conditions. The species concentrations and gas exit temperature were then determined (Fig. 22a, b). From this information, we can calculate dependent process variables such as producer gas yield (Y_p), make gas heating value (Q), and cold gas efficiency (η_{cg}). Also, since the sensible energy of low BTU gas can be used in a combined power cycle, we feel a new parameter describing efficiency is needed. This new variable, the hot gas efficiency, η_{hg} is defined as:

$$\eta_{hg} = \frac{H_p + \Delta H_{pr}}{H_c}$$

where H_p is the combustion enthalpy of the products, H_{pr} is the difference in sensible enthalpy between the products and reactants, and H_c is the combustion enthalpy of the input coal. This parameter describes more accurately the potential efficiency of the reactor since η_{hg} reflects the energy conversion efficiency appropriate to power gas use. The calculated results (Y_p, Q, η_{cg}, η_{hg}) are shown in Figs. 23a,b,c,d; they compare quite favorably with Table X of Chapter II, which shows dependent variable behavior as found in the coal gasification literature.

Producer gas yield maximizes as the OX/C ratio is varied, but shows little dependence on the H_2O/C ratio. The make gas heating value tends to increase as the OX/C ratio is decreased and can go through a maximum if steam input is low. At low OX/C ratios (and consequently, low temperatures) CH_4 concentrations become important (greater than 2% of the make gas yield) and cause cold gas efficiency to increase. The cold gas efficiency also maximizes as the OX/C ratio is varied and increases as the H_2O/C ratio increases (due to CH_4).

Comparison of the cold gas and hot gas efficiency (Figs. 23c,d) reveals the important aspects of considering the sensible enthalpy of the products. First we note a significant overall increase in efficiency.

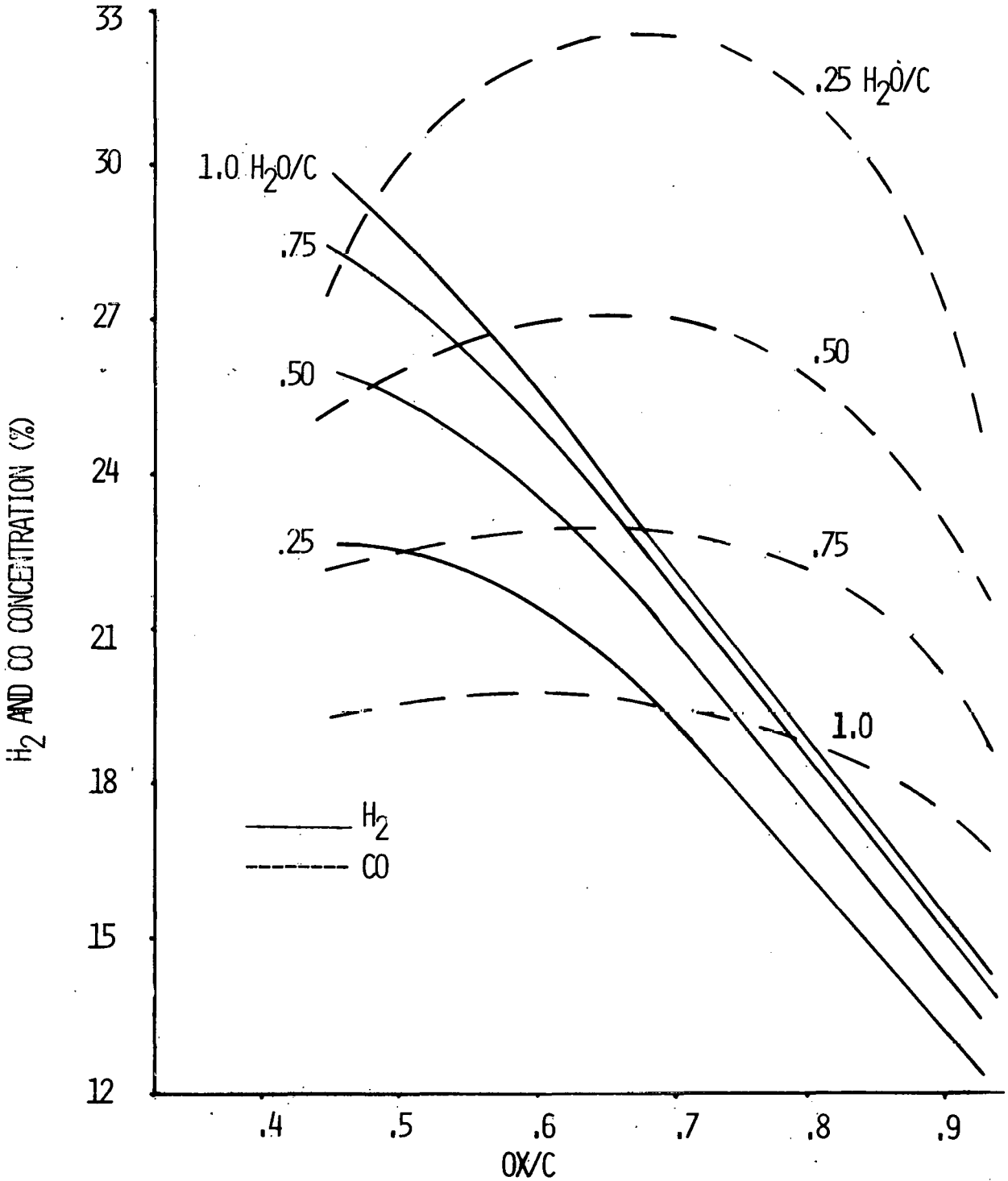

Figure 22a. Equilibrium Predictions for Adiabatic Gasification at 1 atm: H_2 and CO Concentrations

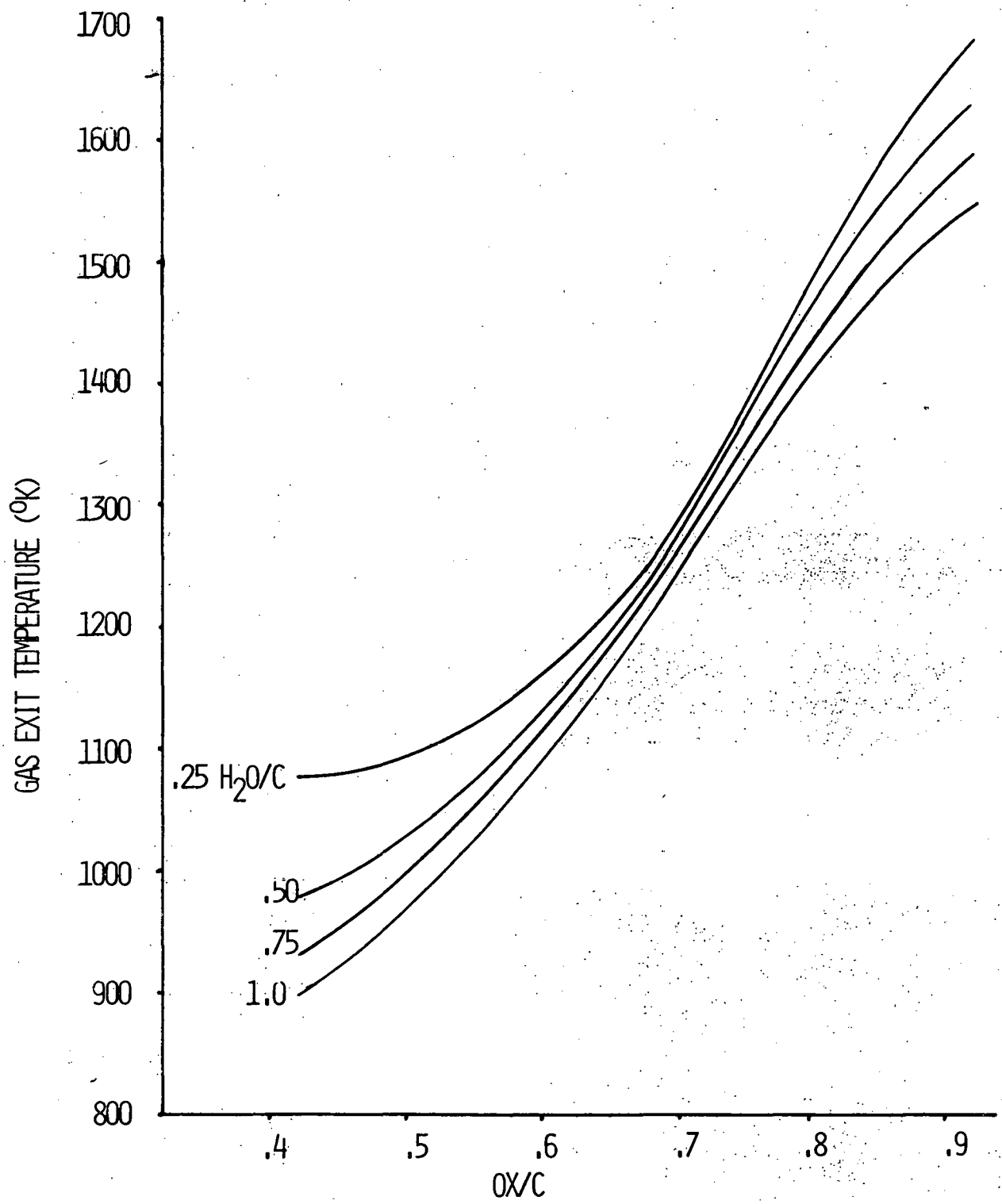

Figure 22b. Equilibrium Predictions for Adiabatic Gasification at 1 atm: Gas Exit Temperature

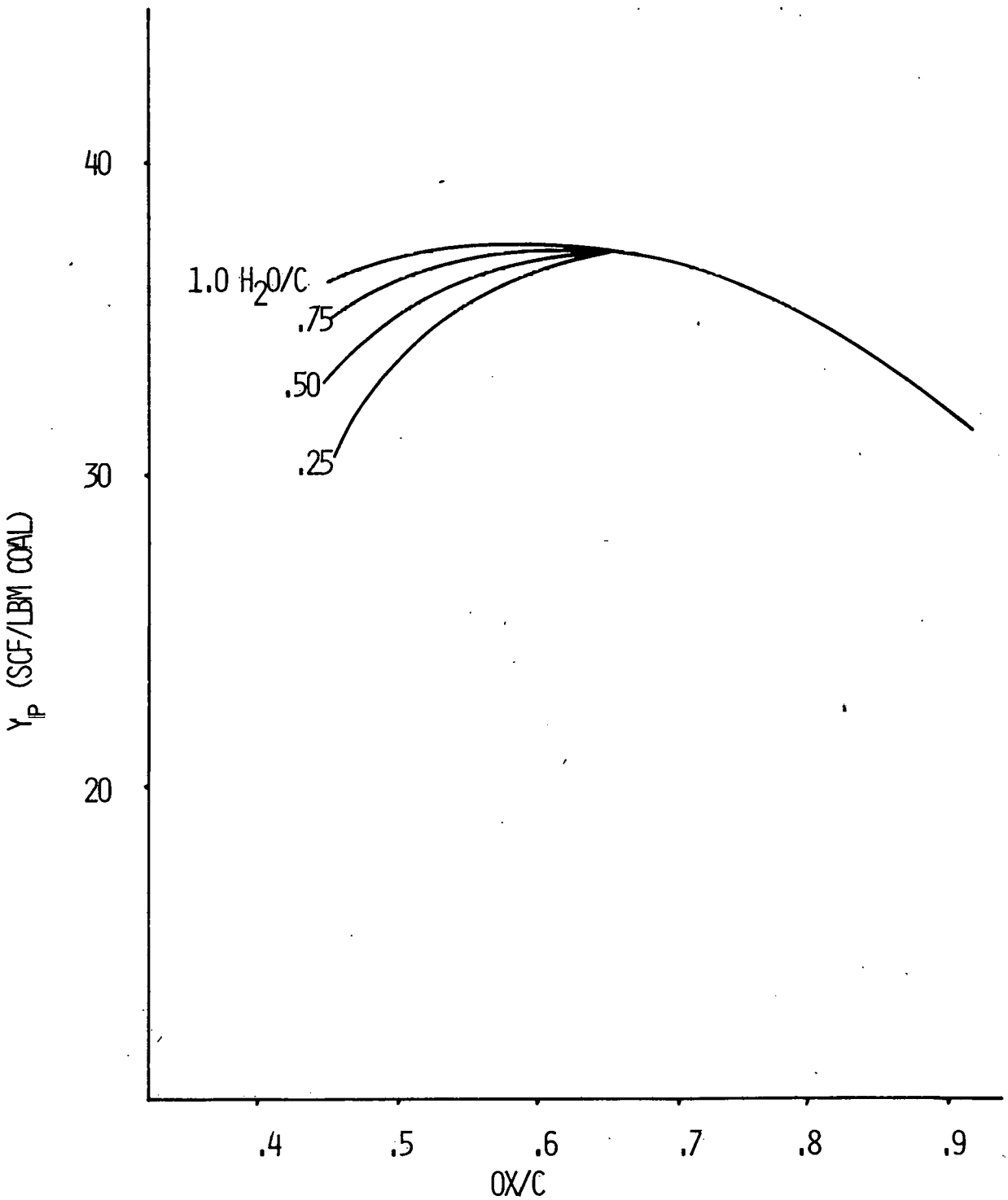

Figure 23a. Dependent Process Variables for Adiabatic Gasification at 1 atm: Producer Gas Yield (Y_p)

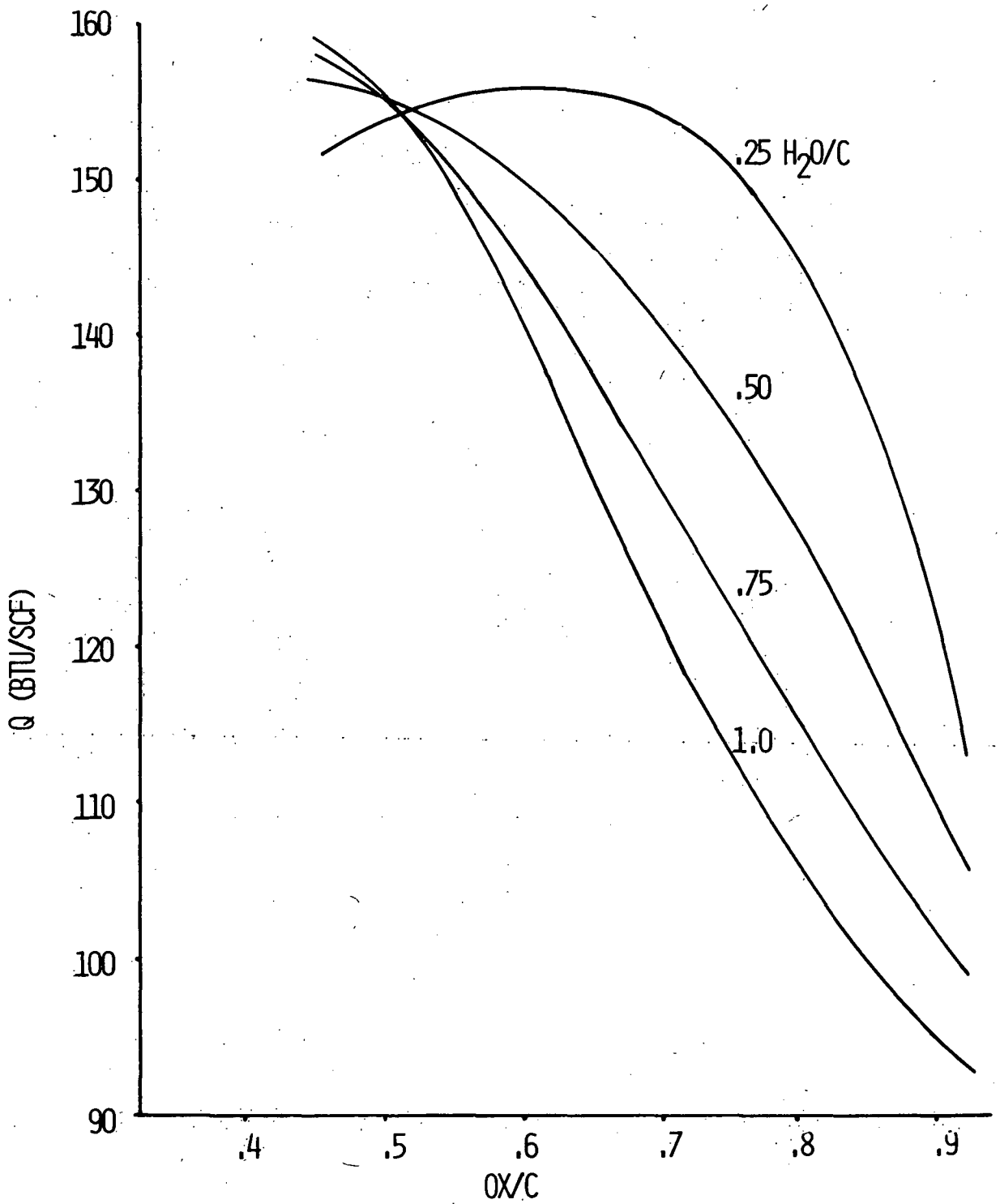

Figure 23b. Dependent Process Variables for Adiabatic Gasification at 1 atm: Make Gas Heating Value (Q)

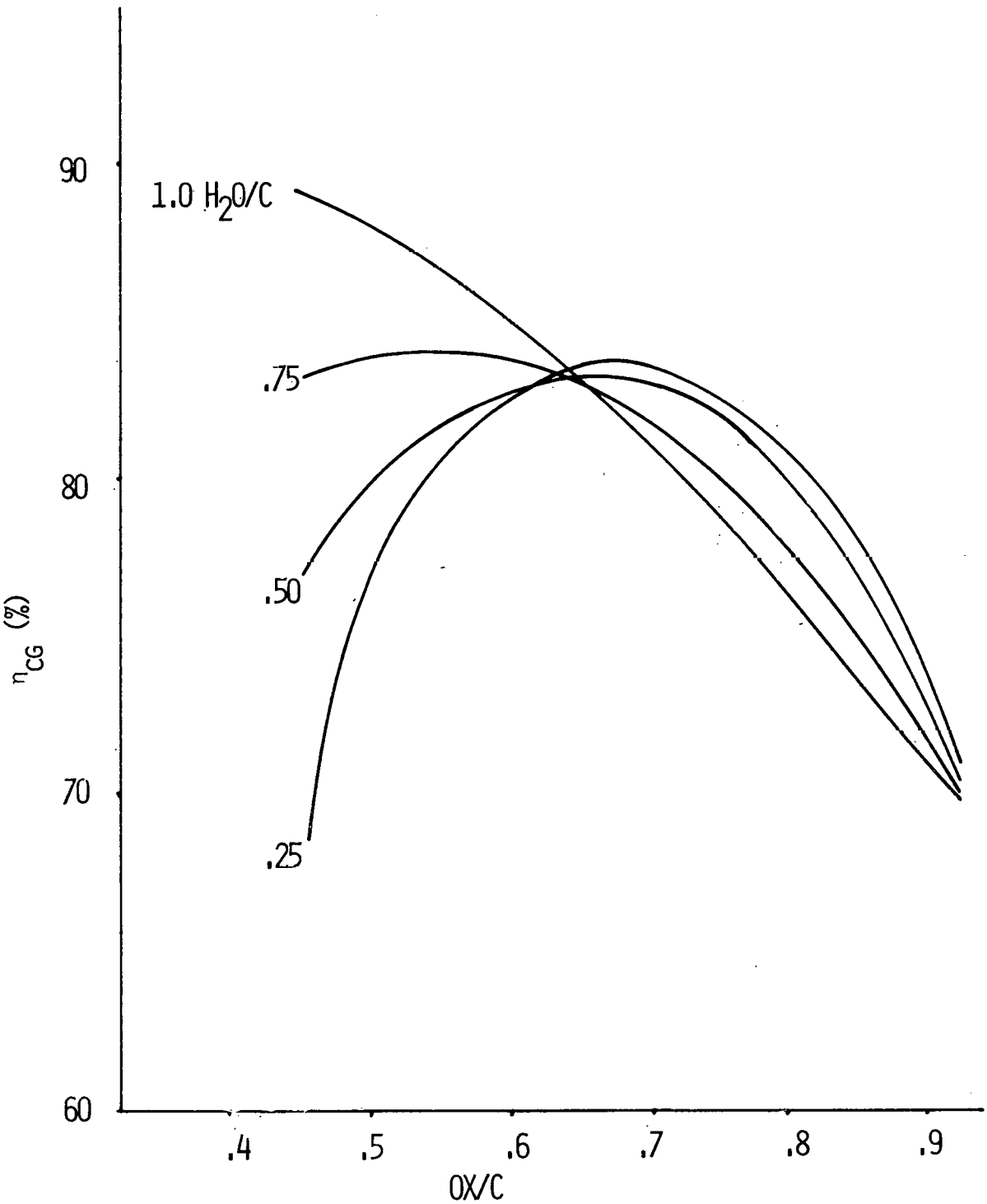

Figure 23c. Dependent Process Variables for Adiabatic Gasification at 1 atm: Cold Gas Efficiency (η_{cg})

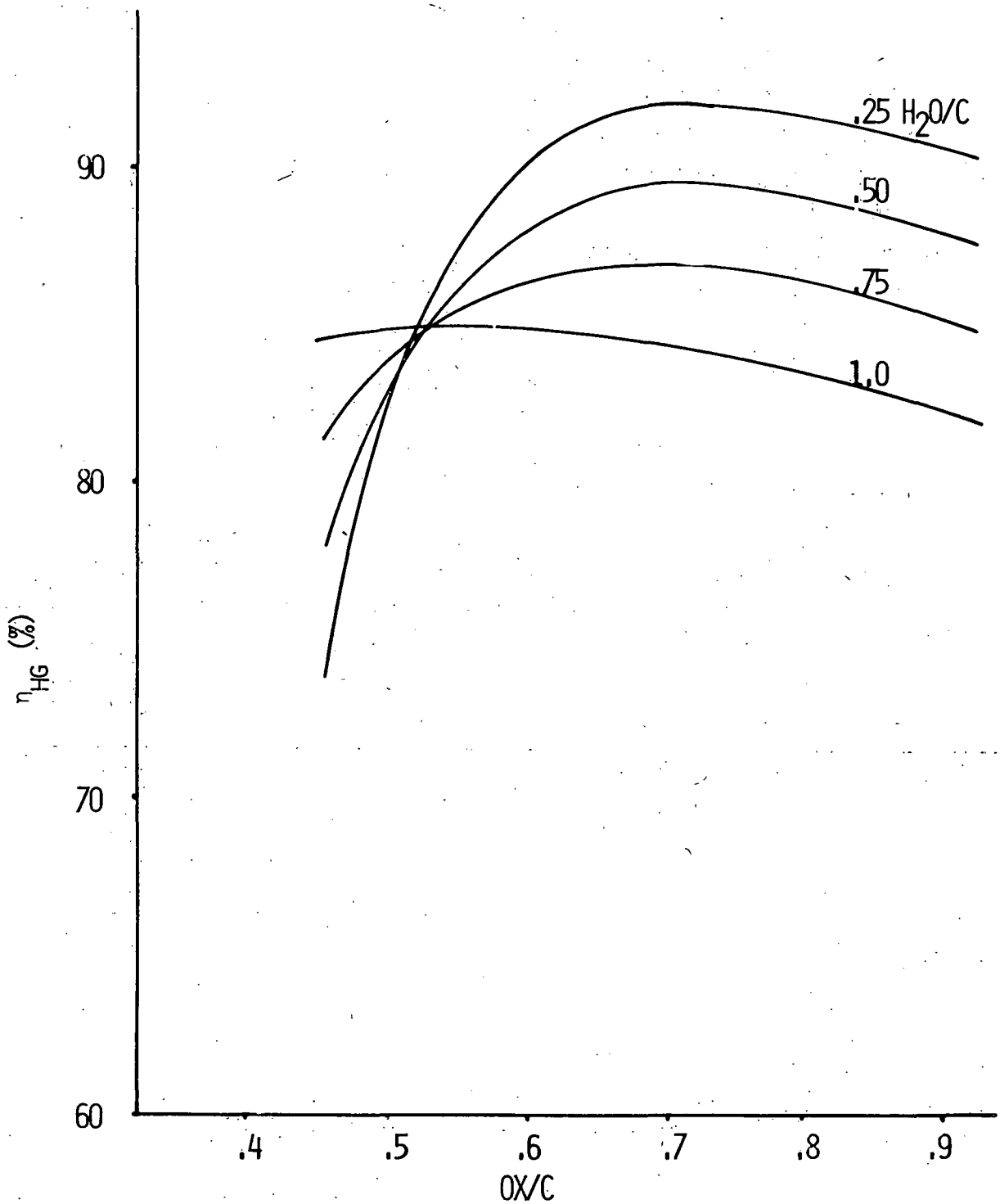

Figure 23d. Dependent Process Variables for Adiabatic Gasification at 1 atm: Hot Gas Efficiency (η_{hg})

Also, the region of maximization is larger, with increasing OX/C ratios causing only slight losses in efficiency. This is of great importance in practical gasifiers since we can increase the OX/C ratio to preserve carbon efficiency and reaction temperature, thus efficiently producing low BTU gas at the high temperatures ideal for combined power cycles.

The effects of operating at elevated pressures (5 and 20 atm) was explored for adiabatic conditions. Gas exit temperature increases noticeably in the low OX/C range, but only slightly in the high OX/C range. Consequently, there is little change in species concentration (and hence efficiency) when operating in the high OX/C range. In the low OX/C range CH_4, CO_2, and H_2O concentrations increase while CO and H_2 concentrations decrease with increasing pressure. At high steam inputs increasing the pressure from 1 to 20 atmospheres causes CH_4 production to increase approximately 2-1/2 times (Fig. 24a). Since CH_4 is favored at high pressure and low temperatures, and H_2 and CO are favored at high temperatures and low pressures, the need for a two stage process becomes evident for the production of SNG. The main advantage of operating at elevated pressures is that the coal throughput may be increased significantly, thus reducing heat loss.

Heat loss was simulated by running the equilibrium reaction at temperatures less than the adiabatic flame temperature (T_a). The effects on the concentrations of CO and H_2 are shown in Fig. 24b. Note that when operating in the high OX/C range, minor heat losses will have little effect on cold gas efficiency since the CO decrease and H_2 increase are of the same magnitude. However, the hot gas efficiency will decrease since the products will exist with lower sensible energy. In general H_2, CH_4 and CO_2 concentrations increase while CO and H_2O concentrations decrease for high OX/C; CH_4, CO_2 and H_2O concentrations increase while H_2 and CO concentrations decrease for low OX/C ratios. At low OX/C ratios heat losses cause CO concentrations to drop drastically, thus causing a loss in cold and hot gas efficiency, make gas heating value, and producer gas yield. When operating at elevated pressures, heat losses cause a drop in carbon efficiency at low OX/C and H_2O/C ratios.

Clearly the importance of the OX/C ratio is seen in all dependent process variables. The qualitative results given from the

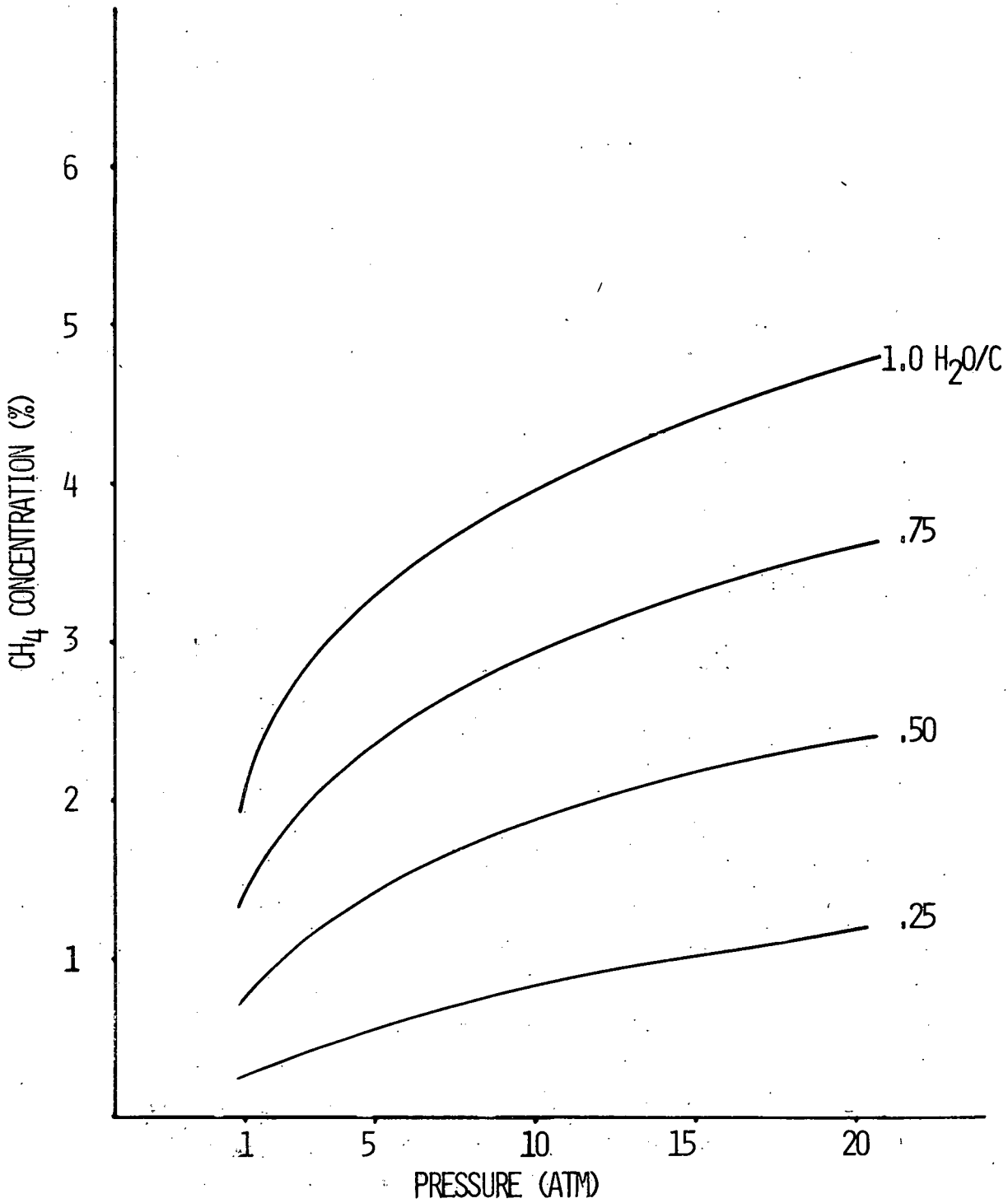

Figure 24a. Effect of Elevated Pressure on Adiabatic CH_4 Concentration (2 lbm air/lbm coal)

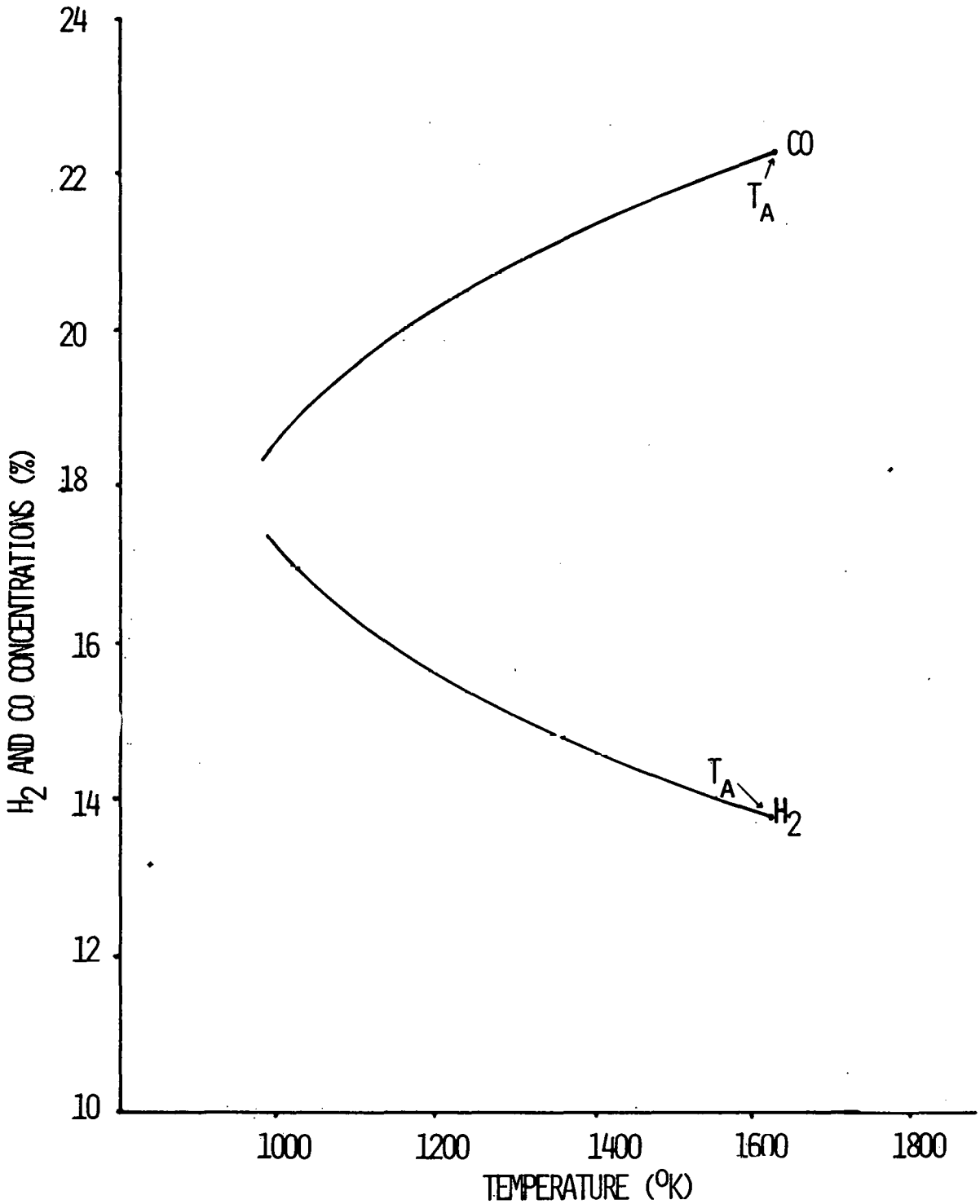

Figure 24b. Effect of Heat Loss on H_2 and CO Concentrations (4 lbm air/lbm coal; 0.5 lbm H_2O/lbm coal)

equilibrium model agree well with those found in coal gasification literature. This implies that most previous processes operated near equilibrium. Further maximization of H_2 and CO can be obtained if flow can be controlled to produce specified reacting regions, and residence times controlled to operate at non-equilibrium conditions.

F. Conclusions

Although no models were found in the literature which pertained to either coal gasification or cyclone combustors, some insight can be gained from previous combustor models. The review of mixing theories suggests that a RTD type mixing model would be favored, as mechanistic models are quite complex and difficult to use. In the model by Beer and Lee (1965), a micromixed PSR was used to represent the swirling portion of a furnace. Micromixing was chosen over macromixing due to the high swirl and temperature in the furnace. A cyclone combustor would also have high temperature and swirl; therefore, a micromixed PSR may be a good approximation for a portion of the cyclone. A major difference for cyclones, however, is the long particle residence time compared to the gas residence time.

Combustion kinetics can be best treated empirically if the proper data is available, but often a theoretical rate expression must be used. An empirical particle burning rate equation such as that used by Beer and Lee (1965) is easily implemented into a combustor model. However, most studies done to date are for anthracite or semi-anthracite coals and not bituminous; therefore, an empirical rate expression may not be feasible. Instantaneous volatile burning rates are acceptable, as the actual burning time is only a few milliseconds (once the volatiles are mixed in air). Also, a Rosin-Rammler size distribution should be used when calculating particle combustion or gasification (Field et al., 1967). Realistic gasification models should also consider homogeneous kinetics; particularly combustion of H_2, CO and CH_4.

VI. GASIFICATION FACILITY DESIGN

Progress on the experimental phase of the investigation is considered in this chapter. The coal handling facility is complete. The test cell electrical and flow systems and the cyclone gasifier have been designed. Construction will begin on both in early August. Calibration of the mass spectrometer and construction of the sampling system will be finished before our initial atmospheric combustion tests.

A. Test Cell

As noted in Table XV, most of the equipment for the test cell is on hand or has been ordered. All equipment that has been ordered is expected prior to the end of July. All valves for the air and nitrogen systems are on hand and construction of these systems is underway. An electrical interlock and control system has been devised, as well as a power distribution system for three phase power to the cell. In addition, we have a preliminary design for a central control panel. Auxiliary panel designs are presently in the conceptual stage.

1. Flow System

Figure 25 is the revised flow system schematic diagram. It incorporates valving, pressure gages, and safety devices not included with previous schematics. Table XVI indicates the symbols used in this and subsequent figures in this section. Sizing of lines and valves has been based on the flow rates indicated in Table XVII. A full scale arrangement based on the schematic has been layed out on the test cell wall. All valves and equipment have been located on the flow layout to reflect their actual physical size and insure that operating difficulties and interference will be minimized. Along with valve positioning, the layout enabled a complete and accurate fitting list

TABLE XV

EQUIPMENT STATUS

Location and Use	Description of Equipment	Cost	Comments
AIR SUPPLY SYSTEM, GENERAL			
ASV - High pressure air shut-off valve, located outside cell	Valve in place		On hand
Air filter	Balston 95S	$ 78.00	Received
AR-1 - Air regulator	Regulator in place		On hand
SV-M - Safety valve	400 psig set press. Safety valve (Kunkle fig. 264)	$ 104.63	Received
P6 - Pressure gage	1500 psig gage		On hand
AIR SUPPLY SYSTEM, PRIMARY AIR			
PA1 - Manual shut-off	600 psig globe valve		On hand
PAC - Control valve	Remotely loaded air control valve		On hand
PAE - Remote shut-off valve	ASCO solenoid valve, 8228A65 (1/4" pipe fittings)	$ 61.50	Received
PAFM - Primary air flowmeter	Thermal Instruments Co. Model 60	$1300.00	Ordered, delivery expected 7/30/76
PAH - Primary air heater	GTE/Sylvania Model CGL138823 process heater, 4 kw	$ 98.00	Received

Location and Use	Description of Equipment	Cost	Comments
PA-2 - Manual shut-off	1/4" high temperature valve		On hand
CV2 - Check valve	Autoclave 1/4" AE speedbite SW Cat. No. SWB 8800	$ 38.00	Received
Feeder	Vibra-Screw live bin feeder	$2600.00	Received
AIR SUPPLY SYSTEM, SECONDARY AIR			
CV1 - Check valve	Positive shut-off, spring loaded check valve		On hand
SA1 - Manual shut-off	10,000 psig valve		On hand
SAC - Control valve	Remotely loaded air control valve		On hand
SAE - Remote shut-off	Magnetrol solenoid valve 1/2" (E33A62)	$ 107.00	Received
SAFM - Secondary air flowmeter	Thermal Instrument Co. Model 60	$1300.00	Ordered
SAH - Secondary air heater	GTE/Sylvania Model PGH138825 process heaters, 3 in series 18 kw total	$ 414.00	Received
SA-2 - Gasifier selection valve SA-3 - Gasifier selection valve	Pacific Valve, Inc., Figure No. 41568Y7, 1" stainless steel valve, packing to be John Crane 187-I		On hand except packing

Location and Use	Description of Equipment	Cost	Comments
AIR SUPPLY SYSTEM, CONTROL AIR SUPPLY			
CA1 - Shut-off valve	1/8" valve		On hand
CAR-1 - Control air regulator for steam system pneumatic valves	150 psi outlet pressure regulator		On hand
CAL-1 - Control air loader for primary air control valve	350 psig outlet/400 psig inlet small volume regulator		On hand
CAL-2 - Control air loader for secondary air control valve	Same as CAL-1		On hand
CAL-3 - Loader for SE-1 CAL-4 - Loader for SE-2	Regulators in place		On hand
P1 - Pressure gage	400 psig gage		On hand
P2 - Pressure gage	400 psig gage		On hand
P3 - Pressure gage	100 psig gage		On hand
P4 - Pressure gage	100 psig gage		On hand
CAT - Control air trip valve	Four way solenoid valve		On hand
P-5 - Pressure gage for supply to steam valve regulators	150 psig		On hand
CASV - Control air safety valve	125 psig set pressure crane safety valve		On hand

Location and Use	Description of Equipment	Cost	Comments
STEAM SUPPLY SYSTEM			
Boiler	Coates Electric Boiler (Neal Engr.)	$3210.00	Ordered
SE-1 - Shut-off/control valve	Autoclave Engr. 6V71B8-OM with air to open operator	$ 150.00	Ordered
SE-1T - Electric emergency trip for SE-1	Asco 3 way solenoid valve, NC operation (Cat. No. 8320A132)	$ 25.00	Received
SE-2 - Shut-off/control valve	Autoclave Engr. 6V71B8-HT-OM with high temp. packing and air to open operator	$ 260.00	Ordered
SE-2T - Electric emergency trip for SE-2	Asco 3 way solenoid valve, NC operation (Cat. No. 8320A132)	$ 25.00	Received
SD-1 - Steam remote operated drain valve	Autoclave Engr. 6V71B4-CM with air to close operator	$ 110.00	Ordered
SD-1P - Pilot valve for SD-1	Asco 3 way solenoid valve, NC operation (Cat. No. 8320A132)	$ 25.00	Received
SD-2P - Pilot valve for SD-2		$ 25.00	Received
SD-2 - Remote operated steam drain valve	Autoclave Engr. 6V71B8-HT-CM with air to close operator and high temp. packing	$ 200.00	Ordered
STH - Steam superheater	GTE/Sylvania Model PGH 138825 process heater, 6 kw	$ 138.00	Received
S-1 - Gasifier selection valve	1/4" high temperature valve		On hand
S-2 - Gasifier selection valve	Same as S-1		On hand

Location and Use	Description of Equipment	Cost	Comments
CV-3 - Check valve	Autoclave Engr. 1/2" AE Speed-bite SW Cat. No. SW8800	$ 42.00	Received
SFM - Steam flowmeter	Thermal Instrument Co. Model 60	$1400.00	Ordered, delivery expected 7/30/76
WATER FEED SYSTEM			
Feedwater tank	10.5 cu. ft. High pressure tank (needs 600 psig hydrostatic test)		On hand
WF-1 - Manual shut-off valve	600 psig 1/4"		On hand
WFF - Fill valve	1/2" 600 psig valve		On hand
WFD - Drain valve	600 psig 1/4"		On hand
WF-2 - Feedwater manual shut-off	600 psig 1/4" valve		On hand
WFV - Vent valve	600 psig 1/4" valve		On hand
NITROGEN SYSTEM			
NR-1 - Nitrogen regulator for purge system	3000/500 psig regulator		On hand
N-2 - Purging solenoid valve	Magnetrol Model #-33AR62 2 way high pressure solenoid valve, N.O. operation	$ 105.00	Received
NR-3 - Boiler nitrogen cap regulator	400/10 psig regulator		On hand

Location and Use	Description of Equipment	Cost	Comments
BN-1 - Boiler nitrogen cap shutoff	600 psig @ 500°F 1/4" high temperature valve		On hand
P7 - Purge N_2 pressure	400 psig gage		
PS-7 - Nitrogen pressure switch	Barksdale Model #1H-H500 pressure switch	$ 20.00	Ordered
P8 - Boiler pressure	400 psig gage		Supplied with boiler
SVN - Nitrogen system safety	250 psig set pressure, 1" Kunkle safety valve		On hand
CV-4 - Coal transport system nitrogen purge check valve	1/4" tubing, positive shut-off check valve		On hand
CV-5 - Secondary air system nitrogen purge check valve	5/8" tubing, positive shut-off check valve		On hand
MISCELLANEOUS			
Steam blowdown tank (BD tank)	4" (approx) diameter tank for separation of water from steam before vent; construct from scrap		Materials on hand
IGNITION SYSTEM			
IGR-1 - Ignition gas regulator	Manually set regulator (3000 psig inlet, 300 psig outlet)		
IGE - Ignition gas remote shut-off valve	1/4" tubing solenoid valve with 1/16" orifice		On hand

Location and Use	Description of Equipment	Cost	Comments
IAE - Ignition air remote shut-off valve	Same as IGE		On hand
IAR-2 - Ignition air regulator	Manually set regulator (400 psig inlet, 300 psig outlet)		On hand
IA-1 - Ignition air shut-off valve	600 psig valve for 1/4" tubing		On hand
P9 - Ignition gas pressure P10 - Ignition air pressure	400 psig gage 400 psig gage		
IG-3 - Gasifier selection valve, ignition gas	Whitey Model No. 43X54 3 way valve		On hand
IA-3 - Gasifier selection valve, ignition air	Whitey Model No. 43X54 3 way valve		On hand
IGBD - Ignition gas burst disk	450 psig burst disk BS&B Type A-2	$ 20.00	
ELECTRICAL SYSTEM, GENERAL			
3ϕ, 240 vac power supply to safety switches	Wiring by physical plant including switches.	$1600.00	Requested
Boiler	See steam system		
Boiler control	SCR power controller with manually adjusted potentiometer. Magnetic contactor supplied internal to boiler to insure positive remote shut-down		Supplied with boiler

Location and Use	Description of Equipment	Cost	Comments
Feeder	Vibra Screw volumetric live bin screw feeder	$2600.00	Received
FDR - Feeder motor starter	GE CR206 magnetic starter 206A102 with 120 vac coil	$ 41.00	
ELECTRICAL SYSTEM, PRIMARY AIR			
CRPAH - Primary air heater trip relay	Allen Bradley Model No. 702BAD92 30 amp contactor	$ 45.00	
PAH-C - Primary air heater temp. control	GTE/Sylvania Model PFR130634	$ 184.00	
PAH - Primary air heater	See AIR SUPPLY SYSTEM, PRIMARY AIR		
ELECTRICAL SYSTEM, SECONDARY AIR			
CRSAH-1 - Secondary air heater trip relay	Allen Bradley Model No. 702BAD92 30 amp contactor	$ 45.00	
CRSAH-2 - Secondary air heater trip relay	Same as CRSAH-1	$ 45.00	
CRSAH-3 - Secondary air heater trip relay	Same as CRSAH-1	$ 45.00	
SAH-1C - 1st secondary air heater manual control	GTE/Sylvania power control module Model No. SCR139884	$ 52.00	
SAH-2C - 2nd secondary air heater manual control	Same as SAH-1C	$ 52.00	

Location and Use	Description of Equipment	Cost	Comments
SAH-3C - 3rd secondary air heater final temperature control	GTE/Sylvania Model PFR130633	$ 235.00	
SAH-1 - Secondary air heaters SAH-2 - Secondary air heaters SAH-3 - Secondary air heaters	See AIR SUPPLY SYSTEM, SECONDARY AIR		
ELECTRICAL SYSTEM, STEAM			
CRSTH - Steam heater trip relay	45 amp Allen Bradley motor starter		On hand
STH-C - Steam temperature control	GTE/Sylvania Model No. PFR130633	$ 235.00	
STH - Steam heater	See STEAM SUPPLY SYSTEM		
ELECTRICAL SYSTEM, REACTORS			
CRRH - Reactor heater control and trip relay	General Electric SCR power controller Model CP1012	$ 197.00	
RH-C - Reactor heater temp. control	General Electric temperature controller Model CD1006	$ 151.00	
VGH - Vortex gasifier heater	Electro-Application clam shell type heater - custom made 8 kw	$ 230.00	
JGH - Jet gasifier heater	Selection pending reactor design		
RH-SS - Reactor heater selector switch	DPDT panel mounted switch with 2 Allen Bradley 45 amp motor starters		On hand

Location and Use	Description of Equipment	Cost	Comments
ELECTRICAL SYSTEM, SAFETY INTERLOCK SYSTEM			
Control relays	3 - 24 VDC 3PDT square D type KTD13	$ 31.80	Ordered
	6 - 24 VDC 2PDT square D type KTD12	$ 55.80	Ordered
	3 - 120 VAC 3PDT square D type KT13	$ 34.65	Ordered
	4 - 120 VAC 2PDT square D type KT12	$ 41.28	Ordered
	2 - 240 VAC 2PDT square D type KT12	$ 24.98	Ordered
Trip relays	2 - General Electric type CR120AD08048AA 24 VDC control relay	$ 100.00	Ordered
Time delay relays	1 - General Electric type CR122A04148AA time delay relay	$ 55.00	Ordered
	1 - Industrial Timer Corp. Model TDAF - 15M		On hand
Pressure switches	2 - Barksdale Model E1H-H500	$ 40.00	Ordered
Pilot lights	38 required, various colors	$ 30.00	Received
Switches	16 - DPPT 10 amp toggle switches		On hand
	2 - 5 amp push button		On hand

Location and Use	Description of Equipment	Cost	Comments
No coal flow signal	Hardware not selected		
No air flow signal	Hardware not selected		
No flame signal	Honeywell flame scanner Type RA890E 112A 2		On hand
COAL HANDLING FACILITY			
Pulverizer	Holmes Brothers Model No. 500	$1180.00	Received
Crusher	Holmes Brothers Model No. 201	$1940.00	Received
Sieve shaker	Gilson Model SS-12R	$ 655.00	Received
Sieves	12 in. diameter brass with brass cloth in sizes #70, #100, #140, #200, #230, #270, #325, #400, and brass pan with lid	$ 296.00	Received
Scales	Ohaus 1000 Optical Projection Autogram Balance	$ 318.00	Received
Ventilation hood	6' x 6' galvanized hood		Donated by Rush Metal Co.

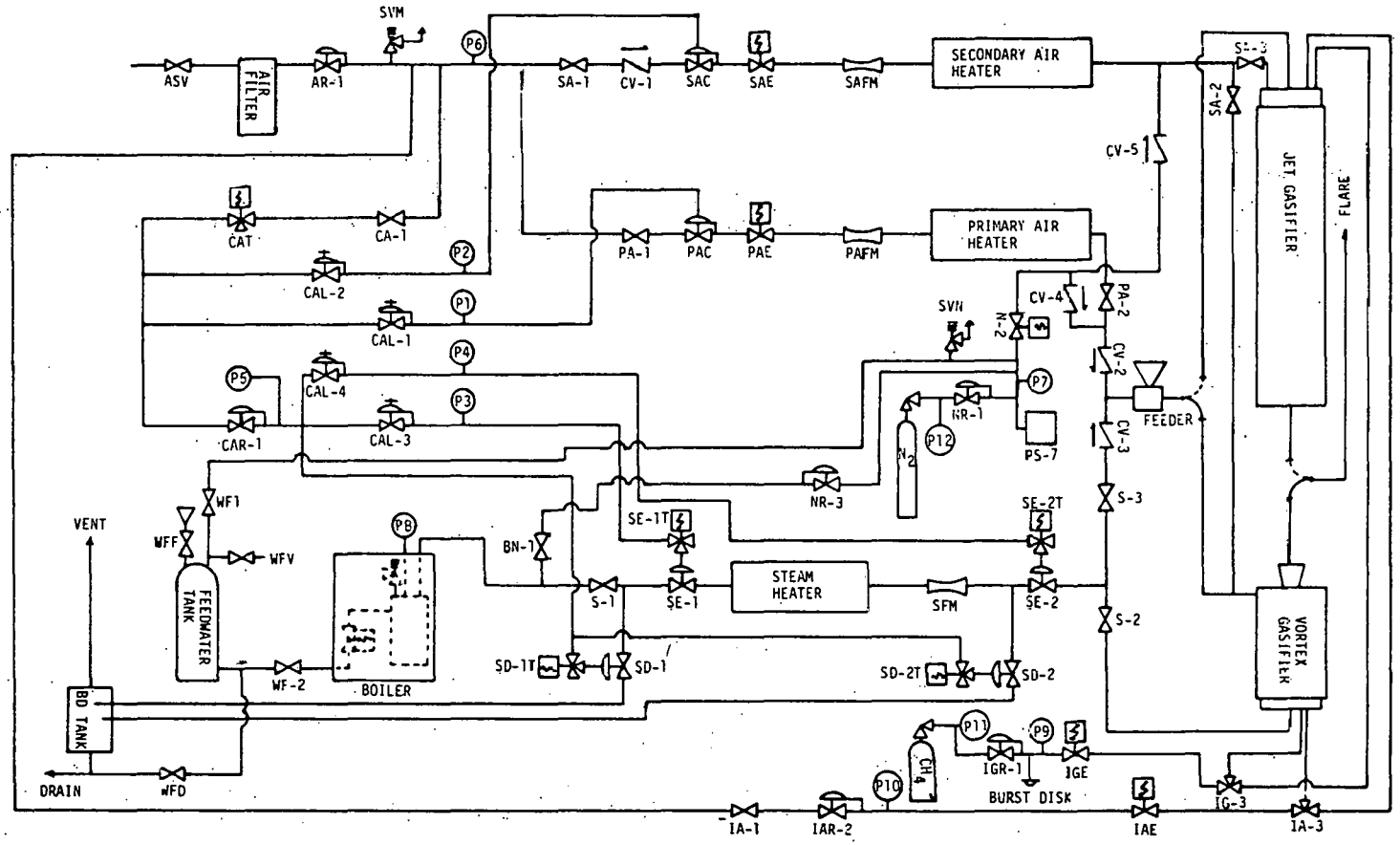

Figure 25. Flow System Schematic

TABLE XVI

MECHANICAL, ELECTRICAL AND LOGIC SYMBOLS

(Note: Letter & number equipment designations noted in Equipment Status List (Table XV))

Manual valve

Feeder

Air operated valve

Manually set pneumatic loader

Pressure regulator

Pressure gage

Three way valve

Check valve

Safety valve

Electrically operated valve

Flowmeter

Interchangeable pipe section used to select gasifier

Burst disk

Indicating light

Toggle switch

Push button

Resistance heating element

Ground

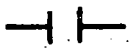
Normally open contact

Normally closed contact

Relay/solenoid coil

Externally switched coil

Fuse

Variable resistor (potentiometer)

Signal input

Signal output

Not (no input gives output)

And (all inputs required for output)

Or (any input required for output)

Location reference (refers to location input received from or output goes to)

Time delay (input is delayed before output)

TABLE XVII

DESIGN FLOW RATES FOR TEST CELL

	Maximum Design Flow	Expected Experimental Range
Coal	40 lbm/hr	7 to 28 lbm/hr
Primary Air	60 lbm/hr	10 to 45 lbm/hr
Secondary Air	450 lbm/hr	20 to 350 lbm/hr
Steam	60 lbm/hr	2 to 20 lbm/hr

to be compiled. All fittings have been ordered.

A rough floor plan for the cell is shown in Fig. 26. The feeder, jet gasifier, vortex gasifier, air heaters and supply systems will be housed in the cell. The boiler and feedwater tank, along with spare equipment and a work bench will be housed in a concrete block building located behind the test cell. All monitoring equipment, electrical relays, and pressure gages handling non-hazardous fluid will be located in the control room. Gas bottles will be located just outside the cell and secured to the building wall.

2. Electrical System

The test cell will be supplied with 24 volt DC, 120 volt AC, and three phase 240 volt AC electrical power. The 24 volt system is used exclusively for actuating solenoid valves and interlock relays. The 120 volt system is used for some relay logic and controls and will also power sampling and data recording systems. The 240 volt system supplies power to the air and steam heaters, feeder motor, boiler and reactor heaters.

2.1 The 240 VAC System. Figure 27 is a power distribution diagram for the three phase 240 volt system. The power will be supplied to safety switches located in the control room. The safety switch for the boiler, however, will be located in the building with the boiler. From these safety switches power will be run to controllers located on the side control panel and then via conduit penetrations into the cell

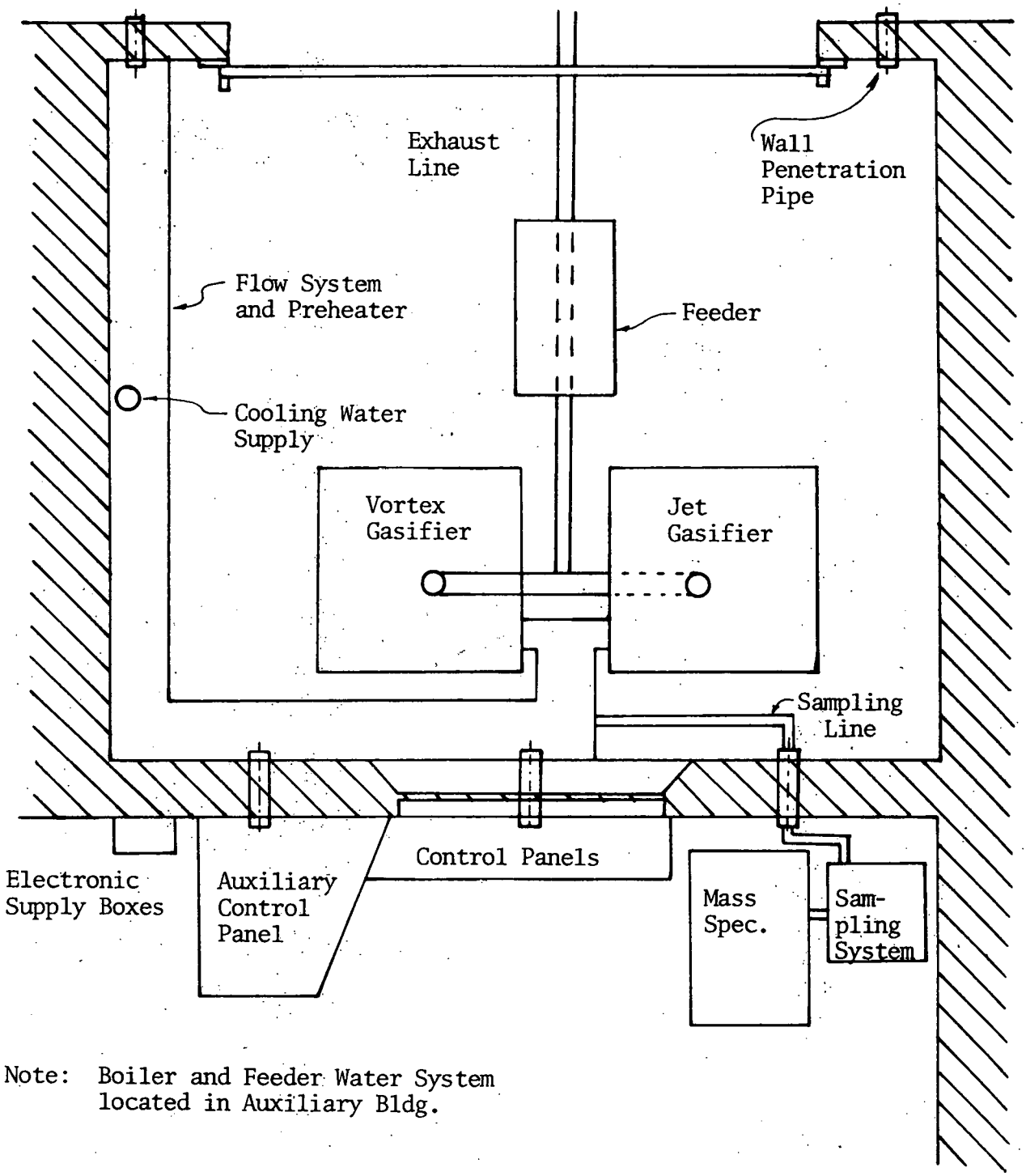

Note: Boiler and Feeder Water System
located in Auxiliary Bldg.

Figure 26. Test Cell Floor Plan

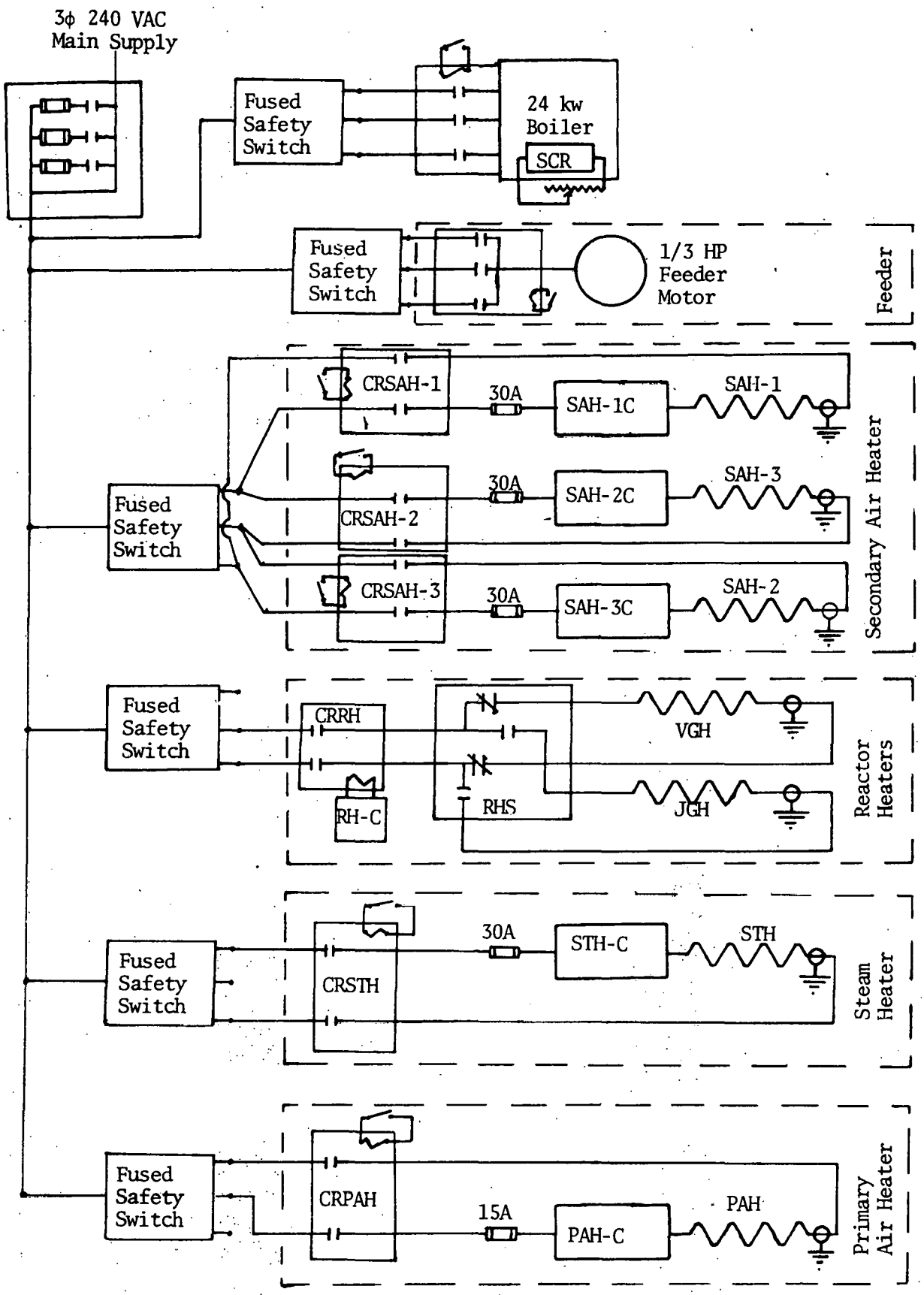

Figure 27. Three Phase Power Distribution System

to the various pieces of equipment. The portion of the control panel used for power distribution will be isolated from portions used for control and monitoring equipment to avoid induced currents and signal noise. Where signal lines are required in the power panel, such as thermocouple inputs to temperature controllers, they will be shielded, as will the temperature controllers. Construction of the three phase power distribution system will begin in late August, after the flow system is nearing completion and the control panels have been constructed.

2.2 Safety Interlock and Control System. The safety interlock and control system is designed to allow an operator to start-up and shut-down the gasification system from the central control panel in an orderly fashion. In addition, certain basic interlocks and trips are provided. Figure 28 is a logic diagram of the safety interlock system. A wiring diagram based on this logic diagram is also complete, but not included. The system provides for remote opening and closing of shut-off valves and pilot light indication of equipment status. Switches are provided to turn various heaters on or off, but heat control will be on the side panel as will flow monitoring. Flow control will be from a panel above the cell observation window. In addition, interlocks will:

(1) prevent the feeder from starting without the ignitor on;
(2) prevent the feeder from running without the primary air or steam supply valve open;
(3) prevent the feeder from running without the N_2 purge system operational;
(4) prevent opening any supply valves with the system tripped;
(5) prevent opening the ignitor fuel supply without both ignitor air and spark on;
(6) prevent operating any heater without the associated supply valve open;
(7) open the nitrogen purge valve upon trip, and insure a 2 minute purge;
(8) open the two steam drain lines upon trip;
(9) prevent resetting a trip until all control switches are normalized.

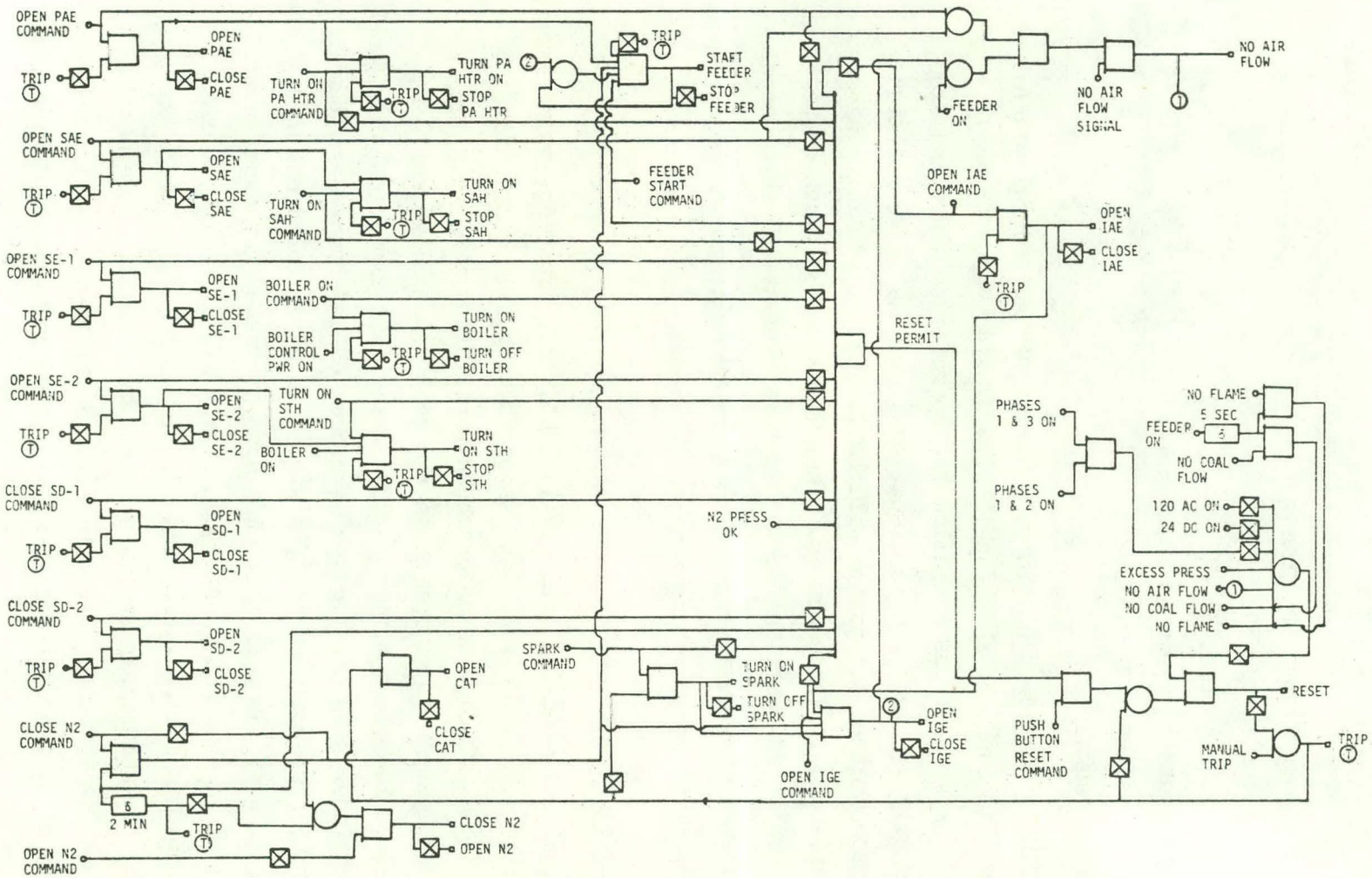

Figure 28. Interlock Logic Diagram

The following conditions will cause a system trip:

(1) loss of 24 VDC power;
(2) loss of 120 VAC control power;
(3) loss of 240 VAC power;
(4) loss of air flow;
(5) loss of coal feed;
(6) loss of flame in the reactor;
(7) system over-pressure;
(8) manual trip.

Figure 29 shows the proposed layout of the central control panel. The philosophy of this panel is to provide "at a glance" indication of system status and allow the operator to start and stop equipment easily. Actual control functions, such as valve position and heater temperature set points will be located on adjoining panels with appropriate color-coded knobs. They will also be arranged to reflect the relative positions of the various elements on the control panel. The control functions are located on an auxiliary control panel to insure a clear indication of system status.

B. Coal Handling Facility

The coal handling facility is complete. Crushing, pulverizing, weighing, size grading, drying, and sample mixing all occur under a 6 foot square hood attached to an overhead ventilating fan. Fig. 30 shows the arrangement of equipment in the coal processing area. This area uses about 50 square feet of a 200 square foot explosion proof cell with the remainder used for storage of processed and unprocessed coal, char, and coke. Unprocessed coal is stored in 55 gallon drums with plastic bag liners. Samples that have been processed for experimental use are stored in 4 gallon plastic containers with air-tight lids.

Compressed air, water, and additional 120 VAC outlets are available in the cell. A water spray system actuated by a manual valve outside the cell provides emergency fire control. Specific equipment installed for the various coal processing steps is listed under "Coal Preparation Equipment" in the Equipment Status List (Table XV).

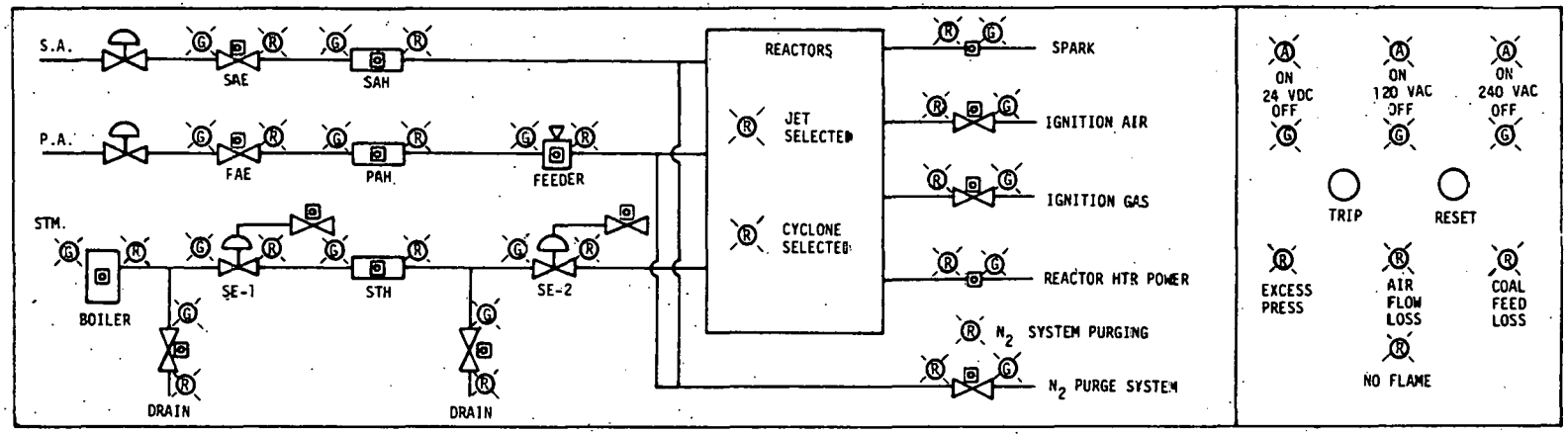

Figure 29. Central Control Panel

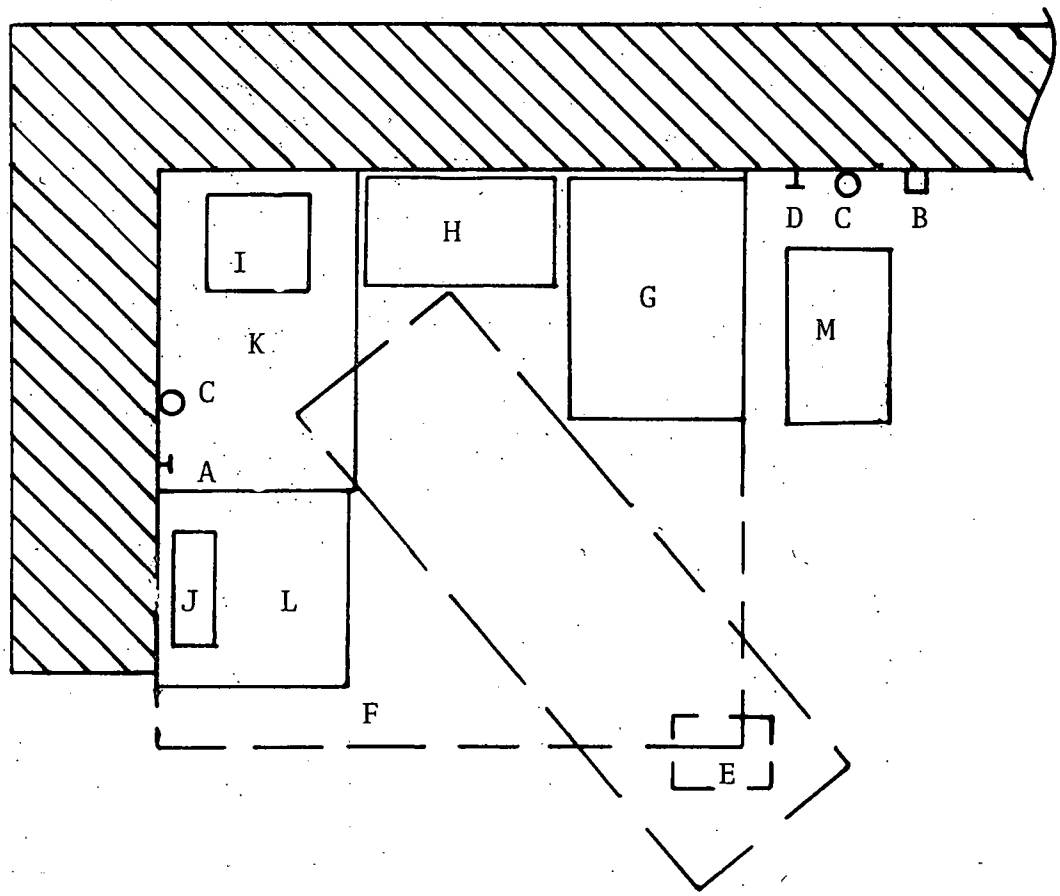

A. Compressed Air (80 psig)
B. 240 VAC 3-Phase Outlet
C. 110 VAC Outlet
D. Water
E. Roof Fan
F. Ventilation Hood
G. Crusher
H. Screen Shaker
I. Pulverizer
J. Scales
K. Steel Table (21 in.)
L. Steel Table (35 in.)
M. Dryer

Figure 30. Coal Handling Facility: Floor Plan

C. Cyclone Gasifier Design

1. Objectives

Our central objective is to determine the suitability of the conventional cyclone combustor for the conversion of pulverized coal to low or middle BTU producer gas. To this end we have designed a laboratory scale cyclone chamber to react 7 to 28 lbm pulverized coal per hour. Measurements of temperature and species concentrations (CO, H_2, H_2O, CO_2, O_2, CH_4, N_2) both within and downstream of the flame and eventual operation at presssures up to 20 atm are planned. The design optimizes geometric parameters and maintains industrial similarity.

2. Reactor Sizing

Reactor size is influenced by three considerations: the diameter ratio of the cyclone to the sampling probe, chamber geometric parameters, and coal throughput (lbm coal/hr ft^3). Residence time, although important, is not an independent consideration; both gas and particle residence times are indirectly related to coal throughput.

To reduce relative flow disturbance by probe insertion, it is desirable to maximize the diameter ratio of cyclone to probe. A typical probe diameter for this application is 3/8 in. For a chamber diameter of 6 in, this results in a diameter ratio of 16. Overall design considerations do not warrant a larger chamber; however, efforts have been directed toward fabricating a smaller probe.

Geometric parameters for cyclone chambers are reviewed in Chapter IV. Dimensionless parameters were selected from those recommended in the literature. Absolute dimensions were determined from these parameters and the reactor volume, which was selected from throughput considerations. Table XVIII lists the geometric design parameters for our chamber; these may be modified to improve high pressure operation.

Coal at throughputs was the most influential consideration in the sizing process. A design objective was the ability to operate throughputs similar to those achieved in both industry and other experimental gasifiers without exceeding coal feed rates of 40 lbm/hr. Figure 31 shows the relationship between coal throughput per atmosphere pressure

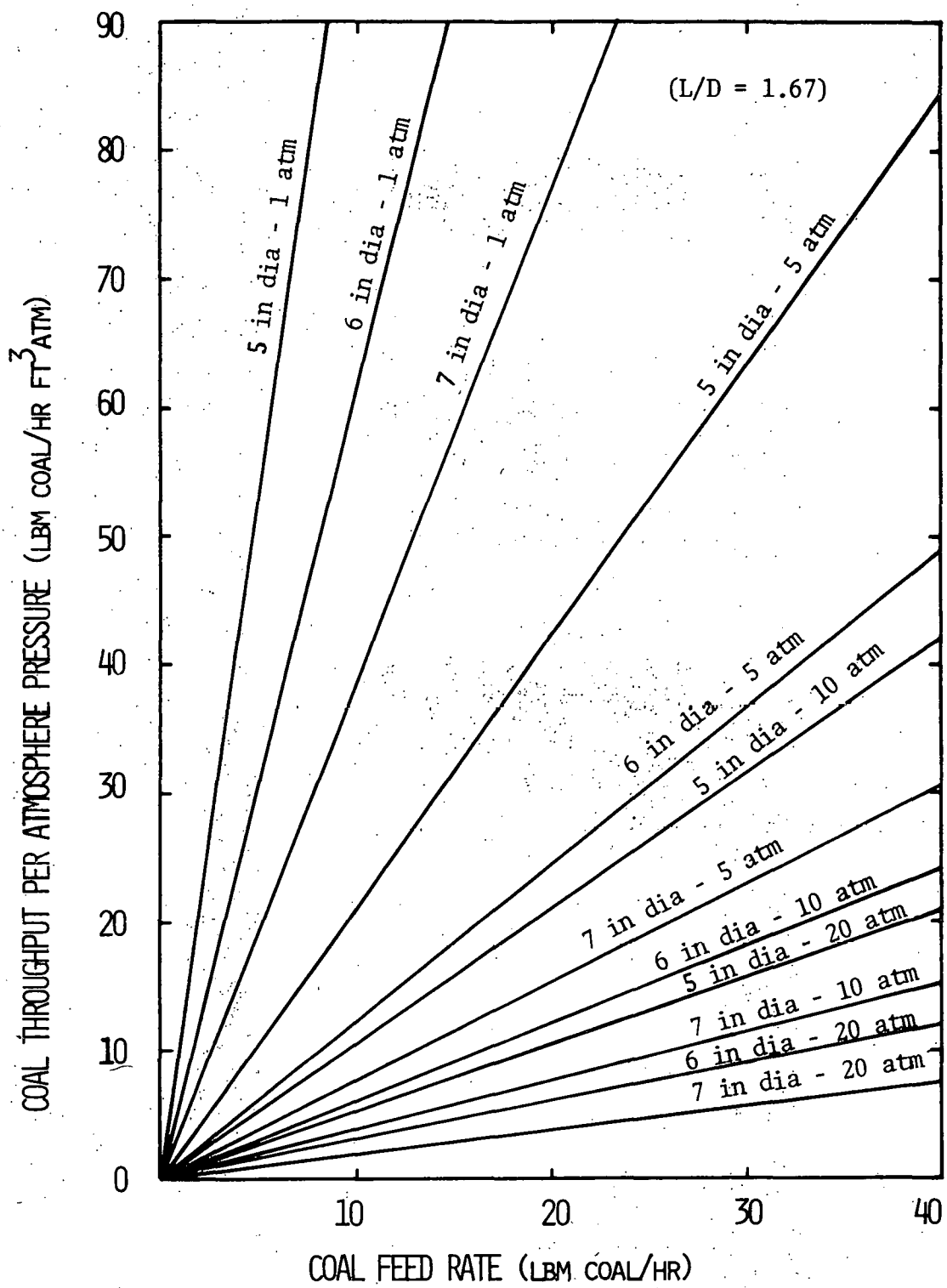

Figure 31. Coal Throughput per Atmosphere Pressure for Various Size Reactors

TABLE XVIII

GEOMETRIC DESIGN PARAMETERS FOR CYCLONE GASIFIER

S	14-28
L/D	1.67
D_e/D	0.33-0.67
N	4
A_t/A_e	0.054-0.215

and coal feed rate for reactors of various diameters at a fixed aspect ratio (L/D). Throughputs obtainable with these reactors can be compared with typical throughputs of actual gasifiers listed in Table VII of Chapter II.

In conventional slagging cyclone combustors, heat release rates per cyclone wall surface area are typically 7×10^5 BTU/hr-ft^2 (G.Moore, 1976). Figure 32 shows the relationships among volumetric, surface, and total heat release rates for various size reactors. It can be seen that surface area heat release rates of 3.5×10^5 BTU/hr-ft^2 (the same order of magnitude as industrial scale) can be achieved at coal feeds under 40 lbm/hr in 5 to 6 inch diameter reactors with L/D = 1.67.

Due to the reduction in throughput at increased reactor volume, chambers with diameters larger than 6 inches were eliminated from consideration. The increased flow disturbance (due to probe insertion) in a smaller diameter chamber was considered to offset the increased throughput capability. Consequently, a 6 inch diameter chamber was selected. At high pressures, however, a smaller chamber may become desirable.

3. Heat Transfer

Heat transfer calculations were performed to determine thermal losses and to aid the materials selection process. Heat loss estimates are imperative due to the high surface to volume ratio of laboratory

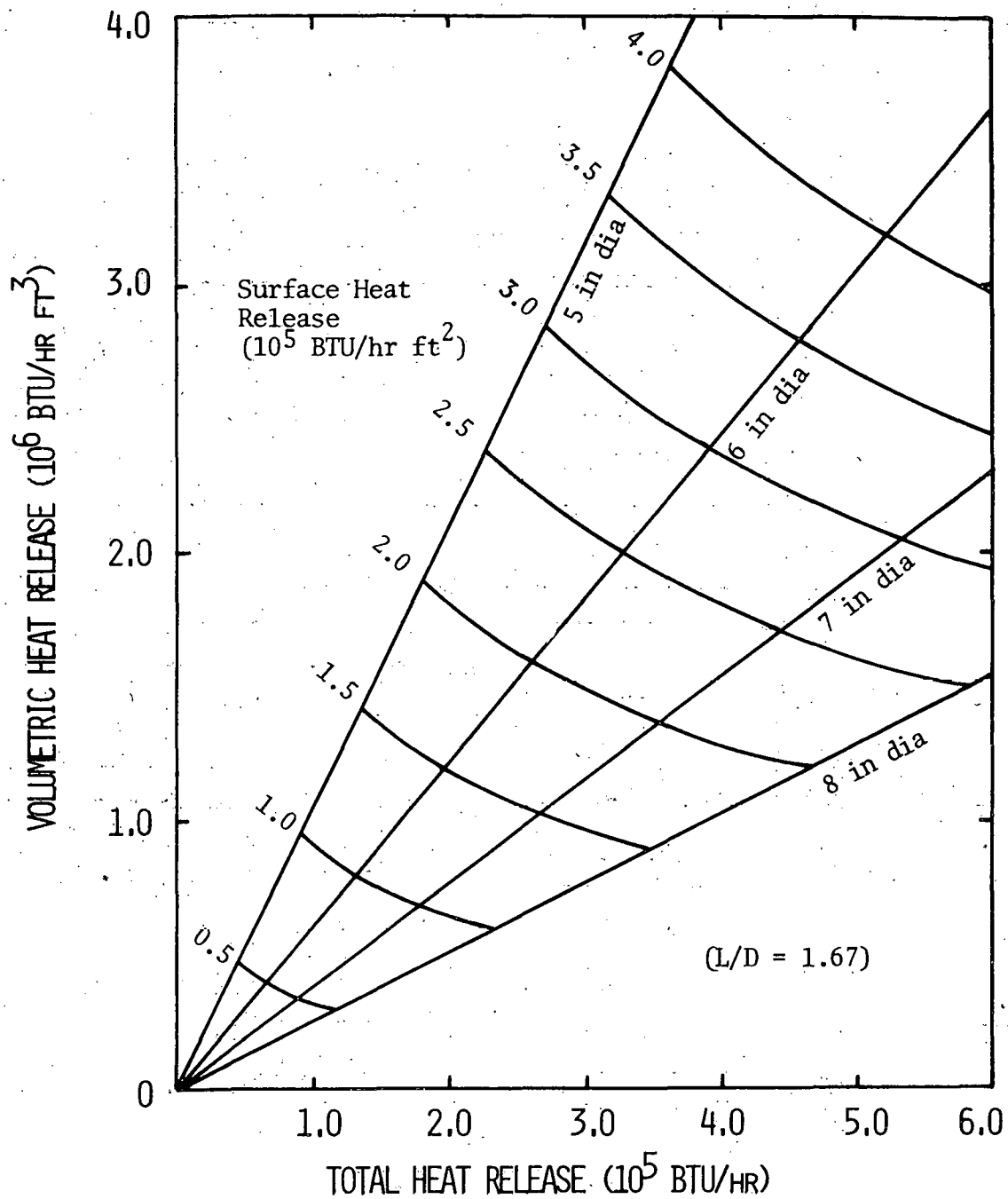

Figure 32. Heat Release Rates for Various Size Reactors

cyclones. Temperature profiles of the reactor assembly under various operating conditions help determine the type and amount of refractory and insulation. These calculations form the basis for heating element selection and pressure vessel design.

Heat transfer calculations were based on the following assumptions: (1) steady state; (2) one dimensional heat transfer; (3) isothermal chamber surfaces; (4) a constant 80°F (300°K) ambient air temperature. One dimensional heat transfer calculations were made in both radial and axial directions, and then summed. A first set of calculations was made for inner refractory wall surface temperatures ranging from 1000 to 3000°F (810 to 1920°K). To compensate for two dimensional transfer effects, a second set of calculations was made for outer refractory wall surface temperatures over the same temperature range. Heat loss estimates for both sets of calculations are shown in Table XIX. The first set of calculations was used to determine various temperatures in the reactor assembly. These temperatures are listed in Table XX for reactor locations shown in Fig. 33.

4. The Reactor Assembly

The reactor assembly is shown in Fig. 33. The reaction zone is 6 inches in diameter and 10 inches long. Pulverized coal and air enter through four equally spaced tangential nozzles in the upper portion of the chamber. Each nozzle has a concentric tubing arrangement; primary air and coal are injected through the inner tube, secondary air through the outer tube. Primary air entrance velocities range from approximately 100 to 300 ft/sec. A torch ignitor for chamber preheating and coal ignition will fire downward from the annulus at the chamber throat.

Steam for gasification will be injected to the core of the chamber from the bottom. We propose that this separate injection of fuel/air and steam, coupled with cyclone flow characteristics, will establish two zones of reaction within a single reactor state: exothermic combustion reactions in the annular zone and endothermic gasification reactions in the core.

TABLE XIX

HEAT LOSS ESTIMATES FOR CYCLONE GASIFIER

T_{wall} (°F)	Inner Surface at T_{wall}			Outer Surface at T_{wall}		
	q_{radial} (BTU/hr)	q_{axial} (BTU/hr)	q_{total} (BTU/hr)	q_{radial} (BTU/hr)	q_{axial} (BTU/hr)	q_{total} (BTU/hr)
1000	1000	100	1100	2150	430	2580
1500	1540	160	1700	3320	660	3980
2000	2080	210	2290	4490	890	5380
2500	2620	270	2890	5650	1120	6770
3000	3170	320	3490	6820	1360	8180

TABLE XX

TEMPERATURE ESTIMATES FOR CYCLONE GASIFIER ASSEMBLY

Inner Wall Temp. (°F)	Ambient Air Temp. (°F)	Tr_2 (°F)	Tr_3 (°F)	Tr_4 (°F)	Tr_5 (°F)	Tx_2 (°F)	Tx_3 (°F)	Tx_4 (°F)
1000	80	930	930	200	200	950	220	220
1500	80	1400	1390	270	270	1430	300	300
2000	80	1860	1850	330	330	1900	380	370
2500	80	2330	2310	400	400	2370	460	460
3000	80	2790	2770	460	460	2850	530	530

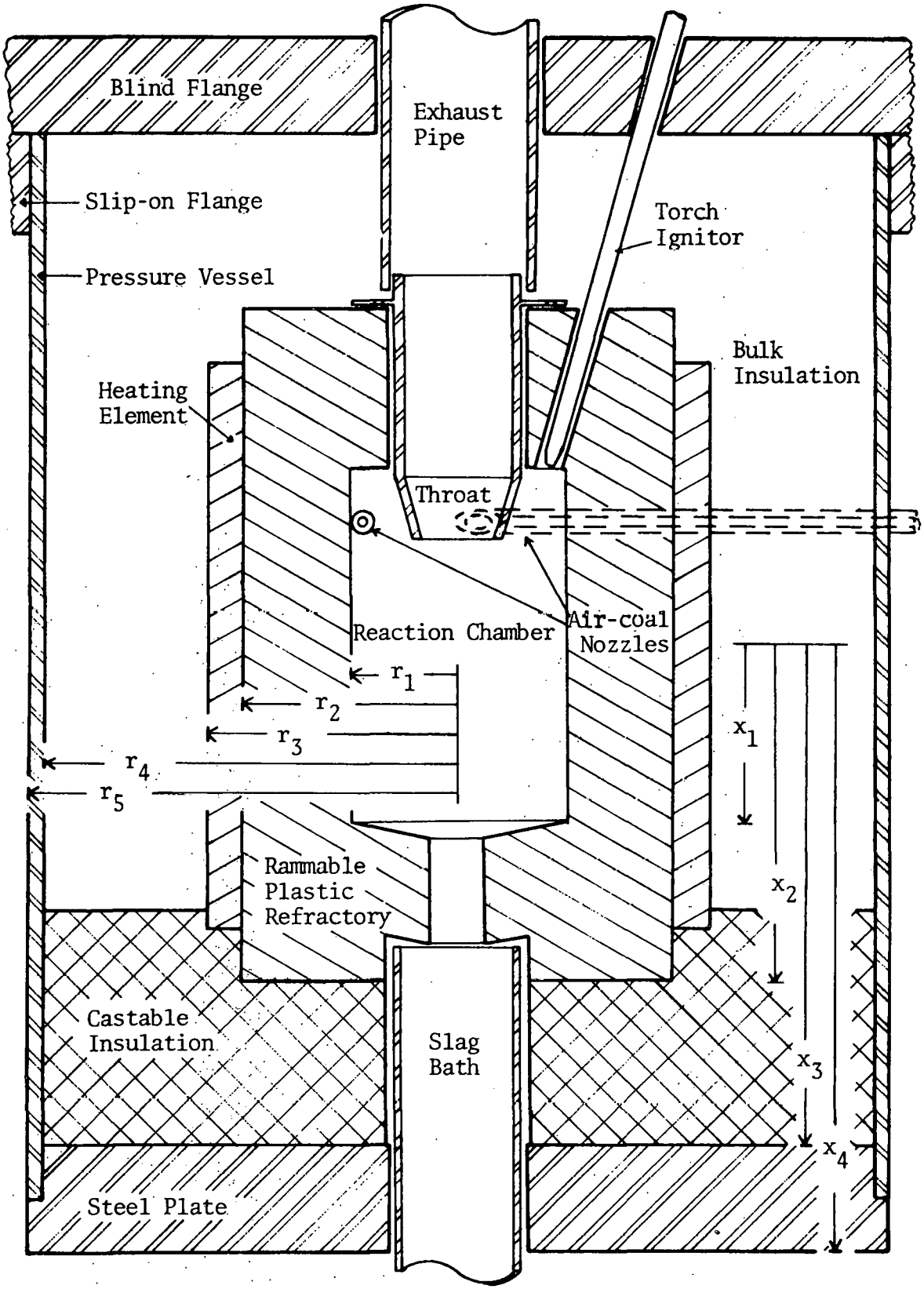

Figure 33. Cyclone Reactor Assembly

Reaction products leave via the conical throat in the chamber roof. Product sampling will initially occur downstream; eventually, however, the chamber interior will be probed. A hole in the chamber floor allows slag to flow to a quench bath.

The walls of the reaction zone are formed from a rammable plastic refractory (Jade Pak-88-P, manufactured by A. P. Green Refractories Co., Mexico, Mo.). This material resists attack by slag and can withstand temperatures as high as 3400°F (2140°K). The cylinder wall is 3 inches thick; the roof and floor are 4 to 5 inches thick. Several inches of lightweight castable refractory (A. P. Green Co.'s Castable Insulation No. 22) supports and insulates the plastic refractory. Bulk insulation fills the void between the reaction chamber and the pressure vessel wall.

Wall heat losses are minimized by four quarter-cylindrical electrical heating elements (Electro-Applications, Inc., Canonsburg, Pa.) which enclose the refractory wall. These elements, 16 inches long, extend beyond the chamber endwalls to promote a flat temperature profile in the reaction zone. A slot in each element allows the four feed tubes to reach the chamber. Total heating capability is 8 kW.

The pressure vessel is fabricated from a 30 inch length of 24 inch seamless pipe (carbon steel, schedule 20). A 3 inch circular steel plate forms a flat head at the bottom; a blind flange bolted to a slip-on flange seals the top. The vessel has been designed in accordance with the ASME Boiler and Pressure Vessel Code to operate at 20 atm.

The major aspects of this design are the symmetric reactant inlet arrangement, the separate combustion and gasification zones promoted by independent steam injection, pressure gasification, operation under slagging conditions, and the use of air with no oxygen enrichment. While several of these features have been previously employed by others, to the best of our knowledge no one has ever incorporated all of them in a single design.

D. Gas Sampling System

Our gasification program is characterized by a unique feature; we will attempt to measure gas-phase composition and temperature not only at the exhaust, but also within each gasifier. Due to the presence of particulates, these measurements will not be straightforward. However, the measurements can be made by an appropriately designed mass spectrometer-probe system.

1. Mass Spectrometer

Based on extensive consultation with seven leading manufacturers of mass spectrometers, we purchased a UTI Q-30C precision quadrupole mass spectrometer system from UTHE Technology International, Sunnyvale, California. The complete Q-30C system has been delivered, and was found to be in working order by a UTI representative.

Only the Q-30C system meets all of the program requirements for a mass spectrometer:

(1) mobility (ion pump)
(2) integrated storage oscilloscope and recorder
(3) automatic scan function and bakeout
(4) rapid response, high pressure inlet system
(5) flexibility
(6) heated inlet system.

In addition, only UTI expressed a willingness to help integrate their mass spectrometer system to our probe/gasifier assembly.

Initial experiments by Dr. Bruce Raby of UTI confirm that the Q-30C system can easily resolve a gas mixture similar to that expected during coal gasification (5.85% CO_2, 3.94% CO, 7.91% H_2, 2.06% CH_4). Use of a Faraday cup, rather than the electron multiplier, will enhance response linearity. Direct measurement of H_2O concentration presents no problem with the heated inlet system. Hydrogen measurements are feasible (even with an ion pump) for $[H_2] < 15\text{-}25\%$. Distinguishing CO from N_2 is achievable for $CO/N_2 > 0.01$ (Damoth and Montgomery, 1972; Singh, 1970).

The UTI Q-30C mass spectrometer is designed as a total system. A vacuum module, display and control module, and quadrupole mass analyzer (UTI 100C) are included. Signal voltages are obtained by a combination Faraday cup/electron multiplier. The inlet system is capable of continuously monitoring a gas stream at 5-50 psia (response time-250 millisec). The entire mass range can be scanned in as little as 75 millisec. The mass range is 1-300 AMU, with an ultimate sensitivity of 100 ppb.

2. Calibration and Data Reduction

A simple calibration facility will soon be designed and built. This system will provide a means of mixing calibration gases from pure gases in known ratios by carefully monitoring partial pressures. Also the facility will be capable of making mixtures containing various amounts of water vapor.

To accurately determine the mole fractions of all species in the gas sample, careful calibration will be necessary. Cracking patterns and relative sensitivities will be determined at conditions duplicating as closely as possible the expected experimental conditions. Calibration gas mixtures will be made in ratios similar to those expected when sampling; pressure and temperature will also be kept close to sampling conditions.

When sampling begins, measurements will be made of all significant peak heights. Because there are more significant peak heights than species present, an overdetermined system of linear algebraic equations will govern the species concentrations. The computer program of McLean and Sawyer (1967), which employs a method of least squares, will be used to solve the system of equations for both the species mole fractions and their standard errors.

3. Sample Inlet System

A preliminary design of the sample inlet system is shown in Fig. 34. The sample gas is pulled from the reactor into a water cooled stainless steel probe where chemical reactions are quenched (Chedaille

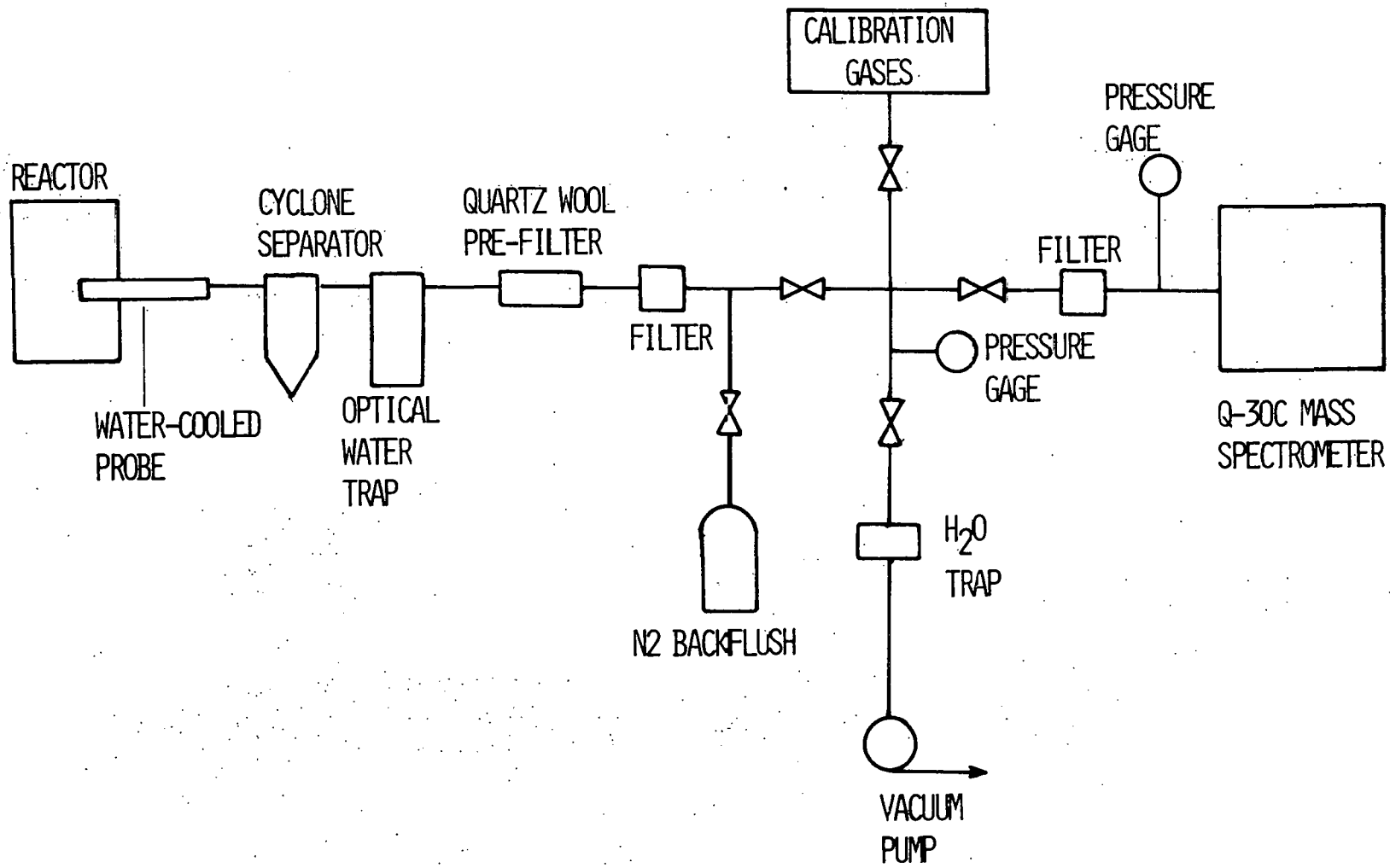

Figure 34. Gas Sampling System Schematic

and Brand, 1972). The cyclone and filters serve to remove particulates which may damage the mass spectrometer and vacuum pump. An optional water trap is included for use when water concentrations become large. A nitrogen backflush is included for purging of part or all of the system. The vacuum pump will pull the sample to the mass spectrometer and can also be used to regulate the sample gas flowrate and pressure at the mass spectrometer inlet. Wherever possible, the inlet lines will be teflon tubing in order to reduce water adsorption, catalytic reactions, and adherence of tars and solids (Fuchs et al., 1974). Heated inlet lines will be used to control the temperature and to avoid water condensation.

4. Probes

A stainless steel water-cooled 3/8 inch O.D. probe is available for sampling reactor exhaust gases. Fine mesh stainless steel screen will be placed over the probe inlet; particles 25 microns in diameter or larger will not enter the probe. Downstream filters will eliminate smaller particulates.

Other probes will be designed for internal reactor probing. Probe designs capable of simultaneous measurement of temperature and concentration will be examined. Material limitations which occur due to the severe reactor environment eliminate the possibility of using sophisticated uncooled probes. Quartz lined, water-cooled probes are presently being examined, and appear suitable for internal reactor probing.

VII. FUTURE EFFORTS

During the next contract year, we expect to meet the following schedule:

(1) Final design and construction of flow system and preheaters, including electrical power and control panels. Complete literature survey and gasifier design. Preliminary construction of gasifiers. Calibrate mass spectrometer. (3 months)

(2) Install steam facility and low pressure feeder. Complete gasifier construction. Build probes and sampling system for integration with mass spectrometer. Test cell and gasifier shakedown. Institute coal/air combustion at 1 atm. (3 months)

(3) Complete measurements and interpret results for coal combustion at 1 atm. Develop entrained flow models. (3 months)

(4) Initiate coal gasification experiments at 1 atm. Construct high pressure coal feeder. (3 months)

During the final year of the contract, we expect to (1) complete the measurements for coal gasification at 1 atm and interpret the results in light of our entrained flow models (6 months) and (2) check the feasibility of coal combustion and gasification at elevated pressures (6 months).

Completion of the gasification facility will provide two reactors representing a microcosm of most practical combustion and gasification devices using pulverized coal and char. Successful probing both externally and internally will allow assessment of the combustion and gasification characteristics of many solid fuels over a range of operating pressures. We are designing the facility with flexibility in mind; thus the reaction vessels can be used for future investigations concerned with related fuels or new reactor configurations.

LIST OF REFERENCES

Abramovich, G. N. (1963), The Theory of Turbulent Jets, (Translation by Scripta Technica Ed: L. H. Schindel) M.I.T. Press, Cambridge, Mass.

Agrest, J. (1965), "The combustion of vegetable materials: A cotton husk combustion problem," J. Inst. Fuel 38, 344.

Baluev, E. D. and Troyankin, Yu. V. (1967a), "Study of the aerodynamic structure of gas flow in a cyclone chamber," Thermal Eng. 14 (1), 84.

Baluev, E. D. and Troyankin, Yu. V. (1967b), "The effect of the design parameters on the aerodynamics of cyclone chambers," Thermal Eng. 14 (2), 99.

Beer, J. M. (1972), "Recent advances in the technology of furnace flames," J. Inst. Fuel, 43, 370.

Beer, J. M. and Chigier, N. A. (1969), "Stability and combustion intensity of pulverized coal flames - effect of swirl and impingement," J. Inst. Fuel 42, 443.

Beer, J. M. and Chigier, N. A. (1972), Combustion Aerodynamics, Wiley, New York.

Beer, J. M. and Lee, K. B. (1965), "The effect of residence time distribution on the performance and efficiency of combustion," Tenth Symposium (International) on Combustion, The Combustion Institute, 1187-1202.

Bodle, W. W. and Vyas, K. C. (1973), "Clean fuels from coal - introduction to modern processes," in Clean Fuels from Coal, Institute of Gas Technology, Chicago, 49-89.

Chedaille, J. and Braud, Y. (1972), Measurements in Flames, International Flame Research Foundation - Crone Russak, New York, 95-98.

Coates, R. L. and Glassett, J. M. (1975), "Experimental and process design study of a fast pyrolytic gasification process," Quarterly Technical Progress Report No. 3, ERDA Fossil Energy Program Contract No. 14-32-0001-1548, Eyring Research Institute, Provo, Utah.

Crowe, C. T. and Pratt, D. T. (1972), "Gas-particle flow in combustion chambers," Paper No. WSCI-72-5, Western States Section, The Combustion Institute.

Dahmen, K. R. and Syred, N. (1975), "The combustion of low calorific value waste gas," Spring Meeting, Central-Western States Section/The Combustion Institute, San Antonio, Texas.

Daily, J. W. and Harleman, D. R. F. (1966), Fluid Dynamics, Addison-Wesley, Reading, Mass., Chapter 6.

Damoth, D. C. and Montgomery, K. L. (1972), "On line monitoring with mass spectrometers," Chem. Eng. Prog. 68 (10), 51.

Elliott, M. A., Perry, H., Jonakin, J., Corey, R. C. and Khullar, M. L. (1952), "Gasification of pulverized coal with oxygen and steam in a vortex reactor," Ind. Eng. Chem. 44, 1074.

Essenhigh, R. H. and Csaba, J. (1963), "The thermal radiation theory for plane flame propagation in coal dust clouds," Ninth Symposium (International) on Combustion, Cornell 1962; Academic Press, N. Y., 111-125.

Farnsworth, J. F., Mitsak, D. M., Leonard, H. F. and Wintrell, R. (1973), "Production of gas from coal by the Koppers-Totzek process," in Clean Fuels from Coal, Institute of Gas Technology, Chicago, 143-162.

Field, M. A. and Gill, D. W. (1967), BCURA Member's Inf. Circ. No. 318.

Field, M. A., Gill, D. W., Morgan, B. B. and Hawksley, P. G. W. (1967), Combustion of Pulverized Coal, BCURA, Leatherhead, U. K.

Fuchs, W., Berman, M., Strakey, J. P., Jr., Ergun, S. (1974), "An automated monitoring system for an experimental coal gasifier," Chem. Inst. 5 (3), 155.

Gordon, S. and McBride, B. J. (1971), "A computer program for calculation of complex chemical equilibrium compositions, rocket performance, incident shocks, and Chapman-Jouguet detonations," NASA SP-273.

Harlow, F. H. and Amsden, A. A. (1971), "Fluid dynamics," Los Alamos Scientific Laboratory, Monograph LA-6700.

Heap, M. P., Lowes, T. M., Walmsley, R. and Bartelds, H. (1973), "Burner design principles for minimum NO_x emissions," EPA Coal Combustion Seminar, Research Triangle Park, North Carolina.

Hedley, A. B. and Jackson, E. W. (1966), "Simplified mathematical model of a pulverized coal flame showing effects of recirculation on combustion rate," J. Inst. Fuel, 39, 208.

Holden, J. H., Strimbeck, G. R., McGee, J. P., Willmott, L. F. and Hirst, L. L. (1960), "Operation of pressure-gasification pilot plant utilizing pulverized coal and oxygen," USBM R15573.

Horn, G., Csaba, J. and Street, D. J. (1966), "Combustion experiments using a pulverized-coal-fired superheater," J. Inst. Fuel, 39, 521.

Hottel, H. C. and Howard, J. B. (1971), New Energy Technology: Some Facts and Assessments, MIT Press, Cambridge, Massachusetts.

Hottel, H. C. and Sarofim, A. F. (1967), Radiative Transfer, McGraw-Hill Book Co., New York.

Howard, J. B. and Essenhigh, R. H. (1967), "Mechanisms of solid-particle combustion with simultaneous gas-phase volatiles combustion," Eleventh Symposium (International) on Combustion, The Combustion Institute, Pittsburgh, 399-408.

Hoy, H. R., Roberts, A. G. and Wilkins, D. M. (1958), "Some investigations with a small cyclone combustor," J. Inst. Fuel 31, 429.

Kalishevskii, L. L. and Ganchev, B. G. (1966), "Study of the aerodynamic structure in cyclone furnaces when burning solid fuel," Thermal Eng. 13 (8), 101.

Kerr, N. M. and Frasier, D. (1965), "Swirl. Part I: Effect on axi-symmetrical turbulent jets," J. Inst. Fuel 38, 519.

Launder, B. E. and Spalding, D. B. (1972), Mathematical Models of Turbulence, Academic Press, London and New York.

Laurendeau, N. M. (1975a), "Theoretical and practical concepts governing production of power gas from coal," Spring Meeting, Central-Western States Section/The Combustion Institute, San Antonio, Texas.

Laurendeau, N. M. (1975b), "Gasification in pulverized coal flames," Report PURDU-CL-75-06 (ERDA-FE-2029-1), School of Mechanical Engineering, Purdue Univ.

Lenzer, R. and Laurendeau, N. (1976), "Gasification of pulverized coal within swirling flows: An interpretive review," Spring Meeting, Western States Section/The Combustion Institute, Salt Lake City, Utah.

Lumley, J. L. and Khajeh-Mouri, B. (1973), "Computational modeling of turbulent transport," Second IUGG-IUTAM Symposium on Atmospheric Diffusion and Environmental Pollution, Charlottesville, Virginia.

McLean, W. J. and Sawyer, R. F. (1967), "Mass spectrometer data reduction and error analysis," Report No. TS-67-4, College of Engineering, University of California, Berkeley.

Mellor, A. M. (1972), "Current kinetic modeling techniques for continuous flow combustors," in Emissions From Continuous Combustion Systems, Cornelius, W., and Agnew, W., Eds., Plenum Publ. Corp., New York, 23-53.

Mellor, G. L. and Herring, H. J. (1973), "A survey of the mean turbulent field closure models," AIAA J. 11, 5, 590.

Moore, G. (1976), General Electric Research Laboratories, Schenectady, N. Y., personal communication.

Mulcahy, M. F. R. and Smith, I. W. (1969), "Kinetics of combustion of pulverized fuel: A review of theory and experiment," Rev. Pure and Appl. Chem. 19, 81.

Nistler, F. (1957), "The Ruhrgas vortex coal dust producer," Coke and Gas 19, 54.

Osborn, E. F. (1974), "Coal and the present energy situation," Science, 183, 477.

Patterson, R. C. (1976), "The combustion engineering and gasification program," Combustion 47 (11), 28.

Perry, H., Corey, R. C. and Elliott, M. A. (1950), "Continuous gasification of pulverized coal with oxygen and steam by the vortex principle," ASME 72, 599.

Pratt, D. T. (1974), "Theories of mixing in continuous combustion," Paper No. 128, Fifteenth Symposium (International) on Combustion, The Combustion Institute, 1339-1351.

Pratt, D. T. (1976), University of Utah, Salt Lake City, Utah, personal communication.

Roschke, E. J. (1966a), "Flow-visualization studies of a confined, jet-driven water vortex," JPL Technical Report No. 32-1004, California Institute of Technology.

Roschke, E. J. (1966b), "Experimental investigation of a confined, jet-driven water vortex," JPL Technical Report No. 32-982, California Institute of Technology.

Rosin, P. O. and Rammler, E. J. (1933), "The laws governing the fineness of powdered coal," J. Inst. Fuel 7, 29.

Schmidt, K. R. (1970), "The rotary flow furnace of Siemens-Agrest," V.D.I. Berichte 146, 90.

Sebastian, J. J. S. (1952), "Powdered-coal gasification," Ind. Eng. Chem. 44, 1175.

Semenov, V. S. and Semenenko, N. A. (1969), "Pattern of combustion and gasification of coal in a cyclone chamber," Thermal Eng. 16 (12), 108.

Singh, T. (1970), "Carbon monoxide reaction in the afterflame zones of the ethylene/oxygen and ethane/oxygen flames," Report No. TS-70-2, College of Engineering, University of California, Berkeley.

Squires, A. M. (1974), "Clean fuels from coal gasification," Science 184, 340.

Strickland, L. D. (1973), "A cold flow mixing study of a vortex coal gasifier," Ph.D. thesis, West Virginia University.

Strimbeck, G. R., Holden, J. H., Bonar, F., Plants, K. D., Pears, C. D. and Hirst, L. L. (1960), "Gasification of pulverized coal at atmospheric pressure," USBM R15559.

Syred, N. and Beer, J. M. (1974), "Combustion in swirling flows: A review," Comb. and Flame 23, 143.

Syred, N., Chigier, N. A. and Beer, J. M. (1971), "Flame stabilization in recirculation zones of jets with swirl," Thirteenth Symposium (International) on Combustion, The Combustion Institute, 617-624.

Tager, S. A. (1971), "Calculating the aerodynamic resistance of cyclone combustion chambers," Thermal Eng. 18 (7), 120.

Tillman, D. A. (1976), "Status of coal gasification," Envir. Sci. Tech. 10 (1), 34.

Traenckner, K. (1953), "Pulverized-coal gasification; Ruhrgas processes," ASME 75, 1095.

Ustimenko, B. P. and Bukhman, M. A. (1968), "Turbulent flow structure in a cyclone chamber," Thermal Eng. 15 (2), 90.

von Fredersdorff, C. (1949), "The continuous gasification of powdered coal suspensions by air-oxygen and air-oxygen-steam mixture," AGA Proc. 31, 705.

von Fredersdorff, C. G. and Elliott, M. A. (1963), "Coal gasification," in Chemistry of Coal Utilization, H. H. Lowry, Ed., Wiley, New York, 892-1022.

Vulis, L. A. (1961), Thermal Regimes of Combustion, McGraw Hill.

Walker, P. L., Jr., Rusinko, F., Jr. and Austin, L. G. (1959), "Gas reactions of carbon" in Eley, D. D., Selwoud, P. W. and Weisg, P. B., Eds., Advances in Catalysis, Academic Press, New York, Vol. 11, 133-221.

Yagi, S. and Kunii, D. (1957), "Studies on combustion and gasification of pulverized coal in a model cyclone generator," Sixth Symposium (International) on Combustion, Reinhold Publ. Corp., New York, 584-590.

BIBLIOGRAPHIC DATA SHEET	1. Report No. ERDA-FE-2029/4	2.	3. Recipient's Accession No.
4. Title and Subtitle GASIFICATION IN PULVERIZED COAL FLAMES First Annual Progress Report			5. Report Date July 1976 (I) 6.
7. Author(s) R. C. Lenzer, P. E. George, J. F. Thomas, N. M. Laurendeau			8. Performing Organization Rept. No. PURDU-CL-76-07
9. Performing Organization Name and Address The Combustion Laboratory School of Mechanical Engineering Purdue University W. Lafayette, Indiana 47907			10. Project/Task/Work Unit No. 11. Contract/Grant No. E(49-18)-2029
12. Sponsoring Organization Name and Address Energy Research and Development Administration Fossil Energy Division 20 Massachusetts Ave., N.W. Washington, D. C. 20545			13. Type of Report & Period Covered (July 1975-June 1976) 14.

15. Supplementary Notes

16. Abstracts

The objective of this program is to investigate the feasibility of using currently available pulverized coal burners to produce power or synthesis gas from coal. Two configurations will be considered: (1) the annular confined jet with secondary swirl, and (2) the vortex tube with tangential entry. The first burner is characterized by a single axial injector of high primary velocity; secondary swirl is used to control mixing and residence times. The second burner is modeled after the cyclone combustor; large residence times and slagging operation should lead to high carbon efficiencies.

Species concentrations and temperature are measured both within and downstream of the gasifier chambers. These profiles are used to assess the influence of process variables such as pressure, solid/gas feed rates, swirl intensity, inlet temperature and geometrical injection pattern on both the rate and extent of coal conversion. Simple models governing entrained flow systems will be developed to further interpret the experimental data.

17. Key Words and Document Analysis. 17a. Descriptors

Pulverized Coal Gasification
Coal Gasification
Pulverized Coal Combustion
Pulverized Coal Burners
Cyclone Burners

17b. Identifiers/Open-Ended Terms

17c. COSATI Field/Group

18. Availability Statement	19. Security Class (This Report)	21. No. of Pages
Release Unlimited	UNCLASSIFIED	169
	20. Security Class (This Page) UNCLASSIFIED	22. Price